

INSIGHT INTO ADENOVIRUS PROGRAMMED DISASSEMBLY FROM  
CRYOEM: THE STRUCTURES OF AD2*ts1* AND THE AD35f+DEFENSIN HD5  
COMPLEX

By

Mariena Silvestry Ramos

Dissertation

Submitted to the Faculty of the  
Graduate School of Vanderbilt University  
in partial fulfillment of the requirements for  
the degree of

DOCTOR OF PHILOSOPHY

in

Molecular Physiology and Biophysics

August, 2009

Nashville, Tennessee

Approved:

Professor Albert H. Beth

Professor Charles E. Cobb

Professor Terence S. Dermody

Professor Hassane S. Mchaourab

Professor Jens Meiler

To my mom, dad and sister, I love you dearly. It is because of you that I am here today. To Raúl, my best friend and companion. To my Ague, who I've missed every day since May of 1995. To CazMan ... keep on beating Ad.



## ACKNOWLEDGEMENTS

I would like to thank my mentor, Phoebe Stewart, who gave me the chance to do fun, exciting and cutting edge research in her lab. Her faith and support were always there for me. I admire her positive attitude, especially at times where it was hard to find a pattern or explanation to a result. Her ideas and energy were critical at every step of the road. And the quality of research which I have done in her lab is superb.

I am grateful for starting my thesis work under the direction of Dr. Susan Sabán. She was the one that got me “hooked” on cryoEM and her technical and teaching skills set an example to follow. Susan is an outstanding microscopist and her attention to detail and insight served as an inspiration all thru the years. Susan has been a great friend and tremendous source of support and inspiration. I have been truly blessed for having her as a friend, lab-mate and mentor.

I am indebted to Dewight Williams, Jian Shi and Mike Lewis for helping me get out of trouble while learning cryoEM. Dewight and Jian were instrumental in speeding the data acquisition with their SAM software, for that I cannot thank them enough. Steffen Lindert has been a great lab-mate along the way. Without him I would not have been able to collect and process the great amount of data for these studies in a short amount of time. Steffen has been a good friend and a great source of scientific and technical questions, all of which made me a better, more inquisitive researcher. Thanks for all the great German chocolate (ist sehr gut!).

I thank all the wonderful collaborators that I was fortunate to work with while doing my thesis and non-thesis related projects. Drs. Glen Nemerow, Jason Smith and Christopher Wiethoff who are remarkable scientists and all of our conversations were a tremendous learning experience. Drs. David Curiel, Dmitry Shayakhmetov and Leonard Rome were instrumental in providing non-thesis related projects that have made a big impact on my scientific development.

I acknowledge the support from the Center for Structural Biology and the Molecular Biophysics Training Program, which funded my research during my second year Vanderbilt. Dr. Walter Chazin has been of great help in this process and I thank him for his interest in my research and career growth. Also, Jarrod Smith, Carrie Lee Kennedy and Matt Binkley who were very nice in assisting with the computer processing needs at the CSB and VAMPIRE. And also the friends at the Jerome lab, Jay, Denny and Mary, thanks for accommodating my grid-baking needs.

I thank my family: my mami and papi are the source of everyday inspiration. Their hard work and wisdom have been with me always. I cannot thank them enough for their support and encouragement. My sister provided a much needed relief and source of laughter along this path. I thank her for being there at all the stages of my graduate career (gracias por las Medallas y Coronas). My grandma Regina who is extremely supportive, loving, and fun. My Aunt María, Aunt Margie, Uncle Georgie and Uncle Willie and my cousins Gloriena, Billie Joe and Brian, who have made me so happy and provided much needed prayers, strength and love. My friends: Sully, Delly, Mayda, Mayra C and

Mayra A, Leri, Noelia, Ama, Ale, Leo, Renier, Willie, Karinna, Chuck, Sepan, Ezelle and Julia, Ida, El “Coro” and “los corillos Boricuas”. All of you made me laugh along this journey and I cannot thank you enough for being the funniest, most awesome friends ever. I thank Raul’s parents, Lianny and José Raúl. Words cannot express how blessed I am to know you. I cannot thank you enough for your calls, prayers, visits, and encouragement. You are an example of what I aspire to be as a Christian and as a researcher. And Raúl: you came into my life unexpectedly and you’ve changed it in so many good ways. You have taught me so much, through words and actions. You are my best friend, companion and boyfriend. You are my blessing. I thank God for each and every one of you. I love you all.

Last but not least I thank the Choir of St. Henry’s Catholic Church in Bellevue. When my spirit was broken your music was always there to lift me up. I thank Mr. John and Ruth Adrian, and Mrs. Mary Corby, Julie Schwartz and Lee Suttle, three of the most beautiful voices I have ever heard. Shellie for being a really cool gal, I wish you a long and prosperous career in publishing, you deserve it! I will miss the choir so very much. Finally I thank the Allens for all their help, you are a wonderful family.

## TABLE OF CONTENTS

	Page
DEDICATION .....	ii
ACKNOWLEDGEMENTS.....	iii
LIST OF TABLES .....	ix
LIST OF FIGURES .....	x
LIST OF ABBREVIATIONS .....	xii
Chapter	
I. INTRODUCTION .....	1
Adenovirus capsid composition .....	1
External capsid proteins .....	2
Additional internal capsid proteins.....	8
Viral Core: Structure and components .....	9
Adenovirus Cell Entry and Capsid Dismantling.....	11
Aim 1: Structure of the Ad2ts1 Mutant .....	13
Ad Immunity Mediated by Human Defensins .....	15
Aim 2: Structure of the Ad35f Vector Complexed with HD5 Defensin ...	16
Concluding Remarks.....	16
II. MATERIALS AND METHODS .....	19
Preparation and isolation of Ad2ts1 .....	19
Cryoelectron microscopy of Ad2ts1 .....	20
Image processing of Ad2ts1 .....	20
Difference map analysis of Ad2ts1 .....	22
Quantification of core-plus-capsid and capsid-only average intensities in cryoEM particle images .....	26
Membrane disruption assay .....	27
Preparation and isolation of Ad35f .....	27
Cryoelectron Microscopy of Ad35f+HD5 .....	28
Image Processing of Ad35f+HD5 .....	28
III. AIM 1: CRYOELECTRON MICROSCOPY STRUCTURE OF THE ADENOVIRUS TYPE 2 TEMPERATURE-SENSITIVE MUTANT 1 REVEALS INSIGHT INTO THE CELL ENTRY DEFECT .....	30
Introduction .....	30

Adenovirus structure and organization:	
Viral components and their locations.....	30
Adenovirus type 2 temperature-sensitive mutant and its role in elucidating Ad cell entry .....	32
Results.....	33
CryoEM structure reveals differences in the Ad2ts1 core compared to the mature Ad core.....	33
The Ad2ts1 penton base is anchored to the viral core .....	44
Density inside the Ad2ts1 hexon cavities is assigned as preprotein VI.....	44
Assignments for preproteins IIIa and VIII on the inner capsid .....	45
Hexon shields protein VI and preprotein VI membrane lytic activity.....	53
Discussion.....	55
The Ad core condenses and becomes less symmetrically ordered during maturation.....	55
Vertex release may require a conformational change that is blocked in Ad2ts1.....	56
IV.    AIM2: CRYOEM STRUCTURE OF AN ADENOVIRUS-HUMAN $\alpha$ - DEFENSIN COMPLEX: INSIGHT INTO BINDING SITES CRITICAL FOR NEUTRALIZATION .....	61
Introduction .....	61
Defensins .....	61
Modes of defensin neutralization.....	62
Elucidating defensin mode of action against adenovirus.....	63
Results .....	65
Stoichiometry of the Ad35f/HD5 interaction .....	65
CryoEM structural study of the Ad35f+HD5 complex .....	78
Difference mapping allows visualization of HD5 on the Ad capsid .....	71
HD5 has multiple binding sites on the top of the hexons in the Ad capsid.....	74
HD5 coats the fiber and tops of the penton base in the Ad capsid .....	80
Discussion.....	86
V.    SUMMARY AND CONCLUSIONS.....	97
Implications for Adenovirus cell entry from our cryoEM study of Ad2ts1 .....	97
Future directions for Ad2ts1 .....	98
Ad-mediated gene delivery.....	100
Antiviral peptides: human Ads and defensins.....	103
Results and implications from the Ad35f+HD5 studies.....	104
Future directions for Ad-defensin .....	105

Appendices .....	108
Appendix 1 .....	108
Appendix 2 .....	145
Appendix 3 .....	146
Appendix 4 .....	147
References.....	148



## LIST OF TABLES

Table	Page
<b>2.1</b> Difference mapping steps .....	23
<b>2.2</b> Composition and mass of the protein/DNA core of human Ad5.....	25

## LIST OF FIGURES

Figure	Page
<b>1.1</b> Diagram depicting the composition of the Ad capsid .....	3
<b>1.2</b> Penton base conformational change induced by fiber peptide binding .....	5
<b>1.3</b> Location of protein IX within the Ad capsid .....	7
<b>3.1</b> CryoEM structures of Ad2 <i>ts1</i> and Ad35f reveal a major structural difference in the core of the virion .....	35
<b>3.2</b> The main differences between Ad2 <i>ts1</i> and Ad35f are on the interior of the icosahedral capsid .....	38
<b>3.3</b> Average radial density distributions of the Ad2 <i>ts1</i> and Ad35f structures .....	40
<b>3.4</b> Masking of the capsid-only and core-plus-capsid regions of a particle image .....	43
<b>3.5</b> Preprotein VI is assigned to density within the cavity of every hexon trimer in Ad2 <i>ts1</i> .....	47
<b>3.6</b> Density assigned to protein IX and preproteins IIIa and VIII are found within Ad2 <i>ts1</i> .....	50
<b>3.7</b> The secondary structure prediction algorithms Jufo, Psipred, and Sam, were used to obtain a three-state prediction for Ad5 protein VIII.....	52
<b>3.8</b> Hexon binding shields protein VI and preprotein VI membrane lytic activity .....	54
<b>3.9</b> Diagram of proposed cell entry events for Ad2 and Ad5 vs. Ad2 <i>ts1</i> .....	58
<b>4.1</b> Stoichiometry of HD5 binding to Ad5 .....	67
<b>4.2</b> CryoEM structures of Ad35f+HD5 compared to Ad35f .....	70
<b>4.3</b> Difference map analysis of three cryoEM structures with a calculated pseudoatomic facet of hexons and pentons .....	73

<b>4.4</b> Difference density corresponding to both HD5 and the hexon surface loops missing from the crystal structure above each of the four unique hexon positions within the asymmetric unit of the 67% Ad35f+HD5 structure.....	77
<b>4.5</b> Difference density corresponding to both HD5 and the hexon surface loops above each of the four unique hexon positions within the asymmetric unit of the 12% Ad35f+HD5 structure.....	78
<b>4.6</b> Difference density from the Ad35f structure corresponding to the missing loops in the hexon crystal structure .....	79
<b>4.7</b> Difference density in the vertex region in both the Ad35f+HD5 67% and 12% structures and the Ad35f structure.....	81
<b>4.8</b> Side views of the vertex region in the Ad35f+HD5 67% and 12% structures and the Ad35f structure .....	84
<b>4.9</b> Postulated critical neutralization site for HD5 based on a combined cryoEM and sequence analysis .....	90
<b>4.10</b> Infectivity assay for various Ad types in the presence of HD5 .....	92
<b>4.11</b> Close up view the postulated critical binding site of HD5 involving the Ad fiber N-terminal region and near the penton base RGD loop.....	95

## ABBREVIATIONS

Ad/Ads = adenovirus/adenoviruses

Ad2ts1 = Adenovirus type 2 temperature-sensitive mutant 1

SCID = severe combined immune deficiency

CryoEM = cryoelectron microscopy

HVR/HVRs = hyper-variable region/regions

Aa/aa's = amino acid/amino acids

TP = terminal protein

HD5 = human  $\alpha$ -defensin 5

HNP1 = human neutrophil peptide 1

CAR = Coxsackievirus and Adenovirus receptor

RGD loop = Arginine, Glycine and Aspartic Acid loop

FSC = Fourier Shell Correlation

SulfoB = Sulforhodamine B

## CHAPTER I

### Introduction

Adenoviruses are large non-enveloped viruses that cause a variety of infections, particularly in the ocular, respiratory, excretory and gastrointestinal systems. These infections are usually non fatal, except in immunocompromised individuals. Ads are used in approximately a third of all ongoing gene and vaccine delivery trials (<http://www.wiley.co.uk/genmed/clinical>). In addition, Ads have been an important discovery tool in molecular biology, for processes such as RNA splicing and virus-induced tumor formation. Though the lifecycle of Ad is well characterized, structural detail of events such as maturation, cell entry and disassembly intermediates is lacking.

#### **Adenovirus capsid composition**

Adenoviruses are composed of 11 proteins, a virally encoded protease and a double stranded linear 36,000 bp DNA genome. Ads were first identified in the 1950s as the causative agent of acute respiratory infections in military recruits (8). These viruses were first visualized by negative-stain electron microscopy in 1950's and their icosahedral shape was noted.

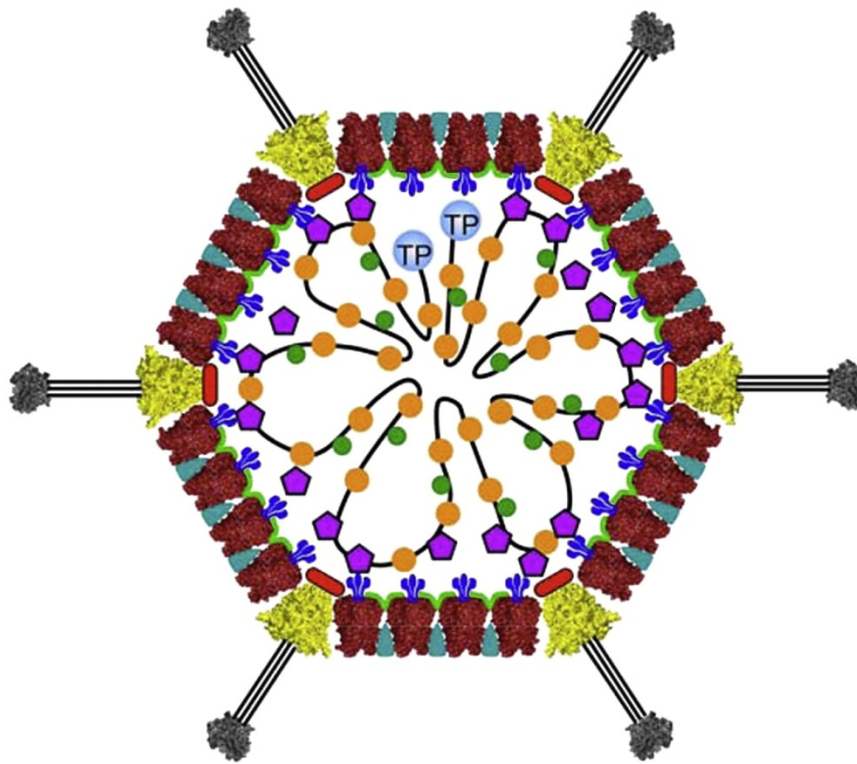
The capsid diameter is over 900Å without taking into account the fiber protein protruding from each vertex of the icosahedron. To date there have been 51 different types of human Ads identified which are classified into 6 species, named A through F, based on their ability to agglutinate blood cells, DNA












sequence similarities, and host immune response. Viruses in species C, which includes Ad 2 and 5, are among the best characterized types of Ad.

### External capsid proteins

The Ad capsid is composed of 3 major proteins: the trimeric hexon found in 240 trimers, the pentameric penton base found in 12 pentamers, and the trimeric fiber also found in 12 trimers. The penton base and trimeric fiber together form the penton located at each icosahedral vertex. The outer capsid also contains protein IX while the inner capsid surface of Ad is coated with proteins IIIa, VI and VIII. The core of the virus does not follow icosahedral symmetry and contains the core proteins V, VII, mu, terminal protein, Ad protease and the DNA **(Figure 1.1)**.

The adenoviral proteins are named according to their migration pattern on SDS-PAGE gels. Hexon, a homotrimer of protein II, is produced in the host cell cytoplasm and its atomic resolution structure has been determined (87). This structure shows that the hexon monomer is rich in  $\beta$  strands. The homotrimer, which forms the majority of the icosahedral capsid, consists of a pseudo-hexagonal base with a triangular top containing the flexible hypervariable regions (HVRs). The 6Å resolution cryoEM structure of the Ad35f vector shows density for the missing HVR loops (124).



<u>Major Capsid Proteins</u>	<u>Minor Capsid Proteins</u>	<u>Core Proteins</u>
 Hexon	 Protein VI	 Terminal Protein
 Penton Base	 Protein IIIa	 Protein Mu
 Fiber	 Protein VIII	 Protein VII
	 Protein IX	 Protein V

**Figure 1.1** Diagram depicting the composition of the Ad capsid. The icosahedrally shaped virus is composed of 11 proteins, the virally encoded protease and the 36kb double stranded DNA genome. The major capsid components, hexon, penton base, and fiber form the icosahedral shell. Protein IX stabilizes the capsid on the outside. Proteins IIIa, VI and VIII associate with the inner capsid surface. The core of the virus is formed by proteins V, VII, Mu, TP and the protease (not depicted), together with the DNA. The core does not follow the icosahedral symmetry of the capsid. The hexon, penton base and fiber knobs are depicted as crystal structures. Adapted with permission from (80).

An atomic resolution structure of the penton base pentamer (protein III), alone and in complex with a fiber peptide (protein IV) has been determined (124). The overall topology of the penton base is similar to that of hexon, a structure rich in  $\beta$ -strands. The penton base crystal structure lacks the RGD-loop, which was not resolved due to flexibility (**Figure 1.2**). There is a slight conformational change at the top of the penton base that occurs when the fiber binds (124). In the 6Å resolution cryoEM structure of Ad35f the density for the missing RGD-loops is observed as well as the conformation of the fiber-bound penton base (89) (**Figure 1.2**).



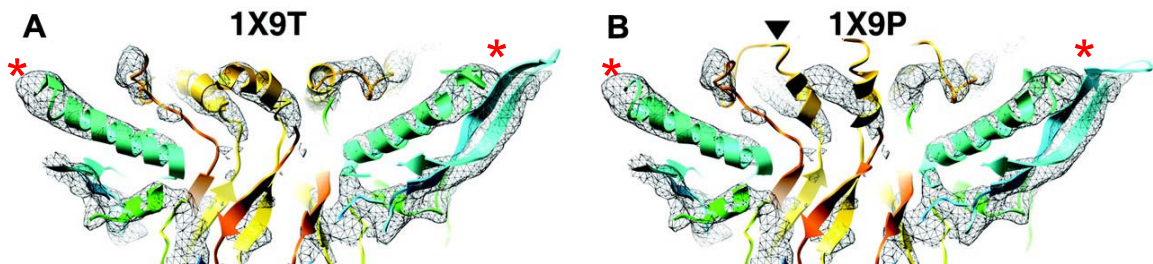


**Figure 1.2** Penton base conformational change induced by fiber peptide binding. Crystal structures of the penton base complexed with the fiber peptide (A; PDB ID: 1X9T) or alone (B; PDB ID: 1X9P) show a slight conformational change at the top of the penton base when the fiber peptide binds (A vs. B, yellow helices). The two crystal structures of the penton base were docked into the 6Å resolution cryoEM structure of the Ad35f vector (gray mesh). The cryoEM structure agrees with the conformation of the penton base with the bound fiber peptide (A). The red asterisks denote the region of the flexible RGD loops. Adapted with permission from (89).

The third major capsid component is the fiber and it is a trimer of protein IV. It is non-covalently bound to the penton base and is responsible for interacting with the CAR or CD46 receptors. The length of the fiber varies according to the serotype, adding 120 to 315Å to the maximal capsid radius (80). Atomic resolution structures of a portion of the fiber shaft, the head (or knob), and the head complexed with Ad receptors have been determined (27, 55, 105, 106). Because the fiber shaft is highly flexible, it is difficult to reconstruct the full length protein by cryoEM or to determine an atomic resolution structure of the full length protein by X-ray crystallography.

The outer capsid protein, IX, is described as a cement protein and viral targeting studies indicate that modification of its C-terminus alters Ad tropism (26). No high-resolution structure of this protein is currently available, but secondary structure prediction algorithms indicate that of all the Ad proteins, protein IX is the only one with a predicted coiled-coil (89). Twelve copies of protein IX are found per facet and form four trimeric clusters with their N-terminal domains and three tetrameric helical bundles with their C-terminal domains (**Figure 1.3**). In the 6Å resolution cryoEM structure of Ad35f, a coiled-coil is observed in the facet between hexons. A cryoEM structure of enhanced green fluorescent protein tagged-protein IX confirms this location (67).

The 6Å resolution cryoEM study and difference mapping analysis has shown that the remaining capsid associated proteins are internal. Their roles in the Ad lifecycle including assembly and programmed disassembly during cell entry are beginning to be understood.

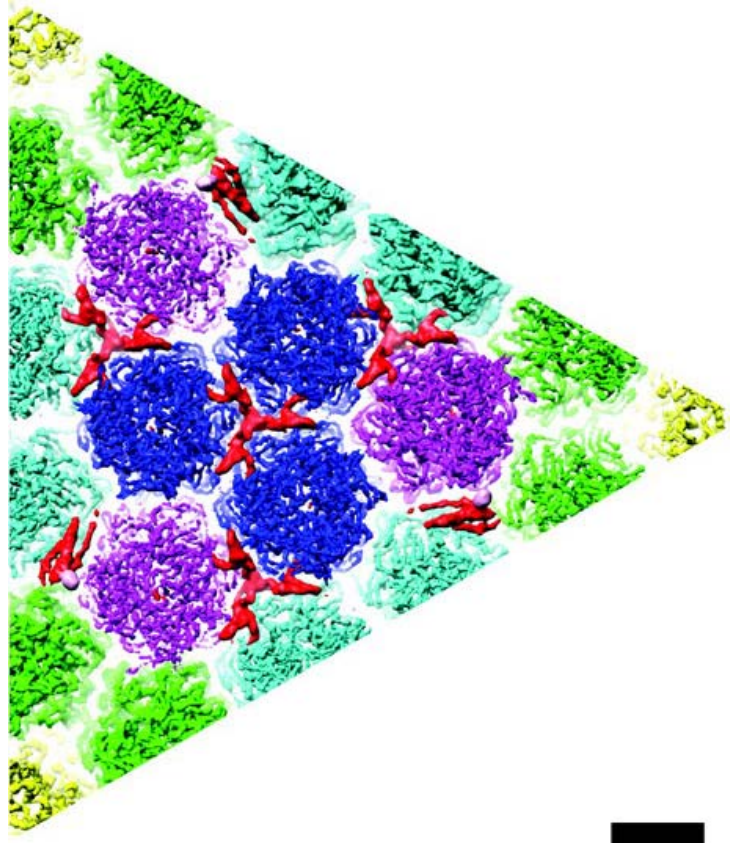


**Figure 1.3.** Location of protein IX (red) within the Ad capsid. A portion of the facet containing three hexons in position 3 (blue) and three hexons in position 4 (purple) is shown. Four copies of the N-terminal domain of protein IX form trimeric clusters, while the C-terminal regions form three tetrameric helical bundles. Scale bar is 50Å. Adapted with permission from (89).

### Additional internal capsid proteins

The inner capsid associated components, proteins IIIa, VI and VIII, are processed by the virally-encoded protease. Temperature-sensitive mutant viruses for protein IIIa, such as the *Adts112* mutant, are defective in viral assembly and maturation, thus protein IIIa's role has been linked to these important processes. The protease removes the C-terminal 15 aa of the Ad5 protein IIIa precursor. Analysis of the Ad35f cryoEM structure with secondary structure prediction algorithms resulted in the assignment of protein IIIa to highly  $\alpha$ -helical regions on the inner surface (89). Structure prediction algorithms indicate that protein IIIa has the highest propensity to form  $\alpha$ -helices of all the adenoviral proteins, with 14 predicted alpha helices with a length of 10 or more residues (89). A structural study involving tagging of the N-terminus of protein IIIa with short peptides, such as six-histidine or FLAG peptides, supports the cryoEM assignment and indicates that protein IIIa's N-terminus faces the inner capsid surface beneath the icosahedral vertices (91).

The second inner capsid protein is VI, which acts as the membrane lytic factor of Ad (118). This protein is produced as a 250 aa precursor. The protease removes 44 residues from precursor protein VI; 33 from the N-terminus and the last 11 C-terminal residues to yield mature VI in Ad2 and Ad5. The C-terminal 11 residues serve as a cofactor for the protease and increase its proteolytic activity by 300-fold (36, 49). Mass spectrometry studies of Ad5 indicate that there are approximately 360 copies of VI within the Ad capsid (58). In the Ad35f structure that contains the mature form of VI, rods of density presumably  $\alpha$ -helices, are

assigned to VI and are located within the hexon cavity (89). Besides mediating endosomal lysis, protein VI has been linked to other events in Ad lifecycle, including protein import of the trimeric hexons to the host cell nucleus during Ad assembly (119).

The third internal capsid protein is protein VIII which is present in 120 copies per capsid or 2 copies per asymmetric unit. The Ad35f structural analysis resulted in assignment of protein VIII to two elongated triangularly shaped regions located below the hexon facet, with one position in the middle of the facet and a second position closer to the vertex and near protein IIIa. Protein VIII has been associated with capsid stabilization as an Ad5 mutant for this protein is more thermolabile than wildtype Ad5 (61). The protease cleaves the Ad5 protein VIII precursor at two sites. It is not known whether all of the cleaved fragments remain within the capsid.

Currently, there is no atomic resolution structure for the three internal capsid components, proteins IIIa, VI and VIII, or their precursor forms. Their locations and copy numbers in the virion have been deduced from biochemical, mass spectrometry and cryoEM studies.

#### Viral Core: Structure and components

Electron microscopy experiments in the 1970's described the core as being composed of spherical particles with a condensed center from which twisted filaments or loops of DNA emanate (9, 21, 44, 81). The core contains five proteins, namely V, VII, mu, TP and the protease together with the ~36,000 bp

genomic dsDNA. CryoEM studies have indicated that the core does not follow icosahedral symmetry, which results in weakly reconstructed density (98, 122). There is a debate on whether the Ad core is incorporated once the capsid is assembled or if the capsid is assembled around a pre-formed core (122).

Early cross-linking studies of the Ad proteins indicated that protein V associates with a dimer of protein VI (16). Therefore it is possible that in immature Ad virions the core and internal capsid surface are connected. Protein VII is the major core protein. It is processed by the viral protease and binds the Ad genome non-specifically to aid in its condensation (122). Two copies of TP are covalently linked to the viral genome and this protein has been proposed to participate in viral replication, possibly acting as a primer for DNA replication (20, 45, 77). Mu is synthesized as a 79 amino acid precursor (protein X) that is processed by the protease at both the N- and C-terminal ends. Mature mu is 19 aa long and is known to associate with the viral DNA *in vitro*, suggesting that mu helps condense DNA in the core, but its function is not clearly understood (15, 16, 50).

Taking into account the copy number and molecular weight for the core components (proteins V, VII, TP, mu, 20-70 copies of the Ad encoded protease, and the genome) the expected mass of the core is approximately 44MDa (Chapter 2, **Table 2.2**). Because cryoEM single particle reconstruction relies on image averaging and the core does not follow the same symmetry as the capsid it is only partially reconstructed. Cryoelectron tomography relies on tilting of the specimen holder and can generate three-dimensional structures

generally to a resolution of 50Å, thus a high-resolution characterization of the Ad core probably cannot be achieved with either three-dimensional EM technique. The core cannot be characterized by NMR as it exceeds the size limitations of this technique (< 100,000 kDa). Because the core does not follow the icosahedral symmetry of the capsid it would also be averaged away in X-ray crystallographic studies. Therefore determining a high-resolution structure of the Ad core is beyond the capabilities of current structural approaches.

### **Adenovirus Cell Entry and Capsid Dismantling**

Ad enters host cells by interacting with two receptors at the cell surface. The first receptor is the coxsackievirus and adenovirus receptor (CAR), which is utilized by most Ad types. Some Ad types interact with CD46 instead of CAR (80). It is the head or knob of the fiber that interacts with CAR or CD46. Atomic resolution structures of the fiber head in complex with either CAR or CD46 have been determined (27, 55, 63, 105). Fiber binds to either CAR or CD46 with high affinity; dissociation constants are in the nM range (1 nM for the fiber-CAR association and 5-15 nM for the fiber-CD46 association) (57, 80). This high-affinity interaction keeps Ad attached to the host cell. CAR is a member of the immunoglobulin superfamily and is involved in the formation of tight junctions in epithelial cells (80). Most Ads use CAR as the primary receptor including Ads of species A, C, E and F, while Ads in species B and D interact with CD46 or sialic acid (80).

The second Ad receptor is  $\alpha$ v integrins ( $\alpha$ v $\beta$ 3 or  $\alpha$ v $\beta$ 5, and in some cases  $\alpha$ M $\beta$ 2 or  $\alpha$ 5 $\beta$ 1), which mediate Ad internalization. Binding of Ad to integrins was described in 1993 (117). The RGD-binding  $\alpha$ v $\beta$ 3 or  $\alpha$ v $\beta$ 5 interact with the RGD loop of the penton base. This interaction triggers signaling pathways in the cell leading to receptor-mediated endocytosis of the virus, via clathrin-coated vesicles (23, 80, 96, 116, 117). The affinity of the penton base-integrin interaction is lower (55 nM) than that of fiber with CAR or CD46 (80, 106). Interaction of integrins activates rearrangement of the cytoskeleton prior to virus internalization (through PI3 kinase and Rho GTPase activation) (116, 117). Once the clathrin-coated vesicle containing Ad is released from the host cell membrane it is delivered to the early endosome, where the environment of this compartment acidified (pH 6-6.5). Acidification of the endosome is thought to trigger the release of the viral proteins at the vertices of the capsid (118). Although some studies indicate that the fibers may fall off earlier than penton base, heat denaturation and low pH-induced disassembly studies indicate that the penton base and 25% of the hexons (presumably the peripentonal hexons) are released together with protein IIIa and 80% of protein VI (37, 118).

Release of protein VI from the inside of the capsid is required for endosomal escape, as protein VI is the membrane lytic factor of Ad (118). Although the precise mechanism of protein VI-mediated membrane destabilization is not understood, residues spanning aa 36-53 are necessary for membrane lytic activity and are predicted to form an amphipathic  $\alpha$ -helix (118). The amphipathic helix may insert into the endosomal membrane, and the



concerted action of a high number of copies of protein VI (~300) may disrupt the membrane by a carpeting, or membrane coating, mechanism (37, 118).

After the virus escapes from endosomes it interacts with motor proteins in the cytosol, such as dynein, which translocate the virus from the endosome to the nuclear pore complex (NPC) (60). Hexons dock at the NPC protein CAN/Nup214. At least two other Ad proteins (VII and terminal protein (TP)) interact with either the NPC or nuclear components to release the Ad genome into the nucleus (12, 21, 60, 86, 122). Three non-Ad proteins assist in the process of genome delivery, histone H1, Hsc70, and CRM1, a nuclear export protein, after which Ad genome transcription begins. The viral proteins are synthesized in the cytoplasm, and are shuttled into the nucleus for assembly of progeny virions. Precursor VI, which has nuclear export and import signals, binds hexons in the cytoplasm and shuttles them into the nucleus for virion assembly (119).

### **Aim 1: Structure of the Ad2ts1 Mutant**

Ad2ts1 is one of a series of chemically-generated Ad mutants first described in 1976. The mutational study was aimed at identifying and describing the Ad genome and the encoded proteins by genetic complementation (6, 111, 112). In the case of Ad2ts1, the defect was traced to a point mutation in the Ad protease, a proline to leucine substitution at position 137 (P137L) (83, 111). This point mutation does not interfere with the proteolytic capacity of the protease, as the mutant protease is able to process the precursor proteins when isolated. The

problem is that the protease is not packaged in the virus when produced at the non-permissive temperature (39°C) (83). Ad2*ts1* particles produced at the non-permissive temperature (Ad2*ts1*-39°C) have a cell entry defect. They are able to enter host cells but cannot escape the endosome and are either recycled to the cell membrane or targeted for degradation in the lysosome. Isolated Ad2*ts1*-39°C particles contain the precursor forms of the Ad proteins IIIa, VI, VII, VIII, X ( $\mu$ ) and TP (111).

In Ad2*ts1*-39°C, the membrane lytic protein VI is not released, and endosomal lysis does not take place. Isolated protein VI, in both its mature and immature forms, can mediate membrane penetration in liposomes. This suggests that the Ad2*ts1*-39°C defect is related to disassembly of the virion during cell entry. This prompted us to investigate the structure of Ad2*ts1*-39°C by cryoEM single particle methods. We envisioned that studying the structure of this mutant virus would increase our understanding of the normal events in assembly, maturation and programmed disassembly of this important human pathogen.

In Chapter 3 I present a 10.5Å resolution cryoEM structure of the Ad2*ts1*-39°C mutant. This structure shows that precursor proteins IIIa, VI and VIII are associated with both the inner capsid surface and the core of Ad2*ts1*-39°C. In contrast, in the mature Ad35f structure these three proteins are associated with the capsid and are clearly separated from the core. Of special interest is the location and structure of precursor protein VI and how it relates to Ad2*ts1*-39°C's inability to undergo programmed disassembly. We present a new model of capsid disassembly for mature Ad2 and Ad5. The critical vertex disassembly step

is blocked in Ad2ts1-39°C. It involves a role for the protease in priming the virion for programmed disassembly during cell entry, including the release of the fiber and protein VI.

### **Ad Immunity Mediated by Human Defensins**

An important step in successful delivery of a transgene or therapeutic agent is to bypass the host's immune system. Ad encounters a plethora of immune system components once it enters its host, one of which is defensin. Defensins are small cationic peptides with potent immune activity that in humans are classified into two groups, alpha and beta defensins, according to the pattern of their disulphide bonds. Defensins are effective against various microbes, including bacteria and both enveloped and non-enveloped viruses, such as HIV-1, influenza A virus, and human papillomavirus (32, 56).

Defensins are expressed by a variety of cells, including neutrophils, Paneth cells, and in the urinary and airway tracts. The mechanism by which defensins disrupt infections is currently not well understood, but in the case of bacteria, fungi and enveloped viruses, is thought to involve membrane disruption. The mechanism of defensin action against Ad has been partially characterized and involves stabilization of the capsid, via direct interaction of HD5 defensins with the Ad capsid. Defensin inhibition of this non-enveloped virus is achieved at low micromolar concentrations ( $IC_{50}$  of 3-4  $\mu$ M), with complete inhibition at concentrations greater than 10  $\mu$ M by preventing the release of the vertex components of the Ad capsid. We present a new model of capsid disassembly

for mature Ad2 and Ad5. The critical vertex disassembly step is blocked in Ad2ts1-39°C.

### **Aim 2: Structure of the Ad35f Vector Complexed with HD5 Defensin**

Since the mechanism of defensin action against enveloped and non-enveloped viruses appears to differ, we wanted to structurally characterize the interaction of human  $\alpha$ -defensin HD5 complexed with the Ad35f vector. The Ad35f vector is composed of the Ad5 capsid pseudotyped with the short Ad35 fiber. The short fiber is advantageous for high-resolution cryoEM studies.

In Chapter 4 I present two structures of Ad35f complexed with human  $\alpha$ -defensin HD5. Difference density analysis revealed multiple binding sites on the outer capsid surface. These include sites on the hexon towers and central depression, as well as on the penton base and fiber. The structural analysis together with the information on which Ad serotypes are neutralized by HD5 and which are not, led to a hypothesis regarding the critical HD5 binding site for neutralization. A model for Ad neutralization by HD5 is presented that involves capsid stabilization and prevention of protein VI release.

### **Concluding Remarks**

In Chapter 2 of the thesis the materials and methods used for these studies are described. Chapter 3 presents the results of Aim I, focusing on the role of the immature capsid proteins of Ad2ts1 in preventing release of the membrane lytic factor at the appropriate time during Ad entry into host cells. Based on our findings we propose that the membrane lytic factor, protein VI,

must be processed by the Ad protease in order to separate from the core and be ready to dissociate from the capsid once the vertex proteins are released in the endosome. Packaging of the protease and timely cleavage of the precursor proteins are critical for producing a fully infectious virion.

Chapter 4 presents two cryoEM structures at 9.6Å and 11.8Å resolution of the Ad35f vector complexed with human  $\alpha$ -defensin HD5. The higher resolution structure has less defensin density coating the outer capsid surface. The lower resolution structure has significantly more defensin density. We have analyzed the possible defensin binding sites in both structures. HD5 density is observed interacting with hexons, penton bases and fibers in multiple sites on the virion surface. We propose a model of neutralization for Ads in which the defensin interferes with the loss of the fiber resulting in a “locking shut” of the capsid that prevents the release of the fiber and of the membrane lytic protein VI.

Chapter 5 presents the conclusions and future directions of these research projects and an overview of Ad programmed disassembly based on our findings. Supplemental chapters S1, S2, and S3 show the results of three additional research projects that I contributed to during my graduate research experience. Chapter S1 presents the 6Å resolution structure of the Ad35f vector. At this resolution  $\alpha$ -helices of 10 or more residues are observed as rods of density. This was confirmed by docking the crystal structure of hexon and penton base into the cryoEM density map. The subnanometer resolution (< 10Å) cryoEM structure allowed a detailed analysis of the capsid associated proteins for which no atomic resolution structures are available (89). Chapter S2 describes a

cryoEM structure of an Ad5 vector complexed with the blood coagulation factor X. Factor X binds with high affinity (229 pM) to the hexon protein. Our cryoEM study enabled visualization of the factor X binding site on the virion (52). Chapter S3 describes a 38Å resolution structure of the vault ribonucleoprotein tagged with a cysteine rich tag to localize the major vault protein's C-terminus. In addition to this Cys-rich tag, IgG and EGF tags were tested for their ability to target vaults to cancer cells. Because of their hollow interior and relatively large size (700Å x 410Å) vaults are proposed as nanodelivery particles that could be engineered to carry molecular cargo and to target and treat specific cells, such as epithelial cancer cells (54). Chapter S4 presents the series of scripts used to perform difference density mapping for Aims 1 and 2.

## CHAPTER II

### Materials and Methods

Contribution note: The Nemerow group prepared the Ad2ts1 and Ad35f samples used for data collection. Steffen Lindert helped with data acquisition and initial image processing for both aims.

#### Preparation and isolation of Ad2ts1

A549 cells were maintained in Dulbecco's complete modified Eagle's medium (DMEM) supplemented with 10 mM HEPES, 2 mM L-glutamine, 1 mM sodium pyruvate, 0.1 mM nonessential amino acids, 100 U of penicillin G/ml, 0.3 mg of gentamicin/ml, and 10% fetal bovine serum. The temperature-sensitive mutant Ad2ts1 was propagated in A459 cells at the non-permissive temperature of 39.5°C. Cells were infected at a multiplicity of infection of 300 particles/cell with Ad2ts1 that had been previously grown at the permissive temperature of 33°C. Infected cells were harvested after nearly complete cytopathic effect, approximately 60 h post-infection. Virus was purified from freeze/thaw lysates by two rounds of CsCl density gradient ultracentrifugation, dialyzed against Tris buffer at pH 8.0 (50mM Tris, 130mM NaCl, and 3mM KCl) and immediately prepared for cryoelectron microscopy. Ad2ts1 particles were compared to wild-type Ad5 particles for the presence of unprocessed (preprotein) capsid proteins as determined by SDS-PAGE.

### Cryoelectron microscopy of Ad2ts1

CryoEM grids were prepared as described by Saban *et al.* (88). Briefly, 6  $\mu$ l samples of Ad2ts1 at a concentration of 614  $\mu$ g/ml were applied to Quantifoil R2/4 holey carbon grids (Quantifoil Micro Tools GmbH) and vitrified using the Vitrobot cryo-fixation device (FEI Company). Data collection was performed on an FEI Polara (300 kV; FEG) transmission cryoelectron microscope operated at liquid nitrogen temperature and 300 kV with a Gatan UltraScan 4kx4k charge-coupled device (CCD) camera. Eight datasets were collected for a total of 7,218 cryoelectron micrographs. Datasets 1 through 4 were collected manually and datasets 5 through 8 were collected using SAM, a semiautomatic data collection routine (95). The absolute magnification for all datasets was  $\sim$ 398kX.

### Image processing of Ad2ts1

A total of 5,544 particle images were selected from the micrographs using the automatic selection program VIRUS (1). The particles were binned to  $250^2$  pixels (4.6Å pixels) for the initial rounds of refinement, and later to  $500^2$  or  $750^2$  for processing with finer pixel sizes (3.1Å and 1.55Å, respectively). The initial microscope defocus and astigmatism parameters were determined with CTFFIND3 (74), and later refined with FREALIGN (39). During the initial stages of refinement only the orientational parameters (translation center and three Euler angles) were refined. In later rounds of refinement, the absolute magnification was also refined on a per particle image basis. The cryoEM structure of Ad35f (89) filtered to 12Å resolution was used as the starting model for refinement. A modified version of FREALIGN was used to allow the input of



externally determined particle centers (89). After each round of refinement several reconstructions were calculated with various thresholds for the “phase residual” parameter calculated by FREALIGN, which is a weighted correlation coefficient between particle and reference (39). The reconstruction with the highest resolution for the icosahedral capsid (radii 300-463Å) as assessed by the Fourier Shell Correlation (FSC) 0.5 threshold was selected as the input map for the subsequent round of refinement. After the final round of refinement, two types of Ad2ts1 density maps were calculated: one including only the capsid radial shell (300-463Å) for resolution assessment, and the other including all radial shells so that the reconstruction would include the core and fibers.

The final reconstruction presented in the figures includes 890 particle images, corresponding to 16% of the data. Additional reconstructions were also calculated with up to 4,229 particles, or 76% of the data. The reconstructions based on larger data subsets are nearly identical to the highest resolution reconstruction based on 16% of the data, except that they have slightly worse resolutions. The map based on 76% of the data has an estimated resolution of 11.7Å at the FSC 0.5 threshold, while the map based on 16% of the data has a resolution of 10.5Å at the FSC 0.5 threshold. In an attempt to examine the core structure, “core-only” reconstructions of Ad2ts1 and Ad35f were calculated with Frealign by setting the outer radius of the map to 300Å or 325Å. We applied various low pass filters with resolution cut offs in the range of 20-100Å to the core-only maps and examined them with UCSF Chimera. No prominent, reproducible features were observed in either the Ad2ts1 or Ad35f core

reconstructions. A temperature factor ( $B = -300\text{\AA}^2$ ) was applied to the highest resolution Ad2ts1 and Ad35f reconstructions to restore high-resolution contrast using the BFACTOR program (<http://emlab.rose2.brandeis.edu/grigorieff>). The FSC and radial density plots were generated with MatLab.

#### Difference map analysis of Ad2ts1

A pseudoatomic facet composed of 18 copies of the Ad5 hexon trimer (PDB ID: 1P30) (87) and three copies of the Ad2 penton base pentamer with fiber peptide (PDB ID: 1X9T) (124) was generated. Optimal docked positions for hexon and penton base were found with the “Fit Model in Map” function of UCSF Chimera (82). The pseudoatomic facet was filtered to the same resolution as the Ad2ts1 or control Ad35f (89) cryoEM structure and subtracted from the cryoEM density map with IMAGIC (104) to reveal density for the minor capsid proteins. Table 2.1 summarizes the steps involved during the difference mapping calculations. All graphics figures were produced with UCSF Chimera.

**Table 2.1.** Difference mapping steps

<b>Step #</b>	<b>Description</b>
1	Names and variables are defined for subsequent steps
2	Cuts region of experimental map for later steps; filters control map to match the experimental map resolution
3	Adjusts control map dimensions to match experimental map dimensions
4	Cuts region of control map matching those of the experimental map
5	Uses UCSF Chimera to coarsely position a facet onto the experimental map
6	Saves individual coordinates of coarsely fitted facet from step 5 for use during step 7
7	Uses UCSF Chimera to accurate fit the facet into the experimental map
8	The fitted facet coordinates are stored relative to the experimental map
9	Converts facet to EM Density (MRC/CCP4); filters and fits the MRC facet properly into the experimental map
10	Normalizes all the maps; the mean and standard deviation values for each map are set equal
11	Applies appropriate threshold values to all the maps (experimental, control and facet) to ensure that the subtraction process is performed correctly
12	Continuation of step 11
13	Continuation of step 11
14	Difference maps are calculated (Map – Map and Map – Facet)

The following assumptions were made for the mass calculations of the Ad2ts1 and Ad5 cores. Monomer copy number per virion: protein II (hexon), 720; protein III (penton base), 60; protein IIIa, 60; protein IV (fiber), 36; protein V, 170; protein VI, 369; protein VII, 633; protein VIII, 120; protein IX, 240; protein X (mu), 125; terminal protein, 2; protease, 43 for mature Ad and 9 for Ad2ts1. The copy number estimates for proteins V, VI, VII are derived from mass spectrometry (58). Biochemical estimates are used for protein X (mu) (12, 50) and terminal protein (12, 84). The protease copy number of 43 in mature Ad is an average of three estimates, 10, 50, or 70 copies per virion (3, 9, 65), and the protease copy number in Ad2ts1 is reduced 5-fold (9). Since the copy number of L1-52K in the mature Ad virion is controversial (18, 48), and since the copy number in the Ad2ts1 virion has been estimated as just one to two molecules (48), we left this protein out of the mass calculations. We assumed a mass of 23.7MDa for the 36kb dsDNA Ad2 and Ad5 genomes. Our calculations indicate that the mass of the Ad2ts1 core is ~46MDa vs. ~44MDa for mature Ad5 core (a 5% difference). When the internal capsid proteins are included in the calculation, the mass of the Ad2ts1 core is ~63MDa vs. ~59MDa for mature Ad5 (a 7% difference). See table 2.2 for details.

**Table 2.2** Composition and mass of the protein/DNA core of human Ad5

Core Component	Processed by the Ad protease	Copy Number	Precursor Mass (kDa) <sup>a</sup>	Mature Mass (kDa)	Total Mass In Immature Core of Ad2ts1 (kDa)	Total Mass In Mature Core (kDa)
V <sup>b</sup>	N	170	41	41	6,970	6,970
VII <sup>b</sup>	Y	633	22	19	13,926	12,027
X(mu) <sup>c</sup>	Y	125	9	2	1,125	250
TP <sup>c</sup>	Y	2	76	37	152	74
Protease <sup>d</sup>	N	43 (mature)  9 (Ad2ts1)	23	23	207	989
dsDNA 35,938bp	N/A	1	23,719	23,719	23,719	23,719
<b>Total</b>					<b>46,099</b>	<b>44,029</b>

<sup>a</sup>The protein masses were calculated using

(<http://www.sciencegateway.org/tools/proteinmw.htm>) and the DNA mass is estimated assuming a molecular weight of 330Da per base.

<sup>b</sup>The copy numbers for V and VII are from mass spectrometry (58).

<sup>c</sup>The copy number for protein X(mu) is from (12, 50) and for TP is from (12, 84) and (84).

<sup>d</sup>The protease copy number in the mature virion is an average of three estimates of 10, 50 or 70 copies (3, 65, 66). The protease copy number in the immature core of Ad2ts1 is estimated as 5-fold lower based on a biochemical estimate (3).

### Quantification of core-plus-capsid and capsid-only average intensities in cryoEM particle images

Subsets of 100 cryoEM particle images included in the highest resolution Ad2ts1 and Ad35f reconstructions were selected for analysis of their 2D projection density. A third subset of 100 Ad2ts1 particle images excluded from the highest resolution reconstruction, but included in the reconstruction based on 76% of the data was also evaluated. IMAGIC (104) was used to translationally center the selected particle images according to the refined FREALIGN centers (x, y). The centered particles were normalized (with the IMAGIC Norm-Variance command) and inverted (with the IMAGIC Arithmetic-with-image command, Invert subcommand) so that protein density would have positive intensity values. Then pixels with negative intensity values were set to zero (with the IMAGIC Arithmetic-with-image command, Threshold subcommand). A circular mask (radius=300Å) was applied to generate core-plus capsid images, and radial masks (inner radius=300Å, outer radius=463Å) were applied to generate capsid-only images (with the IMAGIC Arithmetic-with-image command, Circle and Ring subcommands). The core-plus-capsid images contain projection information from the core as well as from the top and bottom capsid surfaces. The capsid-only images contain projection information from only the capsid around the outer edge of the particle image (Chapter 3, **Figure 3.4**). The IMAGIC Survey command was used to calculate the average intensities for the core-plus-capsid and capsid-only images.

### Membrane disruption assay

Ad-mediated membrane disruption was assessed by the dequenching of sulforhodamine B (Sulfo B) fluorescence upon its release from the liposomes. Fluorescence intensity was monitored using a Tecan Genios microplate reader equipped with 535/20 nm excitation and 585/20 nm emission filters, respectively. Liposomes were diluted to a final phospholipid concentration of 2  $\mu$ M in 100  $\mu$ l of buffer in 96-well plates (catalogue no. 3904; Costar). Various amounts of virus or recombinant Ad proteins in 5 mM HEPES (pH 7.0) were added to the liposomal solutions preequilibrated at 37°C, and the kinetics of membrane disruption were monitored by the increase in SulfoB fluorescence. One hundred percent dye release was determined by adding Triton X-100 to liposomes at a final concentration of 0.2% (wt/vol). The percentage of SulfoB release was calculated by the equation %SulfoB released = 100 x [(F<sub>meas</sub> - F<sub>0</sub>)/(F<sub>tx100</sub> - F<sub>0</sub>)], where F<sub>meas</sub> is the maximum fluorescence intensity measured for each sample, F<sub>0</sub> is the fluorescence intensity in the absence of virus or protein, and F<sub>tx100</sub> is the fluorescence intensity in the presence of 0.2% Triton X-100.

### Preparation and isolation of Ad35f

The Ad35F vector consisting of the Ad5 capsid with the pseudotyped Ad35 fiber was prepared as described in (89). The virus was propagated in A 549 cells and purified by standard CsCl centrifugation (89). Viral protein concentration was determined by the Bio-Rad Protein Assay (Bio-Rad, Richmond, CA) with a

bovine serum albumin standard and used to calculate the viral particle concentration as described by Smith and Nemerow, 2008 (10).

#### Cryoelectron Microscopy of Ad35f+HD5

CryoEM grids were prepared as described by Saban, et al. (89). The complex of Ad35f and HD5 defensin was prepared by incubating HD5 (Peptides International, Inc; Louisville, KY) at a concentration of 20 $\mu$ M with 200  $\mu$ g/mL concentration of Ad35f for 30 minutes at room temperature. 6  $\mu$ l samples of Ad35f-HD5 were applied to C-flat 2/4-4C carbon coated grids (Electron Microscopy Sciences) and vitrified using the Vitrobot cryo-fixation device (FEI Company) or in-house plunging device. Data collection was performed on an FEI Polara (300 kV; FEG) transmission cryoelectron microscope operated at liquid nitrogen temperature and 300 kV with a Gatan UltraScan 4kx4k charge-coupled device camera. A total of 3,000 micrographs were collected in 6 datasets using SAM, an in-house semiautomatic data collection routine (95). The absolute magnification for all datasets was ~398kX.

#### Image Processing of Ad35f+HD5

A total of 3000 particles were selected using the particle program VIRUS (1). The particles were binned to 320<sup>2</sup> pixels for the initial rounds of particle refinement, then, binned to 640<sup>2</sup> and later to 960<sup>2</sup> for image processing with a 1.63Å pixel size. The defocus and astigmatism parameters were determined using the program CTFFIND3 (74). All datasets were initially refined using the previously published structure of the Ad35f vector (89) filtered to 12Å resolution



as the starting model for the program FREALIGN (39). All datasets were refined using a modified code of FREALIGN to allow the input of externally determined particle center. A subset of 348 particles was included in the final structure with a resolution of 9.6Å at 0.5 FSC based on the Fourier Shell Correlation method. A pseudoatomic capsid was built using the Ad5 hexon (PDB ID: 1P30) (84) and the Ad2 penton base (PDB ID: 1X9T) (124) coordinates. Docking of the hexon and penton base coordinates was also used to refine the pixel size of the cryoEM structure. Optimal docked positions for hexon and penton base were found with the “Fit Model in Map” routine of UCSF Chimera (82). Two difference density maps were calculated for data analysis. The first difference density map calculation was done by subtracting the Ad35f cryoEM structure filtered to 9.6Å from the Ad35f+HD5 cryoEM structure. The second difference map was calculated by subtracting facet of 18 hexons and 3 pentons from the 11.8 Å Ad35f+HD5 structure. A B factor of  $-300\text{Å}^2$  was applied to both the Ad35f-HD5 and Ad35f structures using the B-Factor software (38). All graphics figures were generated with UCSF Chimera (82). The FSC plot was generated with the MatLab software.

## CHAPTER III

### **AIM 1: CRYOELECTRON MICROSCOPY STRUCTURE OF THE ADENOVIRUS TYPE 2 TEMPERATURE-SENSITIVE MUTANT 1 REVEALS INSIGHT INTO THE CELL ENTRY DEFECT**

#### **Introduction**

##### Adenovirus structure and organization: viral components and their locations

CryoEM studies of Ad combined with atomic resolution structures of component proteins (hexon, penton base, fiber and protease) have led to a detailed structural model for the mature Ad virion (80). While the Ad protein capsid is icosahedral, the core does not follow the overall symmetry of the particle, and thus the core is not well represented in cryoEM structures (98). The core is composed of the 36kb dsDNA genome complexed with four viral proteins (V, VII, mu, and terminal protein (TP)) and the virally encoded cysteine protease. The core of the mature virion may also contain a few copies of the L1-52K protein (18), a possible scaffolding protein that is present in higher copy numbers in assembling virions (48). The capsid contains the major capsid proteins, hexon, penton base and fiber, together with four minor capsid proteins (IIIa, VI, VIII, and IX). CryoEM difference mapping analyses have led to revised assignments for the locations of the minor capsid proteins with protein IX on the exterior and the other three proteins on the inner capsid surface (29, 89). A scanning transmission electron microscopy (STEM) study indicated that four trimers of protein IX stabilize the group-of-nine hexons in the center of each facet (33). However more recent cryoEM studies indicated that only the N-terminal domain

of protein IX forms these trimeric assemblies (88, 89), while the C-terminal domain, which has a long predicted  $\alpha$ -helix with strong propensity for coiled coil formation, associates in helical bundles at the facet edges (89). Two cryoEM studies support the assignment of the tetrameric helical bundle on the capsid exterior to the C-terminal domain of protein IX (30, 67). Curiously twelve monomers of protein IX per facet assemble into four trimers with their N-terminal domains and three tetramers with their C-terminal domains.

The internal location for protein IIIa below the penton base and surrounding peripentonal hexons was confirmed by a study of virions with N-terminally tagged protein IIIa (91). Although the locations for proteins VI and VIII have not been experimentally confirmed, these proteins are more than likely on the internal side of the capsid as there is no remaining unassigned cryoEM density on the exterior of the capsid. In addition, proteins VI and VIII are two of the viral proteins that are produced in precursor form and cleaved by the viral protease during maturation of the assembled virion (65). The protease is presumed to be packaged within the interior of the virion, and therefore the assignment of proteins VI and VIII to the interior of the capsid where they would be accessible to the protease is logical. Density within the internal cavity of all 240 hexon trimers in the Ad capsid has been assigned to protein VI on the basis of biochemical and temperature-sensitive studies (89, 119).

Ad cell entry begins with attachment of the Ad fiber to either CAR (7) or CD46 (34), which serve as the primary attachment receptors for Ad on most cell types (80). Internalization via clathrin-mediated endocytosis is triggered by

association of the Ad penton base with  $\alpha$  v integrins (117). Escape from the endosome is facilitated by the membrane lytic activity of protein VI, which is released from the virion in the low pH environment of the early endosome (118). The stepwise dismantling of the Ad virion during cell entry has been described biochemically but has not been fully characterized structurally (37). After endosomal escape, the partially uncoated Ad virion is transported along microtubules (100) to the nucleus where the viral genome is inserted into the nucleus via a nuclear pore complex.

#### Adenovirus type 2 temperature-sensitive mutant and its role in elucidating Ad cell entry

Propagation of an Ad2 temperature-sensitive mutant (Ad2*ts*1) at non-permissive temperatures (>39°C) results in the synthesis of virions that have an uncoating defect (68, 75, 77, 111). Although these Ad2*ts*1 particles are capable of interacting with CAR and undergoing internalization via association with  $\alpha$  v integrins, they are unable to escape the early endosome and thus are targeted for degradation in lysosomes (35, 37). The Ad2*ts*1 genetic defect is a point mutation (P137L) in the protease that is linked to a defect in packaging into the virion (83). In wild-type Ad virions, the protease is activated inside nascent virions by the viral DNA as well as an 11 amino acid peptide from the C-terminal end of protein VI (65). The Ad protease mediates the maturational cleavage of six structural proteins: IIIa, VI, VII, VIII, mu, and TP, as well as the presumed scaffolding protein L1-52K (22, 66, 114). In Ad2*ts*1 particles these cleavages do not occur. The presence of the precursor forms of these proteins in Ad2*ts*1 is associated with greater capsid stability (10, 118). Here we present a cryoEM

structural study of the Ad2*ts1* particles that provides insight into the cell entry defect of this temperature-sensitive mutant. Comparison of the Ad2*ts1* structure with that of a mature Ad virion indicates that the major differences are in the interior of the virion. Difference density analysis shows that precursor proteins IIIa and VI connect the inner capsid to the core, preventing the release of the membrane lytic protein VI. Retention of preVI in the capsid results in Ad degradation in lysosomes.

## Results

### CryoEM structure reveals differences in the Ad2*ts1* core compared to the mature Ad core

A 10.5Å resolution cryoEM structure of the immature Ad2*ts1* virion was calculated from 890 particle images selected from a total set of 5,544. Only a relatively low percentage (16%) of the Ad2*ts1* particle images was included in the final, highest resolution reconstruction. Additional reconstructions were calculated including 50-76% of the data, however these had lower resolutions. This suggests either structural heterogeneity between the Ad2*ts1* particles or variable signal-to-noise ratios in the cryoelectron micrographs. A comparison of selected particle images included in the 16% map vs. those rejected from the 16% map but included in the 76% map indicates that there is variation in the signal-to-noise ratio. On average the 76% map includes noisier particle images than are included in the highest resolution, 16% map. We suspect that the long (~360Å) and flexible Ad2 fiber present on the Ad2*ts1* virions may lead to varying

thicknesses of vitreous ice on the cryoEM grids. This would in turn lead to variation in the signal-to-noise ratios in the micrographs. The highest resolution Ad2ts1 cryoEM structure has an estimated resolution of 10.5Å at the Fourier shell correlation (FSC) 0.5 threshold (**Figure 3.1**) (85). A cryoEM structure of the mature Ad35f virion at 6.9Å resolution (FSC 0.5) is shown for comparison (89). The Ad35f vector has an Ad5 capsid pseudotyped with an Ad35 fiber, which is relatively short (~130Å). Except for the different fibers, the Ad35f cryoEM structure serves as a reasonable comparison structure for Ad2ts1. Excluding fiber, the Ad2 and Ad5 structural proteins have identities of 86 to 100%. Therefore the major differences between Ad2ts1 and Ad35f are the fibers (Ad2 vs. Ad35), the variable hexon surface loops, and the presence of preproteins in Ad2ts1.

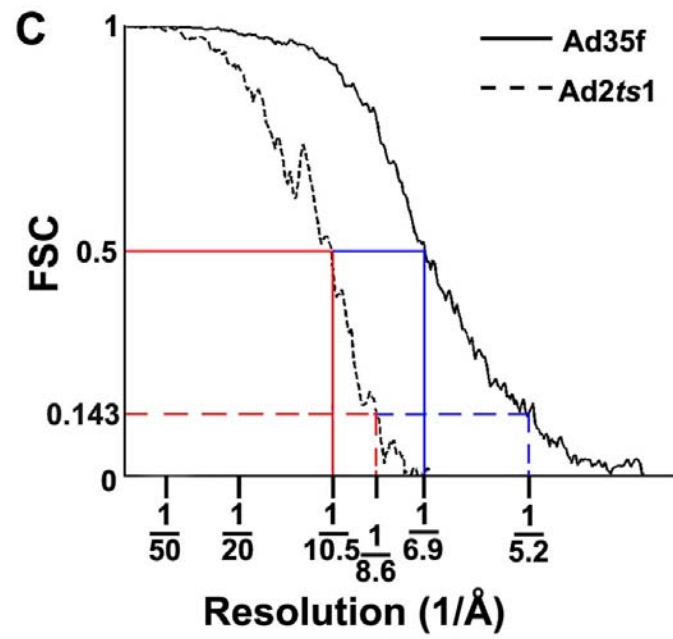
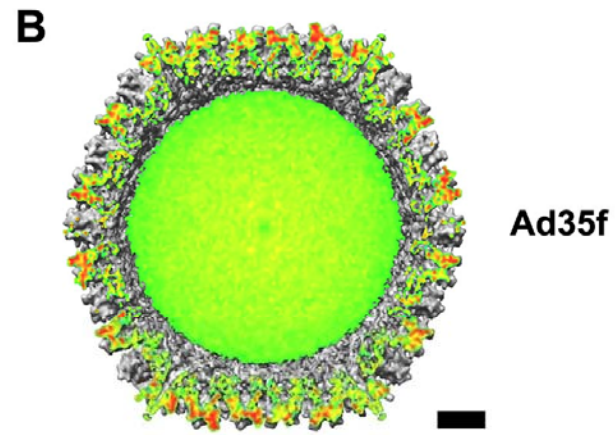
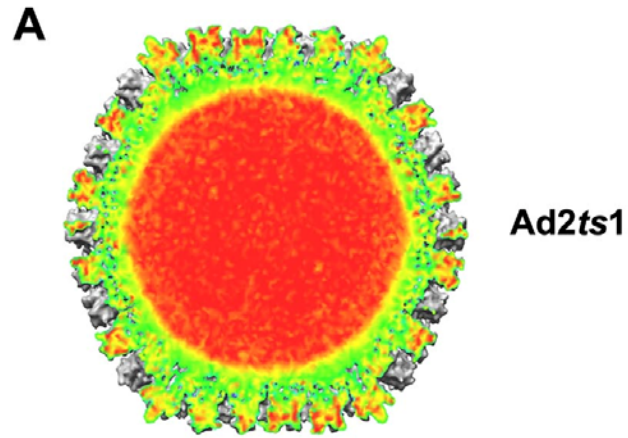


**Figure 3.1.** CryoEM structures of Ad2ts1 and Ad35f reveal a major structural difference in the core of the virion. (A) Cropped view of the Ad2ts1 reconstruction. The crop plane is colored by the density value, with the strongest density in red and the weakest in green. The protein/DNA containing core displays predominantly strong density (red). (B) Cropped view of the Ad35f reconstruction (89) with the crop plane colored as in (A). Both structures are shown filtered to 10.5Å resolution. Scale bar, 100Å. (C) An FSC plot indicating a resolution range for Ad2ts1 of 10.5Å to 8.6Å (10.5Å at FSC 0.5; 9.5Å at FSC 0.3; and 8.6Å at FSC 0.143). The resolution range for Ad35f is 6.9Å to 5.2Å (6.9Å at FSC 0.5; 6.1Å at FSC 0.3; and 5.2Å at FSC 0.143).



When both the Ad2ts1 and Ad35f cryoEM structures are filtered to the same resolution (10.5Å), their outer icosahedral capsid structures appear essentially indistinguishable, but the core regions differ considerably (**Figures 3.1 and 3.2**). When the structures are colored by their reconstructed density values, as in **Figure 3.1**, the Ad35f core (green to yellow) appears weaker than the surrounding capsid (green to red, with red representing the strongest reconstructed density values). In contrast, the Ad2ts1 core (red) appears stronger than its surrounding capsid (green to red). When the two structures are normalized to have the same mean and standard deviations, the average reconstructed density value in the Ad2ts1 core is 44% greater (more dense) than that in the Ad35f core. This effect is also evident in the average radial density profiles of the Ad2ts1 and Ad35f structures (**Figure 3.3**). When the two profiles are normalized on the icosahedral capsids, the core of the Ad2ts1 reconstruction is significantly denser. These findings indicate that either the immature core of Ad2ts1 is more ordered than the mature core of Ad35f or there is significantly more molecular mass within the Ad2ts1 core.

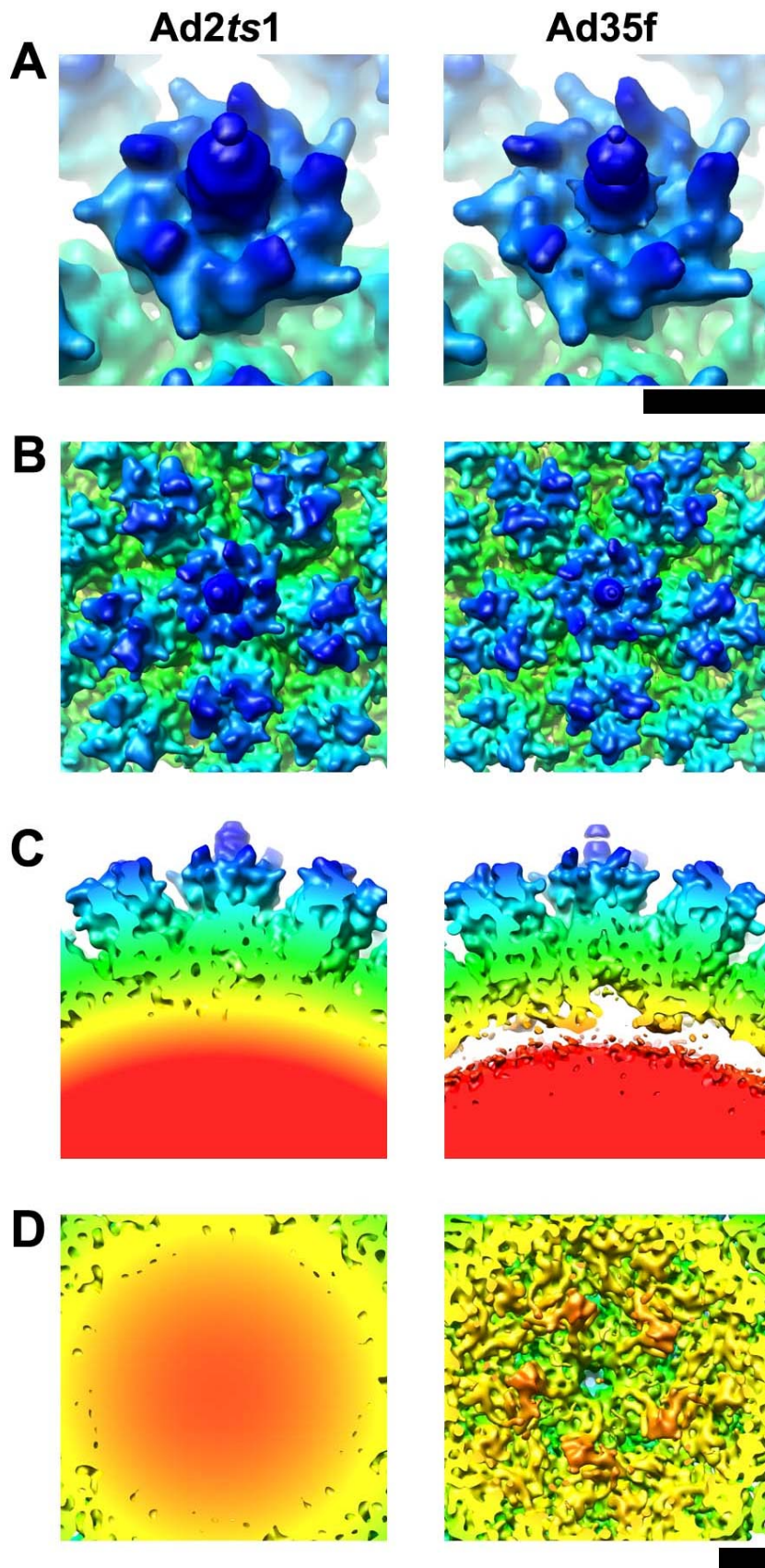


**Figure 3.2.** The main differences between Ad2*ts*1 and Ad35f are on the interior of the icosahedral capsid. (A) Views of the penton base with a segment of protruding fiber. The fiber shaft of both virions is flexible and thus only short portions are reconstructed. Both structures are shown filtered to 10.5Å resolution and radially color coded (300Å = red; 480Å = blue). (B) Outer views of the vertex regions showing a penton base with five surrounding hexons. (C) Side views of the two vertex regions at similar isosurface contour levels. The Ad2*ts*1 capsid (yellow to blue) is closely associated with and connects to the core of the virion (red). In contrast, the Ad35f capsid is separated from the core by a gap in the density. (D) Inner views of the vertex regions showing the core density for Ad2*ts*1 and the resolved internal capsid density below the penton base and surrounding hexons for Ad35f. Scale bars, 50Å.

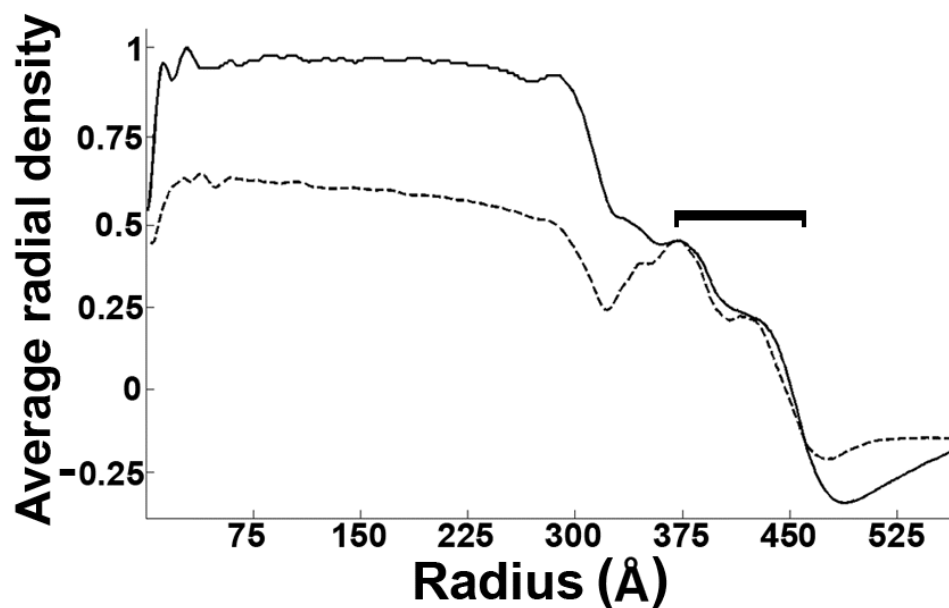


**Figure 3.3.** Average radial density distributions of the Ad2ts1 and Ad35f structures. Profiles for Ad2ts1 (solid line) and Ad35f (dashed line) were calculated with the IMAGIC-5 Threed-radial density-options routine. The two profiles were normalized in the radial shell (370-463Å) indicated by the bracket and corresponding to the outer portion of the icosahedral capsid.

The proteome of the mature Ad5 virion has been analyzed in detail by mass spectrometry (18, 58, 62). Numerous biochemical and PAGE analyses (43, 47, 76, 77) have indicated that the protein composition of Ad2*ts*1 is similar to that of the mature virion but with precursor forms of multiple viral proteins and a ~5-fold reduction in the encapsidation of protease. We estimated the total molecular mass of the Ad2*ts*1 and Ad35f cores by considering the copy numbers and molecular masses of the core components in both their immature forms (for Ad2*ts*1) and mature forms (for Ad35f). We also assumed that all of the small cleavage products generated by the Ad protease would be released from the virion. These calculations indicate a difference of 5 to 7% in total molecular mass between the Ad2*ts*1 and Ad5 cores depending on whether or not the inner capsid proteins (IIIa, VI, and VIII) are included in the calculation (**Table 2.2**). Although the mature core may have a slightly smaller total molecular mass than the immature core of Ad2*ts*1, our calculations indicate that the mass difference is not great enough to explain the significantly stronger reconstructed density of the Ad2*ts*1 core. The results of the molecular mass calculations for the Ad2*ts*1 and Ad35f cores are supported by an analysis of the cryoEM particle images of Ad2*ts*1 and Ad35f. Using a subset of particle images included in either the highest resolution Ad2*ts*1 reconstruction or the Ad35f reconstruction, we quantitated the average signal intensity from the core-plus-capsid within a radius of 300Å and the average intensity from the capsid-only within the radial shell of 300 to 463Å (**Figure 3.4**). The ratio of the core-plus-capsid average intensity to the capsid-only average intensity in the two-dimensional projection images is

essentially the same for Ad2*ts*1 and Ad35f, indicating that the Ad2*ts*1 core has approximately the same total molecular mass as the mature Ad core. Our working hypothesis for the observed core difference in the two structures is that the Ad2*ts*1 has an increased level of icosahedral order.

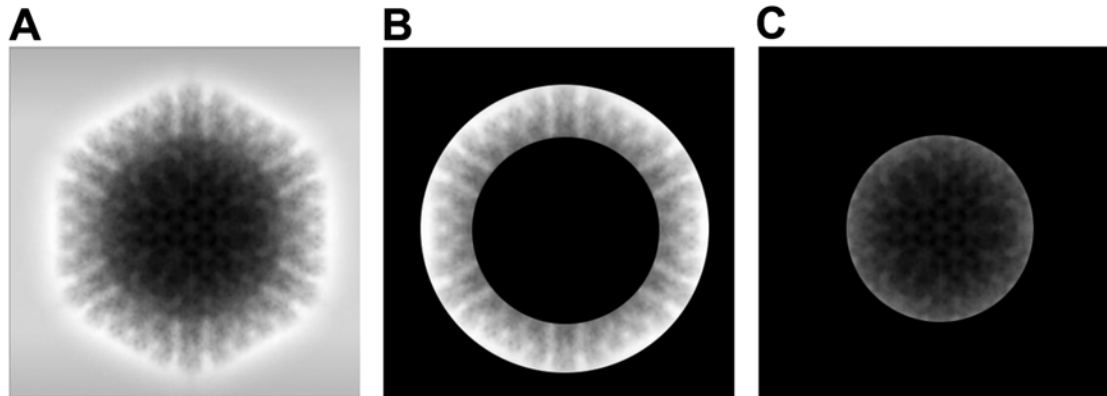


**Figure 3.4.** Masking of the capsid-only and core-plus-capsid regions of a particle image. (A) A projection of the Ad2ts1 reconstruction at 10.5Å resolution viewed along a 3-fold symmetry axis is shown to simulate a particle image. The signal-to-noise ratio of this projection image is significantly better than that of the cryoEM particle images. (B) The simulated Ad2ts1 particle image with inner and outer radial masks applied to isolate the capsid-only region. (C) The simulated Ad2ts1 particle image with a circular mask applied to isolate the core-plus-capsid region. Since the particle image represents a projection of the density within the whole particle, the central region of the particle image contains information from both the core and the capsid.

The cryoEM reconstruction also shows that the Ad2*ts1* core extends to and appears to connect with the capsid (**Figure 3.2 C**). CryoEM reconstructions of mature Ad virions, in contrast, show the core to be separated from the capsid with a prominent gap below the capsid inner surface. These observations indicate that the Ad core condenses, or undergoes a structural rearrangement, during the maturation process. This conclusion is supported by a study showing that Ad2*ts1* chromatin is more resistant to micrococcal nuclease digestion than mature Ad chromatin (76). Since the Ad2*ts1* core appears to be connected to the capsid, condensation of the genome may be inhibited. The immature core might possess a greater degree of icosahedral order by virtue of its association with the capsid, and this could lead to a denser core in the reconstruction even without a significant difference in total mass.

#### The Ad2*ts1* penton base is anchored to the viral core

One of the Ad2*ts1* reported phenotypes is its failure to release the fibers during cell entry (34), while wild-type Ad virions are thought to lose their fibers or vertices early in the cell entry pathway (37). This phenotype is somewhat difficult to explain because neither the penton base nor the fiber is cleaved by the viral protease, and thus Ad2*ts1* contains the same forms of these proteins as in Ad2. Comparison of the vertex regions of the Ad2*ts1* and Ad35f cryoEM structures reveals no obvious difference between the outer proteins of the virion that could explain this property (**Figure 3.2 A and B**). The crystal structure of the Ad2 penton base with the N-terminal region of fiber (124) can be fit equally well into the vertex regions of the Ad2*ts1* and Ad35f cryoEM structures. When the vertex



region is viewed from inside the virion, well-resolved density below the penton base of Ad35f is observed, while only the dense core of Ad2ts1 can be seen (**Figure 3.2 D**). The density below the penton base includes protein IIIa (89, 91), which presumably interacts with the N-terminal tails of penton base (aa 1-51) missing from the crystal structure. Preprotein IIIa is cleaved by the protease, with the C-terminal 15 residues removed for both Ad2 and Ad5. The sequence of preprotein IIIa from these two serotypes indicates that there are 3 Arg residues in the C-terminal peptide removed by the protease, disconnecting capsid and core. We speculate that these positively charged Arg residues may interact with the viral dsDNA genome. After protease cleavage of protein IIIa, the C-terminal Arg-rich peptide may remain associated with the core. The cryoEM structure of Ad2ts1 indicates that penton base is anchored to the viral core, presumably via the precursor form of protein IIIa.

#### Density inside the Ad2ts1 hexon cavities is assigned as preprotein VI

To more fully compare the structures of the minor capsid components in Ad2ts1 and Ad35f, we docked the atomic resolution structures of hexon (87) and penton base with the N-terminal fiber peptide (124) into the cryoEM density and generated difference maps for both virions. The Ad2ts1 difference map shows density on the external capsid surface corresponding to the fiber shaft, the RGD-containing loop of penton base, surface loops of hexon missing from the crystal structure, and protein IX (**Figure 3.5 A**). In addition, the difference map also reveals density inside the cavity of every hexon trimer in the shape of a “plug”, which connects to the viral core (**Figure 3.5 B and C**). Less prominent density

within the Ad35f hexons has also been assigned to protein VI on the basis of both biochemical and molecular genetic information (89, 119). Preprotein VI is cleaved by the protease, removing 33 aa from the N-terminus and 11 aa from the C-terminus for both Ad2 and Ad5. We tentatively assign the plug density found inside the cavity of every hexon in Ad2*ts1* as the precursor form of protein VI.

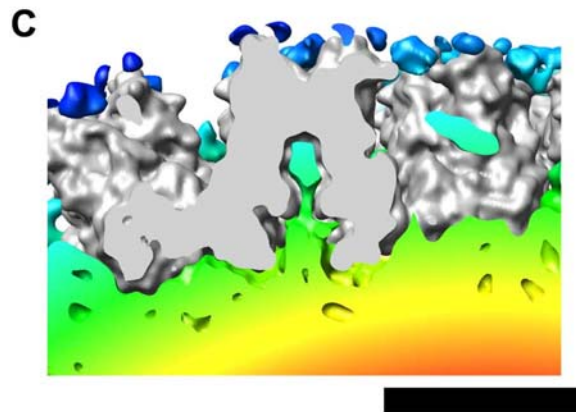
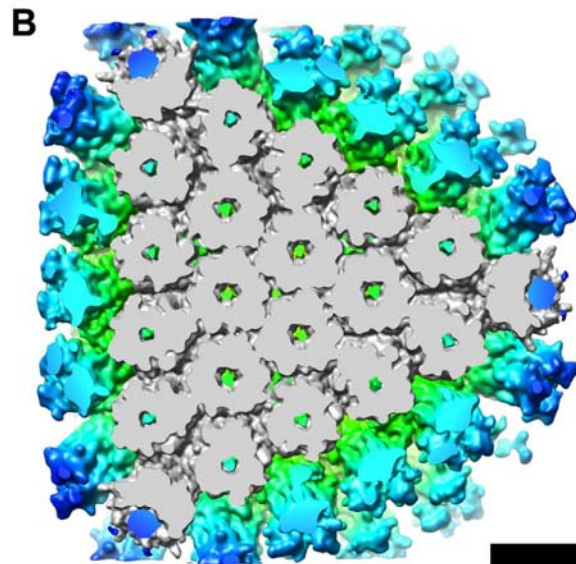
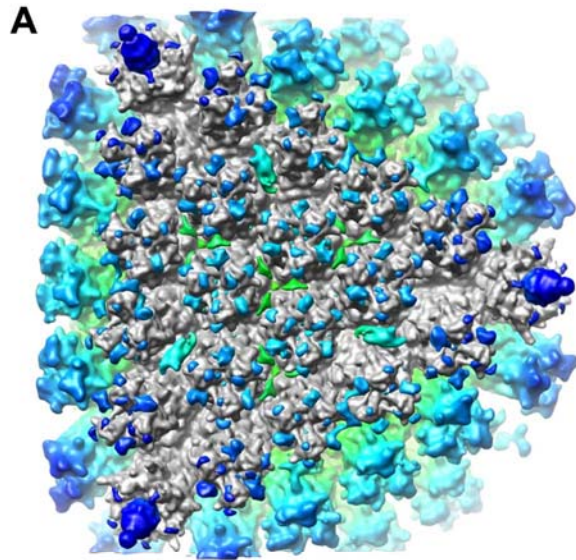


**Figure 3.5.** Preprotein VI is assigned to density within the cavity of every hexon trimer in Ad2ts1. (A) An enlarged facet (gray) consisting of docked crystal structures of 18 hexon trimers and 3 penton base pentamers is shown filtered to 10.5Å resolution. The facet is superimposed on the Ad2ts1 difference density, which is radially color coded as in **Figure 3.2**. The external difference density includes the protruding fiber shaft, surface loops of hexon and penton base missing from their respective crystal structures, and density assigned to protein IX. (B) Cropping away the top ~80Å of the facet reveals difference density inside of every hexon trimer (green). Similar density within the Ad35f hexons has been assigned to protein VI (89). The density within every hexon of Ad2ts1 is tentatively assigned as preprotein VI. (C) Side cropped view of a peripentonal hexon within the facet (gray) with the internal difference density in the shape of a “plug”, which connects to the Ad2ts1 core (yellow to red). Scale bars, 100Å.

### Assignments for preproteins IIIa and VIII on the inner capsid

On the exterior capsid surface the Ad2ts1 difference map reveals density assigned to the N- and C-terminal domains of protein IX (**Figure 3.5 A**). The dense core of Ad2ts1 complicates the analysis of the internal capsid proteins; however, strong density is observed at the locations assigned to mature proteins IIIa and VIII in Ad35f (**Figure 3.6 B**). While the mature forms of proteins IIIa and VIII are separated from the core in Ad35f, the precursor forms in Ad2ts1 appear to be anchored to the core. Both preproteins IIIa and VIII are cleaved by the protease, which could lead to their separation from the core. Mass spectrometry experiments indicate that the Ad5 preprotein VIII is cleaved at two sites with resulting fragment 1 (12.1 kDa) and fragment 3 (7.6 kDa) retained in the mature virion (58). It is not clear whether fragment 2 of protein VIII is retained or released. The resolution of the Ad35f cryoEM structure, 6.9Å, is high enough to reveal  $\alpha$ -helices within protein IIIa and the density assigned to protein VIII (89). The observation of one relatively long (~35Å)  $\alpha$ -helix in the protein VIII density (**Figure 3.6 C**) is consistent with the secondary structure prediction of a ~22 aa  $\alpha$ -helix in fragment 1 (**Figure 3.7**). The more moderate resolution of the Ad2ts1 cryoEM structure, 10.5Å, does not show clearly resolved  $\alpha$ -helices. Nevertheless, Ad2ts1 does contain a density rod at the same site, suggesting that the N-terminal region of preprotein VIII (aa1-111) is associated with the capsid.

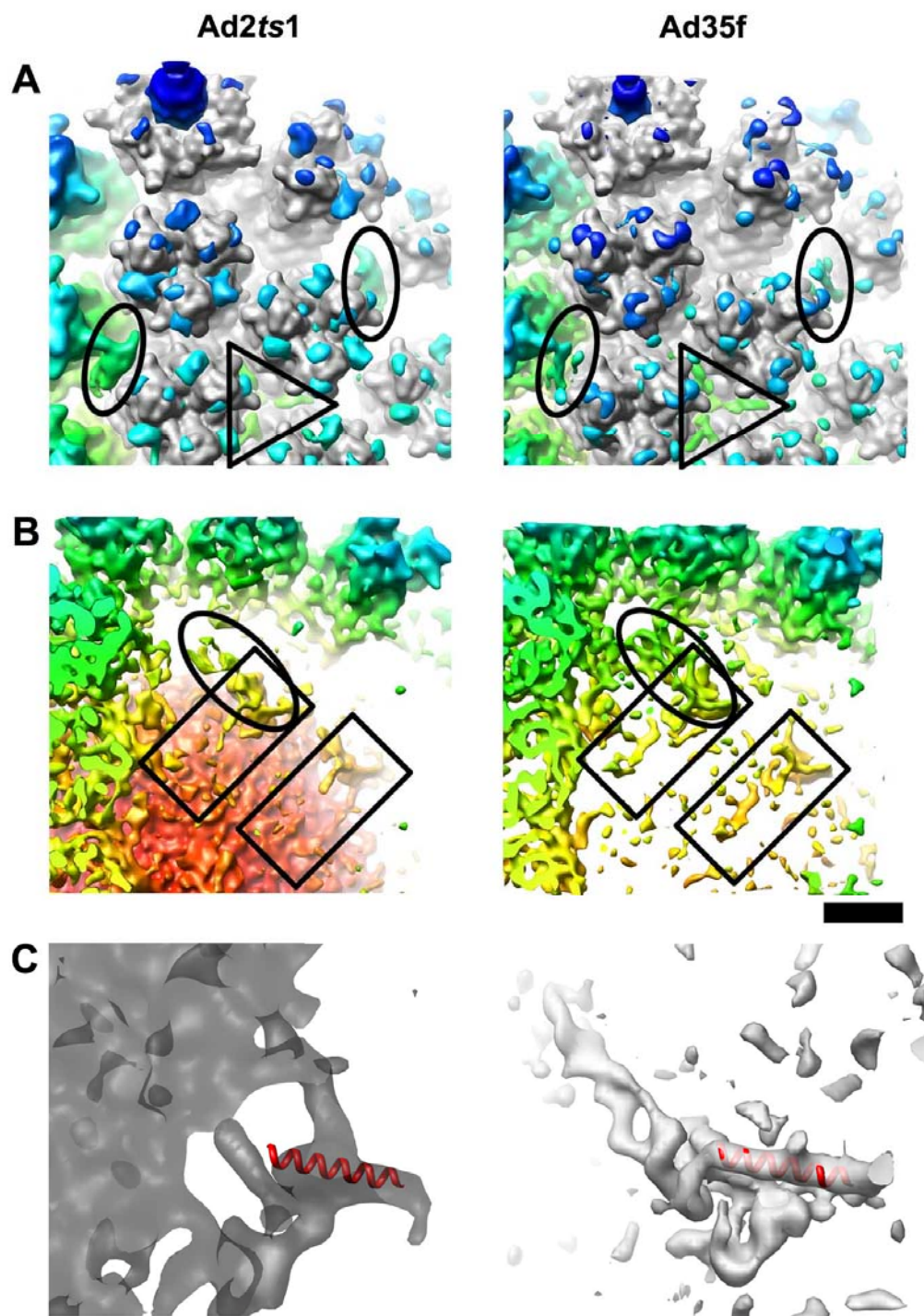


**Figure 3.6.** Density assigned to protein IX and preproteins IIIa and VIII are found within Ad2ts1. (A) The Ad2ts1 difference map (filtered to 10.5Å) and the Ad35f difference map (filtered to 10.5Å resolution) are shown superimposed on a portion of the facet (gray). The density assigned to the N-terminal domain of protein IX is outlined with triangles, and that assigned to the C-terminal domain of protein IX is within ovals (89). (B) Cropping away the top ~100Å reveals internal difference density below the penton base and hexons assigned to preproteins IIIa (oval) and VIII (rectangle) in Ad2ts1, and the mature forms of proteins IIIa and VIII in Ad35f. (C) Rotating by 180° and enlarging one copy of preprotein VIII (left, transparent) or mature protein VIII (right, transparent), shows the density assigned to the predicted 22aa  $\alpha$ -helix (red) in fragment 1 of protein VIII. In panel C the Ad35f density is shown filtered to 6.9Å so that  $\alpha$ -helical rod is well resolved. The internal Ad2ts1 difference density in panels B and C is shown with a relatively high isosurface contour level ( $0.65\sigma$  versus  $0.37\sigma$  in panel A) so that the density assigned to precursor proteins can be resolved from the core. The Ad35f difference density is shown with an isosurface contour level of  $0.85\sigma$  to reveal the  $\alpha$ -helical nature of the C-terminal domain of protein IX, as well as proteins IIIa and VIII. In panels A and B the Ad2ts1 and Ad35f difference density maps are shown radially color coded as in **Figure 3.2**. Scale bar, 50 Å.

## Protein VIII, secondary structure prediction

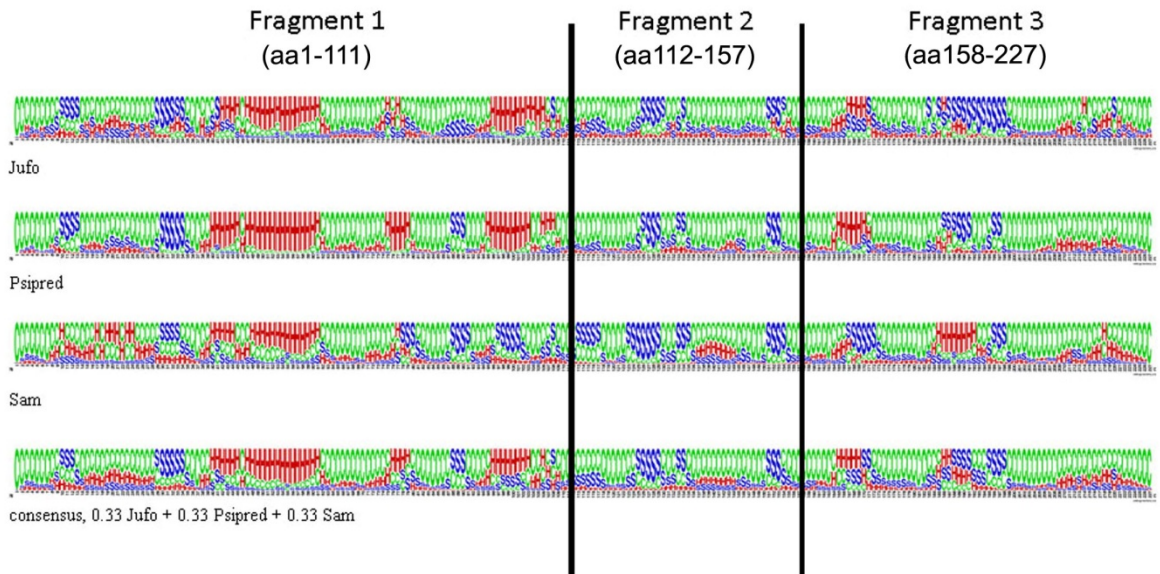


**Figure 3.7.** The secondary structure prediction algorithms Jufo (72, 73), Psipred (51), and Sam (13, 53) were used to obtain predictions for Ad5 protein VIII. To increase confidence in the secondary structure prediction, a three-state consensus prediction of the three methods was created by averaging the individual predictions (96). Alpha-helical regions are indicated by red “H” symbols,  $\beta$ -strand regions by blue “S” symbols, and random coil regions by green “C” symbols. The two Ad protease cleavage sites are indicated by vertical bars. The consensus sequence indicates an  $\alpha$ -helix of ~22 residues in fragment 1, or two closely spaced  $\alpha$ -helices of 6 and 15 residues with a gap of 1 residue.



### Hexon shields protein VI and preprotein VI membrane lytic activity

Protein VI has long been referred to as a hexon-associated protein (28, 70). More recently, protein VI has been identified as a membrane lytic factor of Ad (118). Both recombinant protein VI and its precursor form possess membrane lytic activity in liposome disruption assays. Here we present data showing that purified hexon inhibits the membrane lytic activity of both protein VI and preprotein VI (**Figure 3.8**). Inhibition was saturable with a maximal reduction in membrane lytic activity of ~60%. These results indicate that the membrane lytic domains of protein VI and preprotein VI are equivalently shielded by hexon.

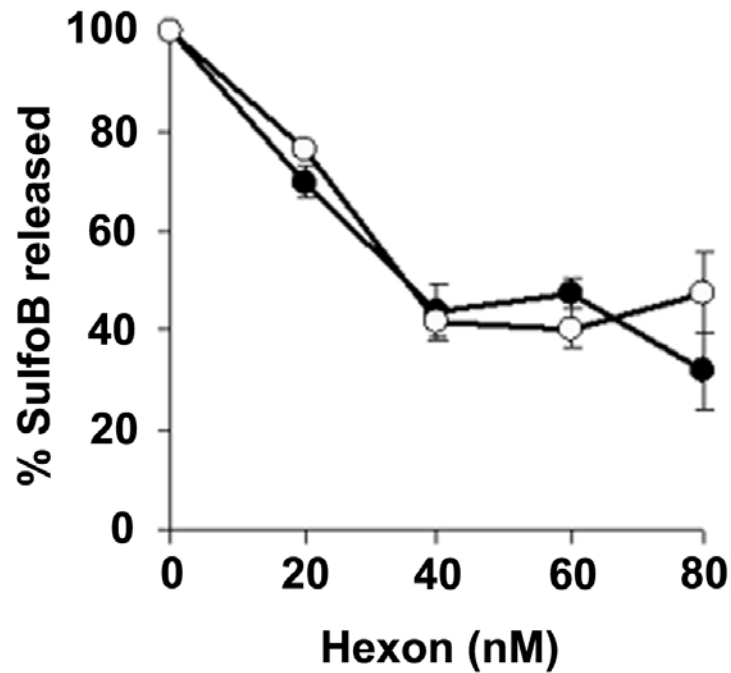


**Figure 3.8.** Hexon binding blocks protein VI and preprotein VI membrane lytic activity. Recombinant protein VI or preprotein VI was incubated with increasing amounts of purified hexon for 30 minutes before addition to SulfoB-containing liposomes at 37°C. The percentage of SulfoB released was measured 15 min after protein addition to liposomes. Protein VI (black circles) or preprotein VI (white circles) was present at a final concentration of 20 nM. The plateau at ~40% of SulfoB released suggests that hexon does not completely block the membrane lytic activity of protein VI or preprotein VI.

## Discussion

### The Ad core condenses and becomes less symmetrically ordered during maturation

The Ad2*ts1* cryoEM structure indicates that the core of this mutant virus is connected to the icosahedral capsid and that the core may have partial icosahedral order. As the wild-type Ad core undergoes maturation, which involves the proteolytic cleavage of precursors of seven core and inner-capsid proteins, the core condenses and separates from the icosahedral outer capsid leading to a less icosahedrally arranged structure for the DNA/protein viral core. The moderate resolution ( $\sim 10\text{\AA}$ ) of the Ad2*ts1* cryoEM structure does not allow us to visualize precisely which precursor proteins are mediating the capsid/core association in Ad2*ts1*. However, two studies have found that capsid protein VI interacts with the core protein V (16, 68). Therefore, we think that preprotein VI, which is present in  $\sim 369$  copies per virion (58), binds to both hexon in the capsid and protein V in the core and contributes to the observed capsid/core connection in Ad2*ts1*. This conclusion is in agreement with observations by Mirza and Weber that preprotein VI is associated with Ad2*ts1* cores isolated by pyridine treatment, but protein VI is not associated with mature cores (76, 77). Preprotein IIIa, which is present in 60 copies per virion and which is underneath the vertices, is also likely to contribute to the observed Ad2*ts1* capsid/core connection. The protein IIIa precursor may be anchored to the Ad2*ts1* core by its arginine-rich C-terminal peptide region. The protease removes the arginine-rich region, and thus the mature protein IIIa may be more closely associated with the capsid than the core.

### Vertex release may require a conformational change that is blocked in Ad2ts1

A conformational change in the vertex region has been proposed after the interaction of Ad with integrins on the cell surface (36). Alternatively, conformational changes in the vertex proteins may be triggered by the low pH environment of the endosome. These conformational changes are thought to lead to release of the vertex proteins, including penton base, fiber, protein IIIa, and the membrane lytic protein VI (118). Comparison of the Ad2ts1 cryoEM structure with that of Ad35f, which contains the mature Ad5 structural proteins with an Ad35 fiber, indicates no obvious differences on the outer surface of the icosahedral capsid. However, differences are found on the inner surface of the capsid below the penton base. Docking of the crystal structure into the cryoEM structures shows that the N-terminal 51 aa tails of penton base, which are missing from the crystal structure, are oriented toward the viral core (29, 88, 89). We have previously postulated that the N-terminal tails of penton base interact with protein IIIa in the mature Ad virion (89). This interaction also likely occurs in Ad2ts1 with preprotein IIIa. Anchoring of the penton base to the Ad2ts1 core via the preprotein IIIa may block the proposed conformational change in the vertex region (**Figure 3.9**). Additionally, anchoring of the hexons to the immature core by preprotein VI may also contribute to the higher stability of Ad2ts1. The stability of Ad2ts1 can be partially overcome by high temperature. *In vitro* uncoating assays with Ad2ts1 indicate that ~50% of penton base, fiber, and protein IIIa is released at neutral pH and 50°C, while ~100% of preprotein VI is retained in the virion (118). In contrast, wild-type Ad5 virions exposed to the same pH release

the vertex proteins (penton base, fiber, and protein IIIa) together with protein VI and at a lower temperature ~45°C. Another study comparing the uncoating of Ad2ts1 and Ad5 found that for Ad5 at neutral pH, protein VI and fiber both dissociated at 49°C. For Ad2ts1 fiber dissociation occurred at 49°C, but preprotein VI dissociation was only observed above 67°C (10). This uncoating information together with the Ad2ts1 structure indicates that vertex release is inhibited in Ad2ts1 and that even if this inhibition is overcome with high temperature (50 to 67°C), preprotein VI remains firmly anchored to the immature core.

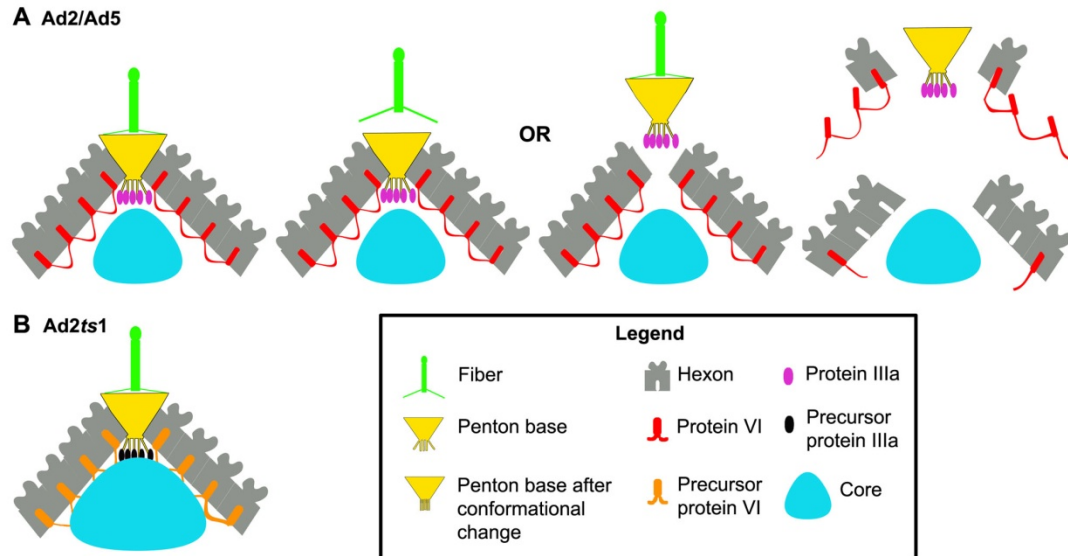


**Figure 3.9.** Diagram of proposed cell entry events for Ad2 and Ad5 vs. Ad2ts1. (A) One vertex of an Ad2 or Ad5 virion is shown schematically (left). The location of protein IIIa (magenta ovals) underneath the penton base is as assigned by a cryoEM study (89) and confirmed by a peptide tagging study (91). The position of protein VI (red) within the cavity of every hexon trimer is as assigned by cryoEM (89). We propose that a critical step of disassembly is either release of the fiber or release of the fiber/penton base complex (middle). Vertex release is associated with release of 25% of the hexons and 80% of protein VI (right), as shown by Wiethoff *et al.* (118) for Ad5 at temperatures over 45°C. (B) One vertex of an Ad2ts1 virion is shown schematically, with preprotein IIIa (black ovals) and preprotein VI (orange) anchored to the immature DNA/protein core (cyan). The association of preprotein IIIa with both the N-terminal tails of penton base and the viral core may impede the release of the vertex proteins (fiber, penton base and preprotein IIIa). In addition, anchoring of preprotein VI to the core may block its release.

It has been shown previously that both protein VI and preprotein VI have membrane lytic activity (118). We present data indicating that hexon can shield the membrane lytic activity of both the mature and preprotein forms of protein VI equally well. Thermal disassembly studies indicate that mature wild-type Ad virions release ~80% of penton base with ~25% of the hexons in the Ad capsid, and a large percentage (~80%) of protein VI (118) following heating at 43°C and higher temperatures. If the cryoEM density assignment for protein VI is correct and protein VI is associated with all of the hexons in the capsid, then homotypic interactions between protein VI monomers would explain the simultaneous release of a high percentage of this protein (**Figure 3.9 A**) (89). Uncoating assays indicate the preprotein VI is not released from Ad2ts1 even at 60°C (pH 7.4). The cryoEM structure indicates that preprotein VI is associated with both the capsid hexons and the immature core (**Figure 3.5 B**) and presumably the interaction with the core is stronger. Since preprotein VI is not released, Ad2ts1 cannot escape from the endosome in a timely manner and is targeted to lysosomes for degradation (36).

In conclusion, the cryoEM structure of Ad2ts1 reveals a virion in which the core protein/DNA has not condensed and separated from the capsid as in mature Ad. The interaction between the capsid and core is presumably mediated by one or more of the precursor proteins, with IIIa and VI being likely candidates. Preprotein IIIa has an arginine rich C-terminal peptide tail, which is cleaved by the protease and which may associate with the dsDNA viral genome. Protein VI associates with core protein V (16, 68), and preprotein VI is retained in pyridine

cores (77), making it a second likely candidate. The cryoEM observation that the Ad2*ts1* capsid and core are associated is consistent with functional studies showing that Ad2*ts1* is more stable than wild-type mature virions (43, 118).

The finding that Ad2*ts1* fails to release its vertex proteins (36), combined with the cryoEM observation of no obvious differences between the external surface of Ad2*ts1* and a mature Ad virion, indicates that the capsid/core connection plays a role in the disassembly defect of Ad2*ts1*. Our structural analyses suggest that vertex release and disassembly are impeded in Ad2*ts1* by linkage of the penton base to preprotein IIIa and the immature core.



## CHAPTER IV

### **AIM 2: CRYOEM STRUCTURE OF AN ADENOVIRUS-HUMAN $\alpha$ -DEFENSIN COMPLEX: INSIGHT INTO BINDING SITES CRITICAL FOR NEUTRALIZATION**

#### **Introduction**

##### Defensins

Defensins are small cationic peptides that present one of the first lines of protection against pathogens. They are expressed in a variety of cells and are active against a wide range of microbes, including Gram-positive and -negative bacteria, enveloped viruses such as HIV and human influenza A virus and non-enveloped viruses such as adenovirus and human papillomavirus.

Human defensins are classified into two groups, alpha and beta defensins, according to their pattern of disulfide bonds. Both alpha and beta defensins are short polypeptides (18 to 45 residues), cationic and have three intramolecular disulfide bonds with different disulfide pairings. Human alpha defensins are expressed in a variety of cells including neutrophils, Paneth cells, and epithelial cells of the small intestine and airways. Beta defensins are mostly expressed in epithelial cells. Both types of defensins are constitutively active, but can be upregulated upon exposure to a pathogen.

### Modes of defensin neutralization

Defensins act in a variety of ways to neutralize infections caused by bacteria, fungi, and enveloped and non-enveloped viruses. Human  $\beta$ -defensin hBD-2 neutralizes *E. coli* by preventing bacterial adhesion. Bacterial flagellin appears to be involved in the induction of hBD-2 synthesis and neutralizes not only *E. coli*, but also *Salmonella*, among other pathogens (78, 92, 93, 102). Isolated *E. coli* flagellin induces hBD-2 mRNA expression in Caco-2 cells (92). Flagellin, the structural protein of the bacterial flagellum, participates in bacterial adhesion and stimulates production of interleukin-8 and nitric oxide in addition to hBD-2.

For HIV, human  $\beta$ -defensins interfere with infection in various stages of the lifecycle. Defensins hBD-2 and hBD-3, which are expressed in the mouth, appear to interfere with HIV reverse transcription, as no cDNA provirus can be detected when these defensins are expressed. hBD-2 and hBD-3 might also interact with receptors necessary for HIV cell uptake (such as CXCR4), and thus prevent internalization of the virus. Human  $\alpha$ -defensins also interfere with HIV infection (14, 19, 32, 56, 115, 121).

In addition to preventing adhesion and/or internalization of pathogens, defensins and related peptides are known to disrupt intracellular signaling of the pathogen or to form pores to puncture the membrane of a pathogen (14, 19, 24, 25, 41, 42, 46, 59, 71, 79, 90). For adenovirus, which lacks a lipid envelope, the

mechanism of defensin neutralization is likely to differ from that used to neutralize other pathogens.

#### Elucidating defensin mode of action against adenovirus

The Nemerow group has shown that human  $\alpha$ -defensins HNP1 and HD5 neutralize Ad5 infection by direct association with the capsid (10). Species A, B and C Ads appear to be neutralized by HD5 but not species D Ads (JG Smith and GR Nemerow, **Figure 4.10**, unpublished results). Using Ad5 vectors expressing enhanced green fluorescent protein (eGFP), Smith and Nemerow established that HNP1 inhibits Ad5 infection up to 20-fold with an  $IC_{50}$  between 5 and 6  $\mu$ M. HD5 is more potent and has an  $IC_{50}$  of 3-4  $\mu$ M. It also completely blocks Ad5 infection at high concentration (>5  $\mu$ M), unlike HNP1. They also found that HD5 inhibits an early step in Ad cell entry, but does not interfere with virus attachment and internalization. Ad5, in the presence of neutralizing levels of HD5, is efficiently internalized but does not escape the endosome and is targeted for degradation.

Smith and Nemerow showed that disassembly of the vertex region and release of the membrane lytic protein VI is inhibited by two human  $\alpha$ -defensins (10). Release of protein VI is necessary in order for Ad to escape from the endosome. The Ad/defensin complex is similar to the temperature-sensitive Ad2 mutant, Ad2*ts1*, in that it cannot release protein VI in the endosome and thus is targeted for degradation in the lysosome. When neutralizing concentrations of HD5 are added to Ad at 4°C and in the absence of cells, nearly complete

inhibition of viral infection is observed when the Ad/HD5 mixture is warmed to 37°C and introduced to A549 cells. When HD5 is added after Ad is warmed to 37°C and introduced to A549 cells, partial inhibition is observed. These results point to an inhibition of Ad infection at an early step of the Ad lifecycle as HD5 exhibits a time-dependent inhibitory effect. Normally Ad2 reaches the nuclear pore complex within 45min of binding to the cell surface.

In another experiment designed to test viral disruption of the endosomal membrane, ribotoxin  $\alpha$ -sarcin was mixed with Ad in the presence or absence of HD5 and HNP1. The toxin alone cannot enter cells. After metabolic labeling with  $^{35}\text{S}$ -Met, cell samples were tested for incorporation of  $^{35}\text{S}$ -Met into newly synthesized proteins. When the experiment is performed with wild-type Ad without defensin, the toxin gets into cells and  $^{35}\text{S}$ -Met incorporation is reduced by 90% with 50 ng virus/ml corresponding to 4000 particles/cell. With the *Ad2ts1* mutant, 100 ng virus/ml causes only a 25% reduction in  $^{35}\text{S}$ -Met incorporation. Ad in the presence of HD5 or HNP1 behaves similarly to *Ad2ts1*. These results indicate that Ad complexed with either HD5 or HNP1 is impeded in its ability to disrupt the endosomal membrane.

Incubation of Ad5 at temperatures between 43°C to 73°C causes the loss of both fiber and protein VI. When *Ad2ts1* produced at non-permissive temperature is incubated at the same temperatures, the fiber is lost in a similar manner as Ad5, but protein VI is retained and only released at higher temperatures. When Ad5 is incubated with 5 $\mu\text{M}$  HD5, the fiber is partially stabilized with the capsid and protein VI is retained as in *Ad2ts1* (10).

The precise mechanism of how human  $\alpha$ -defensins might stabilize Ad virions and block infection remained elusive after the biochemical studies of the Nemerow group, prompting us to determine a cryoEM structure of Ad in complex with HD5 in an attempt to shed light on the mechanism of neutralization.

## Results

### Stoichiometry of the Ad35f/HD5 interaction

Before we began the cryoEM study, the Nemerow laboratory estimated the stoichiometry of HD5 binding to Ad5. We wanted to confirm that HD5 bound with a high enough copy number to be observed by cryoEM at  $\sim 10\text{\AA}$  resolution. The initial stoichiometry experiments involved mixing Ad with HD5 labeled with Alexa Fluor 488, but unfortunately labeled HD5 was found to aggregate. Therefore, the final stoichiometry experiment was performed with unlabeled HD5. High-resolution Tricine gels, combined with a very sensitive protein stain (Deep Purple) and a sensitive imaging system (GE Healthcare Typhoon) were used to determine the stoichiometry of the complex (JG Smith and GR Nemerow, personal communication). HD5 was bound to Ad on ice, followed by removal of unbound HD5 with a histodenz density gradient. The sample was then reduced and boiled prior to separation of the proteins by SDS-PAGE and quantification of bound HD5 by comparison with the major structural proteins of Ad (hexon and penton base).

Saturation was achieved at approximately  $10\ \mu\text{M}$ , or  $\sim 1,000$  HD5 molecules per Ad virion as indicated by the highest plateau in **Figure 4.1**. A

lower plateau was also observed in the 6-8  $\mu\text{M}$  range, which corresponds to  $\sim 500$  HD5 molecules per Ad virion. These plateaus may indicate the presence of both high affinity and low affinity binding sites. Because of the difficulties associated with determining stoichiometry by gel quantification, these results are probably accurate to within a factor of two (GR Nemerow, personal communication). Therefore, a concentration of HD5 of 20  $\mu\text{M}$  was used to form the complex with Ad for the cryoEM study. This HD5 concentration is within the highest plateau in the stoichiometry plot (**Figure 4.1**), and is above the concentration found in an independent experiment for complete neutralization of Ad5 (5  $\mu\text{M}$ ) (10).

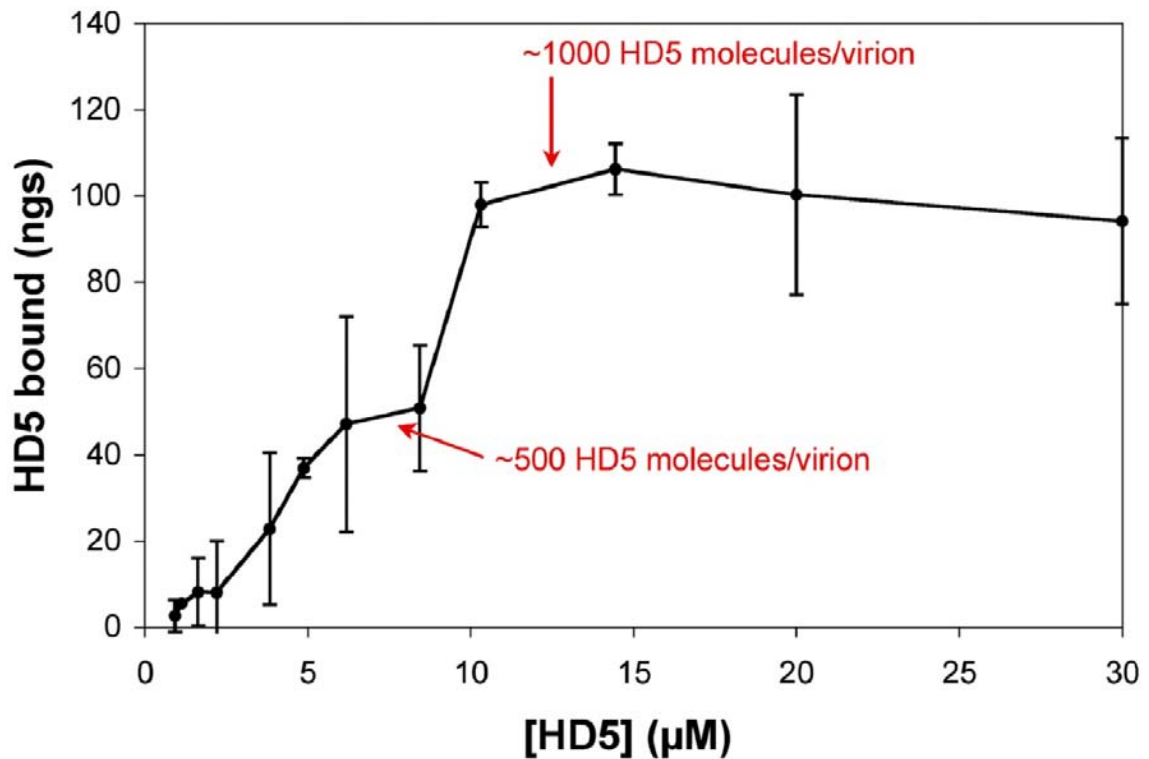


**Figure 4.1.** Stoichiometry of HD5 binding to Ad5. Unlabeled HD5 was complexed with Ad5 and quantitated by high-resolution gel analysis. Saturation was achieved at ~10 µM, or 1000 HD5 molecules per Ad virion (Unpublished results, JG Smith and GR Nemerow). There is also a lower plateau at 6-8 µM, or ~500 HD5 molecules per virion. The observation of two plateaus might indicate both high and low affinity binding sites for HD5 on the Ad virion. However, there is not much difference in the “high” and “low” affinity values and the error bars are large. Therefore, this result will be confirmed before publication.

## CryoEM structural study of the Ad35f+HD5 complex

For our cryoEM study we used the Ad35f vector, which consists of the Ad5 capsid pseudotyped with the Ad35 fiber. This vector is neutralized by HD5 (97), and the short Ad35 fiber is ideal for cryoEM studies as the sample can be embedded in relatively thin ice (86). Sample embedded in the thinnest possible ice results in cryoEM particle images with the best signal-to-noise ratio. Cryoelectron micrographs with better contrast are obtained for Ad35f than for Ads with long fibers. A high-resolution structure of the Ad35f vector (6.9Å at FSC 0.5) has been determined, and this structure provides a control for the Ad35f+HD5 cryoEM structures presented here (89).

We found that Ad samples with concentrations in the range of 150 to 200 µg/mL (1-1.3 nM) are suitable for cryoEM studies. These concentrations lead to nicely spaced virions in the holes of a cryoEM grid and are ideal for data collection. To ensure a high occupancy of HD5 on all possible binding sites of the virion, we prepared an Ad35f/HD5 mixture with an HD5 concentration of 20 µM and an Ad concentration of 1.1 nM (160 µg/mL).

**Figure 4.2** presents the cryoEM structures of Ad35f both with and without HD5. Two cryoEM structures of Ad35f+HD5 were determined, each including a different percentage of particle images. We found that the highest resolution was achieved with only a small percentage of the Ad35f+HD5 dataset. The Ad35f+HD5 structure based on 12% of the data (348 out of 3000 particle images) has a resolution of 9.6Å at the FSC 0.5 threshold. In contrast, the Ad35f structure



based on 67% of the data (2032 out of 3000 particle images) has a lower resolution of 11.8Å (FSC 0.5). Visually, it appears that the Ad35f+HD5 67% map has much more bound HD5 than the Ad35f+HD5 12% map. We hypothesize that HD5 binds heterogeneously to the virion and that selection for the highest resolution data resulted in a cryoEM structure composed of a subset of particle images. It is possible that the Ad35f+HD5 12% structure contains high affinity HD5 binding sites. Alternatively, the 12% structure may contain the most icosahedrally positioned HD5. The data selection is based on a FREALIGN phase residual, which measures how well particle images agree with a matching projection of the cryoEM structure. It seems that a thick coating of HD5 on the Ad virion lowers the resolution of the structure.

The Ad35f+HD5 67% structure shows a significant amount of extra density around the fiber and above the penton base compared to Ad35f (**Figure 4.2**). These additional sites mostly form a second layer of defensin molecules on the Ad capsid surface, and therefore may be lower affinity sites. This observation is consistent with results of Smith and Nemerow who noted that defensins interact with the vertex region of the virion. In an attempt to localize the critical binding sites of HD5 on the Ad capsid, a difference mapping analysis was performed for both the Ad35f+HD5 67% map and the Ad35f+HD5 12% map.

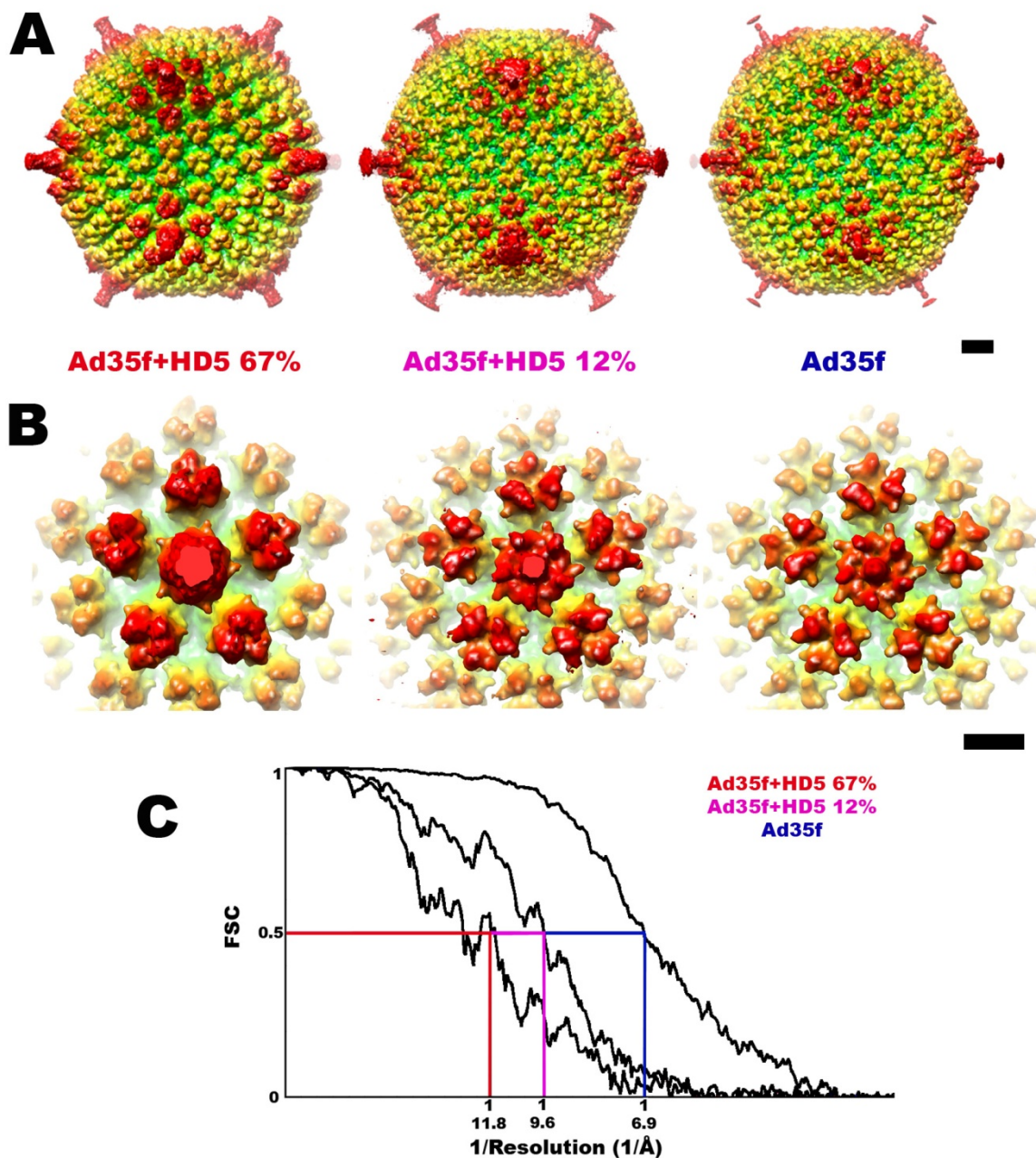


**Figure 4.2** CryoEM structures of Ad35f+HD5 compared to Ad35f. (A) CryoEM structure of Ad35f+HD5 including 67% of the data (left), 12% of the data (center), and Ad35f without HD5 (right). The 3 structures are radially color coded with the fibers and penton base in red (radii >463Å) and the hexons in orange to green (radii 463 Å to 369Å). (B) Enlarged view of the vertex regions of the Ad35f+HD5 and Ad35f structures. Scale bars, 100Å. (C) An FSC plot indicating a resolution for the Ad35f+HD5 structure with 67% of the data of 11.8Å (FSC 0.5); for the Ad35f+HD5 structure with 12% of the data, of 9.6Å; and a resolution for the Ad35f structure of 6.9Å (FSC 0.5).

### Difference mapping allows visualization of HD5 on the Ad capsid

The Ad35f+HD5 structure based on 67% of the data shows extra density attributable to HD5 on the fiber and on the top of the penton bases and hexons. With the Ad35f+HD5 structure based on 12% of the data it is less clear whether there is density that can be attributed to HD5. However, the small mass of an HD5 monomer (3839 Da) compared to the large mass of the Ad virion (150 MDa) might make it difficult to discern HD5 in the Ad/HD5 complex. To identify the defensin binding sites on the Ad capsid, difference maps were calculated by subtracting a pseudoatomic facet from each cryoEM structure.

The pseudoatomic facet consists of 18 hexons and 3 penton bases and is built by fitting the crystal structures of the Ad5 hexon (PDB ID: 1P30) and Ad2 penton base and fiber peptide (PDB ID: 1X9T) into the cryoEM density. The fitting was performed with the UCSF Chimera routine “Fit Model into Map” (82). Since the Ad35f vector contains the Ad5 capsid proteins (except for the fibers), it is reasonable to use the Ad5 hexon and Ad2 penton base crystal structures to build the pseudoatomic facet. The Ad2 and Ad5 penton bases sequences are 98% identical. Once the pseudoatomic facet is built, it is then converted into a density map with the `pdb2mrc` command in EMAN2 (92). The map subtraction step is performed using the IMAGIC-5 “Threed-Two-Volumes-Operations” routine (104). The subtraction of a calculated density map from the cryoEM structure allows for a more uniform difference map than the subtraction of an experimental cryoEM map from another cryoEM map. There is no “ringing” in a calculated density map of the facet as there is in an experimental cryoEM map induced by

imperfect correction of the defocus and astigmatism in the original cryoelectron micrographs. Subtraction of a pseudoatomic facet from Ad35f (without HD5) allows for visualization of the hexon and penton base loops and fiber segments not observed in the X-ray crystal structures (**Figure 4.3 C**). The difference mapping analysis also reveals the density for protein IX on the outer-capsid surface. Protein IX cannot be included in the pseudoatomic facet, as no atomic resolution structure of it has been determined. In the Ad35f+HD5 difference maps (**Figure 4.3, A and B**) we find that HD5 coats the outer-capsid surface, in particular on top of the hexons, and at the icosahedral vertices on top of the penton base and around the fiber.

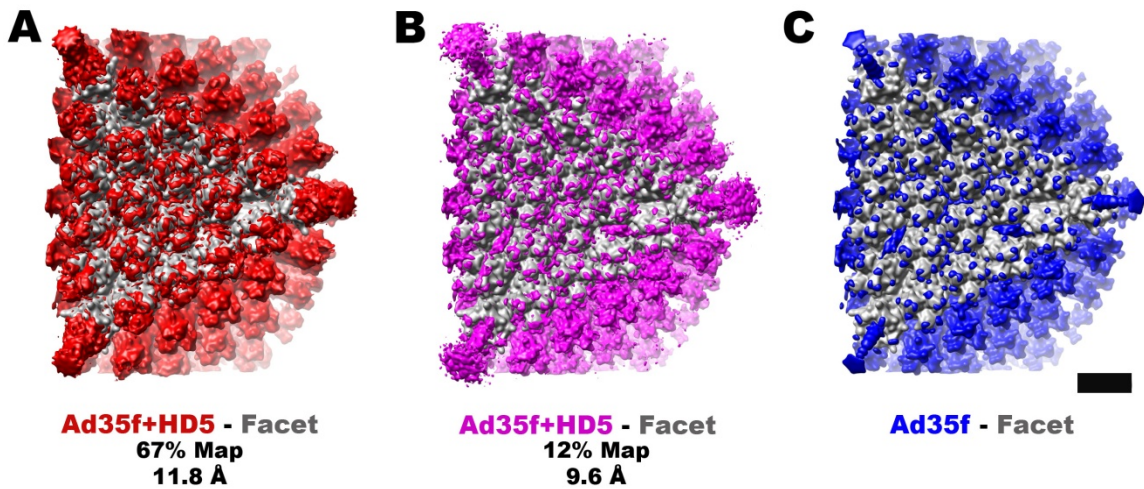


**Figure 4.3.** Difference map analysis of three cryoEM structures with a calculated pseudoatomic facet of hexons and pentons. A facet (gray) was generated by fitting the atomic resolution structures of 18 copies of the Ad5 hexon (PDB: 1P30) and three copies Ad2 penton base and N-terminal fiber peptide complex (PDB: 1X9T) into an icosahedral facet of the Ad35f+HD5 structures (A and B) and the Ad35f structure (C). In A and B the density on top of the facet corresponds to HD5 as well as the missing residues of hexon, penton base, fiber and protein IX. In C, the density on top of the facet corresponds only to the missing residues of hexon, penton base, fiber and protein IX. Scale bar is 100Å.

### HD5 has multiple binding sites on the top of the hexons in the Ad capsid

To take a closer look at the defensin binding sites on hexon, we manually docked the HD5 crystal structure (PDB ID: 1ZMP) into the Ad35f+HD5 difference maps. Hexons are distributed in four unique positions within the asymmetric unit of the icosahedral Ad capsid. Hexons in position 1 are immediately adjacent to the penton base. Hexons in position 2 are located next to hexon 1 and contact another hexon 2 at the icosahedral 2-fold axes. Hexons in position 3 are found at the center of the icosahedral facet, at the icosahedral 3-fold axes. Hexons in position 4 surround hexons in position 3. These hexon positions have been defined previously by Saban et al., 2006 (89). **Figures 4.4 and 4.5** show the difference density observed above each unique hexon position for both the 67% and 12% Ad35f+HD5 structures.

Difference density above the hexons in the Ad35f structure without defensin is shown for comparison in **Figure 4.6**. We note that the Ad35f difference density above hexons appears more regular than the Ad35f+HD5 difference density. The Ad35f difference density corresponds to the loops missing from the Ad5 hexon crystal structure (45 residues) (87). Some of these residues form hyper-variable regions (HVRs), which are the most divergent regions among hexons of different types (87, 89). The largest missing region spans residues 136 to 164, which forms a loop at the top of hexon and which contain several glutamic and aspartic acid residues (PDB ID: 1P30). As the same loops are missing for each hexon (in positions 1-4), it is not surprising that the Ad35f difference density over each hexon is almost the same. In contrast, the

Ad35f+HD5 difference density is more variable above each of the four hexon positions. We conclude that HD5 binds to the flexible loops at the top of hexon and likely induces conformational changes. HD5 may alter the conformation of these loops in multiple ways, leading to less regular difference density as observed in the Ad35f+HD5 difference maps.

In the 67% Ad35f+HD5 difference map, hexons in positions 1 and 2 have a thick coating of the difference density, while hexons in positions 3 and 4 are more moderately coated (**Figure 4.4**). The difference density was displayed as a mesh for manual docking of the HD5 crystal structure (PDB ID: 1ZMP) (101). Multiple HD5 monomers were docked into the observed difference density, resulting in an average of 12.5 HD5 molecules above each hexon. Fifteen HD5 molecules were fit above hexon 1, 13 HD5 molecules were fit above hexon 2, and 11 HD5 molecules were fit above hexons 3 and 4. Given the intermediate resolution of the cryoEM structures (9-12Å), and the heterogeneous binding pattern of HD5 to the capsid, it is not possible to fit HD5 with the precision of atomic resolution. These docked HD5 positions are only meant to give a general sense of how HD5 might bind to the hexons.

Binding at the top of the hexons is expected, since HD5 has an overall positive charge, and the depression at the center of the hexon trimer is negatively charged. CryoEM structures of Ad in complex with blood coagulation factor X (fX) have shown density attributable to the positively charged factor fX Gla domain at this same central depression of hexon (2, 52, 108, 110). Some of

the loops missing from the Ad5 crystal structure are also negatively charged such as aa 136-164, presenting additional reasonable binding sites for HD5 on hexon.

In the 12% Ad35f+HD5 structure, hexons in positions 1 and 2 also display more difference density than hexons 3 and 4 (**Figure 4.5**), but overall the amount of difference density is significantly less than in the 67% Ad35f+HD5 structure. As for the 67% structure, manual docking with the HD5 crystal structure was performed. Twelve HD5 molecules were docked above the hexons in positions 1 and 2. Nine and 7 HD5 molecules were docked above the hexons in positions 3 and 4, respectively. Defensins docked in the 12% Ad35f+HD5 structure might represent the highest-affinity binding sites above the hexons. Our manual docking experiment indicated that an average of 10 HD5 molecules might be bound to hexons in the 12% Ad35f+HD5 structure. An average of 12.5 HD5 molecules might be bound to hexons in the 67% Ad35f+HD5 structure. There are 240 hexon trimers in the Ad capsid; therefore, we estimate that there are 2,400 to 3,000 possible HD5 binding sites just on hexons of the Ad capsid. However, we suspect that only a fraction of these possible sites are occupied on any one Ad virion because of the overlapping nature of the modeled sites.



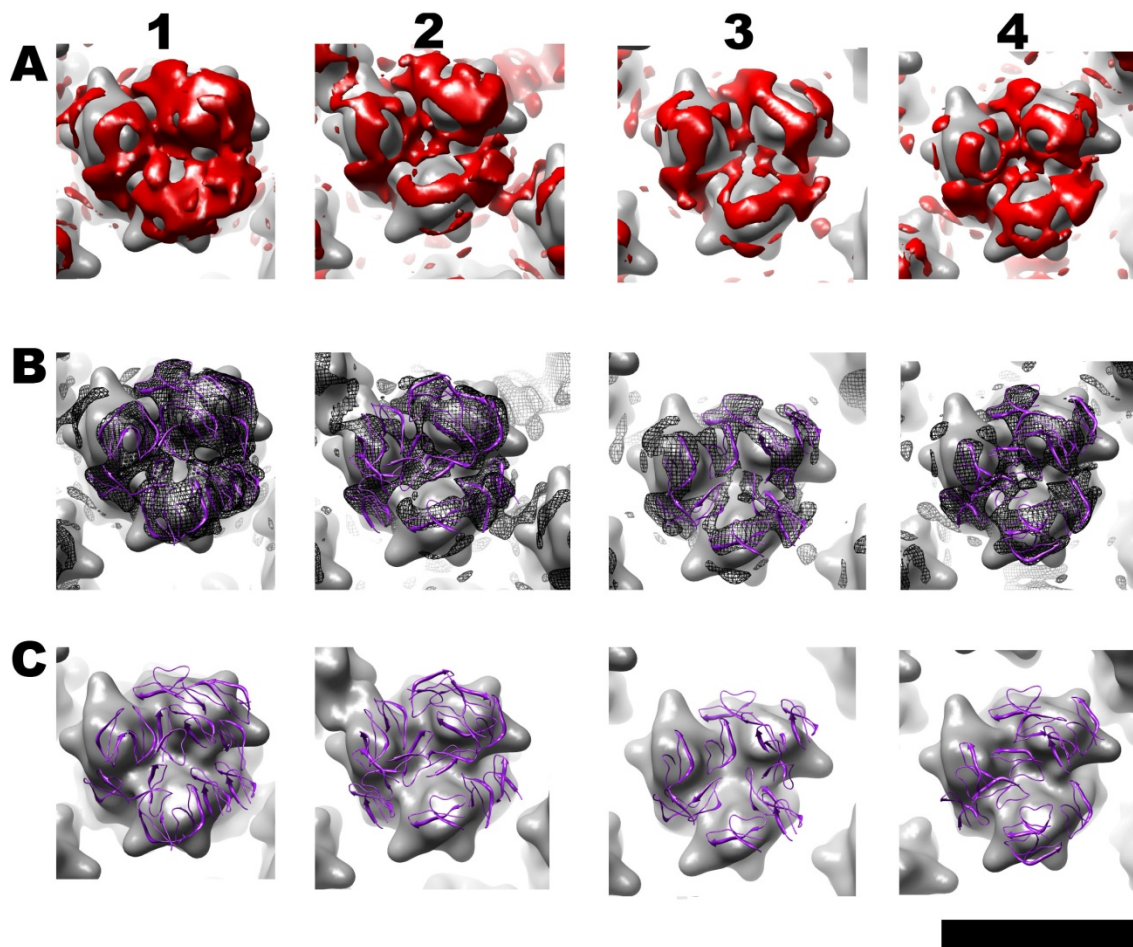


**Figure 4.4.** Difference density corresponding to both HD5 and the hexon surface loops missing from the crystal structure above each of the four unique hexon positions within the asymmetric unit of the 67% Ad35f+HD5 structure. The four unique positions of hexon are: position 1, next to the penton base; position 2 next to hexon 1 and contacting another hexon 2 at the 2-fold axis; position 3 in the middle of the facet, at the 3-fold axis and position 4, surrounding the hexons in position 3. The numbers above each column represent the hexon positions. (A) The difference density above each unique hexon position is shown in red. Hexons in positions 1 and 2 appear to display more difference density than those in positions 3 and 4. (B) The difference density is shown as a mesh with multiple copies of the HD5 crystal structure (PDB ID: 1ZMP) (purple) manually docked into the difference density. (C) The difference density is removed to show the manually docked defensin molecules more clearly. Eleven to 15 copies of HD5 were docked above each hexon position (position 1 = 15 HD5 molecules, position 2 = 13 HD5 molecules, positions 3 and 4 = 11 HD5 molecules each). Scale bar is 100Å.

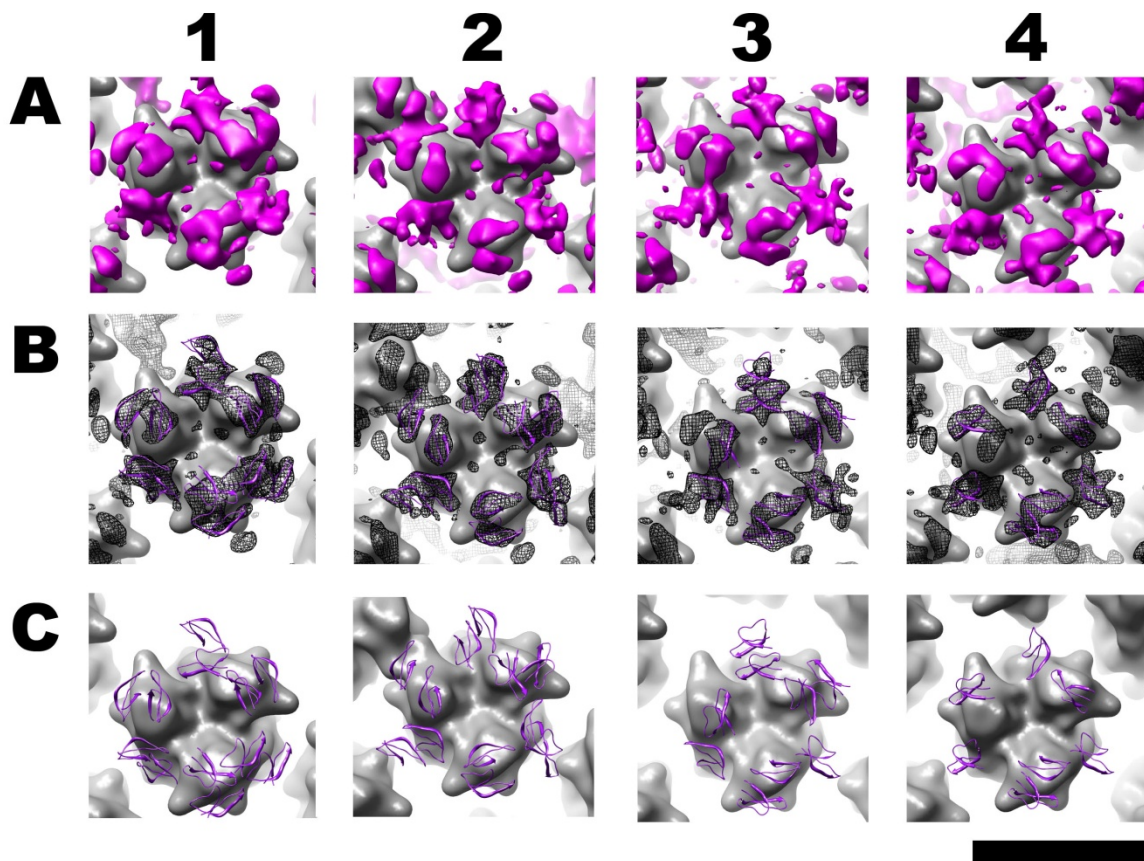


**Figure 4.5.** Difference density corresponding to both HD5 and the hexon surface loops above each of the four unique hexon positions within the asymmetric unit of the 12% Ad35f+HD5 structure. The four unique positions of hexon are indicated above each column. (A) The difference density above each unique hexon position is shown in magenta. (B) The difference density is shown as a mesh with multiple copies of the HD5 crystal structure (PDB ID: 1ZMP) (purple) manually docked. (C) The difference density is removed to show the manually docked defensin molecules more clearly. An average of 10 copies of HD5 were docked above each hexon position (position 1 = 12 HD5 molecules, position 2 = 12 HD5 molecules, position 3 = 9 HD5 molecules and position 4 = 7 HD5 molecules). Scale bar is 100Å.

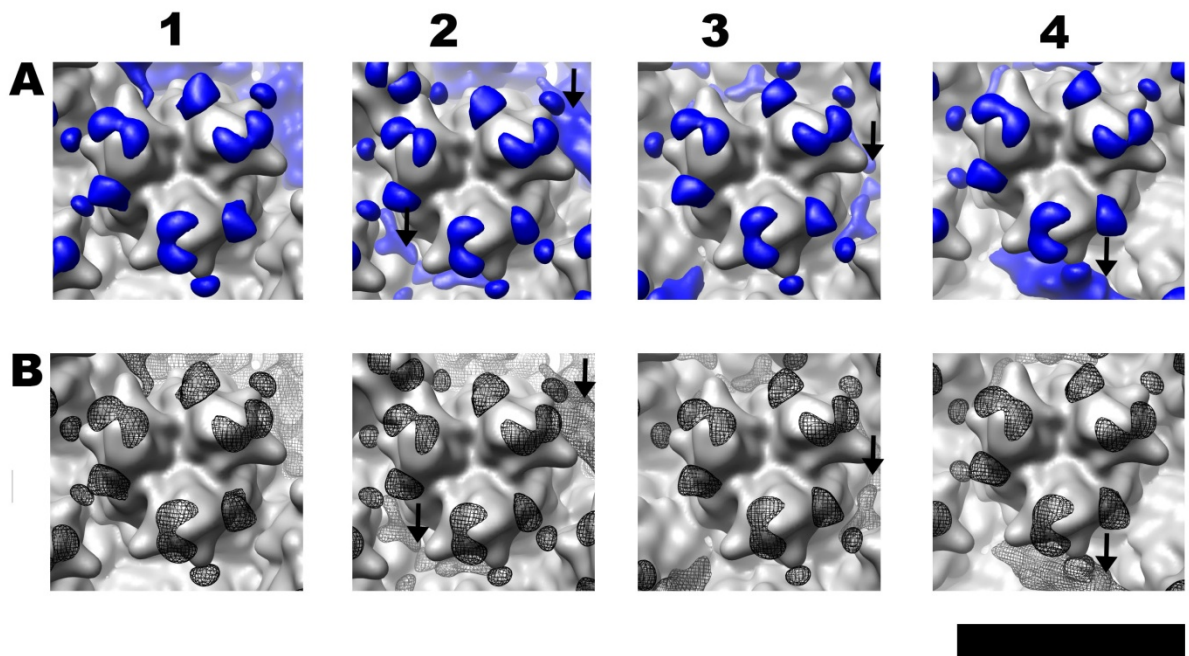


**Figure 4.6.** Difference density from the Ad35f structure corresponding to the missing loops in the hexon crystal structure. The four unique positions of hexon are indicated above each column. Arrows indicate density assigned to protein IX, next to hexons in position 2, 3 and 4. (A) The difference density above each unique hexon position is shown in blue. (B) The difference density is shown as a mesh. Note that the difference density above each unique hexon position is similar. Scale bar is 100Å.

### HD5 coats the fiber and tops of the penton base in the Ad capsid

Difference density attributable to HD5 is not only observed above the hexons, but also at the vertex region, above the penton base and coating the Ad fiber. **Figure 4.7** shows the difference density at the vertex region for both the Ad35+HD5 67% and 12% structures. The Ad35f+HD5 67% structure shows extensive difference above the penton base, while the 12% Ad35f+HD5 structure has significantly less difference density. **Figure 4.7** also shows the difference density corresponding to the Ad5 penton base RGD-containing loop (residues 297-374) and the Ad35 fiber. The pseudoatomic facet used for difference mapping contains the Ad2 penton base in complex with an Ad2 fiber peptide (PDB ID: 1X9T). This structure is missing the RGD loops of the penton base (residues 297 to 374) as well as the fiber shaft and knob (29, 106, 124). Therefore, the control Ad35f difference density corresponds to the penton base RGD-containing loop and the Ad35f fiber shaft. The fiber knob is flexible and not completely reconstructed.

In their biochemical studies, Smith and Nemerow found that Ad, in the presence of neutralizing levels of HD5, was efficiently taken up by host cells suggesting that HD5 does not interfere the association of Ad with  $\alpha v$  integrins (10). There are numerous negatively charged residues in the RGD loop of the Ad2 penton base and in the Ad35 fiber shaft. However, we suspect that only a fraction of these possible sites are occupied on any one Ad virion because of the overlapping nature of the modeled sites.

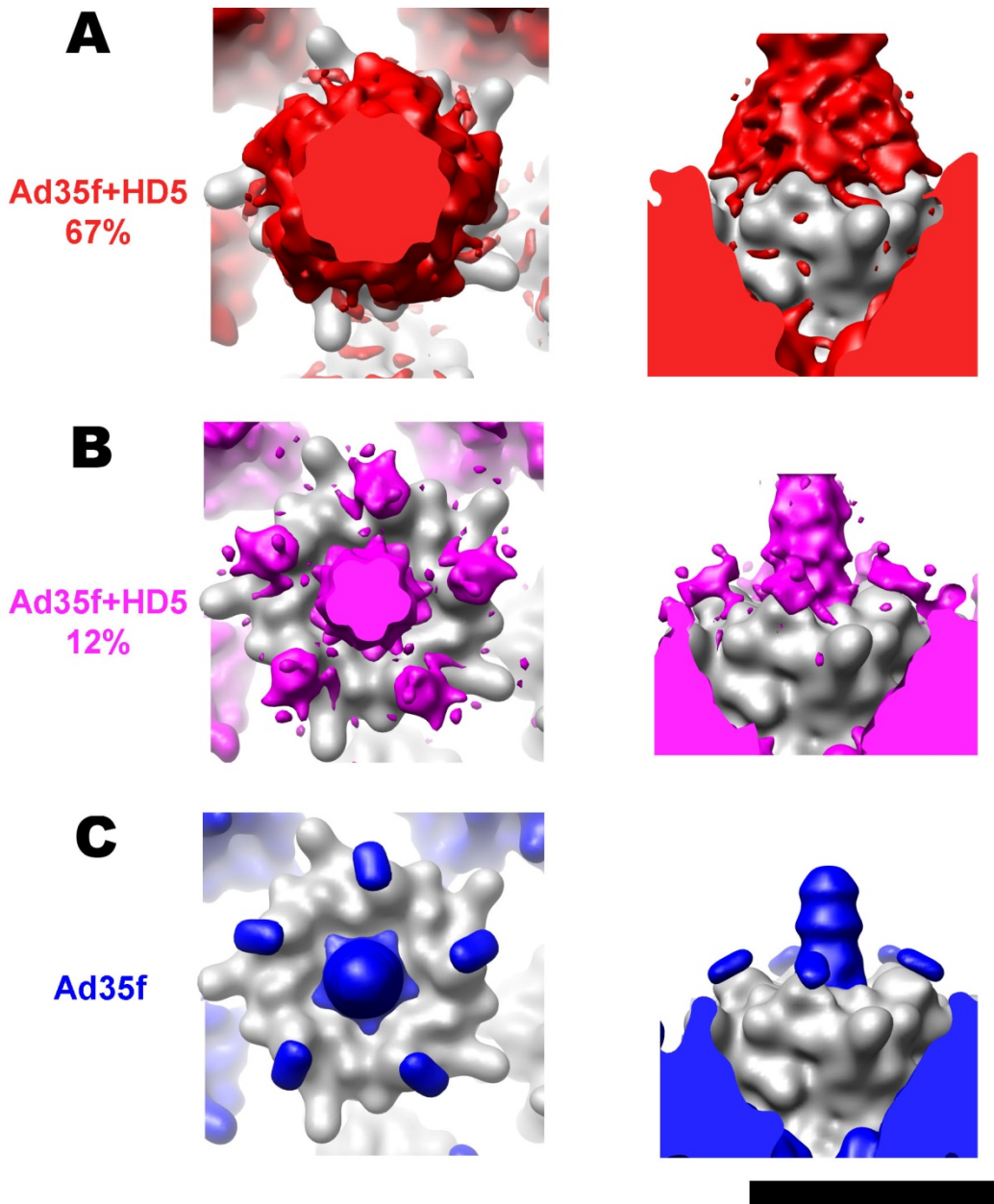


**Figure 4.7.** Difference density in the vertex region in both the Ad35f+HD5 67% and 12% structures and the Ad35f structure. (A) Top and side views of the vertex from the Ad35f+HD5 67% structure. (B) Top and side views of the vertex from the Ad35f+HD5 12% structure. (C) Top and side views of the vertex from Ad35f showing difference density corresponding to the RGD-containing loop of the penton base and the fiber shaft. Scale bar is 100Å.

As performed for the difference density over the hexons, copies of the HD5 crystal structure were manually docked into the difference density in the vertex region (**Figure 4.8**). This difference density displays 5-fold averaging due to the icosahedral symmetry imposed during the reconstruction process. There is a structural mismatch between the 5-fold penton base and 3-fold fiber, therefore the fiber density is inappropriately averaged in the cryoEM structures (89). To help interpret the difference density corresponding to the fiber, 4 triple  $\beta$ -spiral repeats from the Ad2 fiber (PDB ID: 1QIU) were manually docked into the difference density. The Ad35f fiber shaft is predicted to have 6 triple  $\beta$ -spiral repeats but the full length of the fiber is not reconstructed due to flexibility. During positioning of the HD5 molecules, the sites corresponding to the RGD loops were avoided.

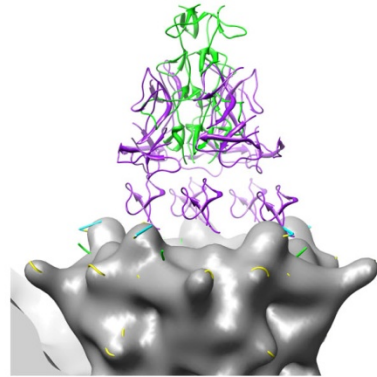
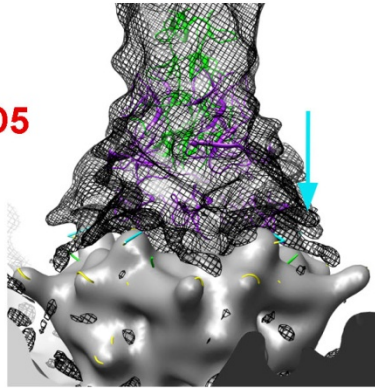
In our models, HD5 density appears to surround the fiber shaft in the 67% Ad35f+HD5 structure, while only very few copies of HD5 appear to bind in the 12% Ad35f+HD5 structure. Fifteen HD5 monomers were docked into the difference density observed above the penton base and surrounding the fiber in the Ad35f+HD5 67% structure, while avoiding the RGD-loop region. In the 12% Ad35f+HD5 structure only 5 HD5 monomers were docked into the observed difference density. Oligomerization of HD5 molecules might occur (JG Smith, personal communication), which could explain the thick layer of the difference density in the Ad35f+HD5 67% structure.

There are 12 vertices per virion; therefore, our modeling studies indicate 60 to 180 possible HD5 binding sites on the vertices of one Ad virion. There

could also be additional HD5 binding sites on the rest of the fiber shaft and the fiber knob, which are not completely reconstructed due to flexibility. Binding of HD5 to Ad does not interfere with the Ad-CAR/Ad-CD46 interaction or with the Ad-integrin interaction, which triggers viral internalization. Based on these cryoEM results, we conclude that defensins neutralize Ad by locking the fiber to the penton base. Fiber loss may be a first key step during Ad programmed disassembly; therefore, locking the fiber to the capsid may prevent release of the membrane lytic protein VI.

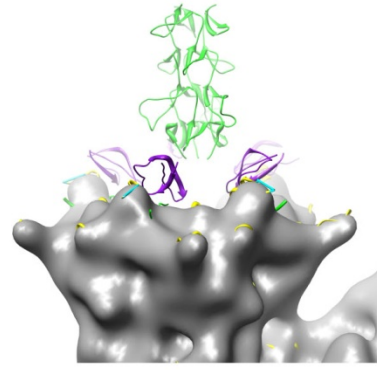
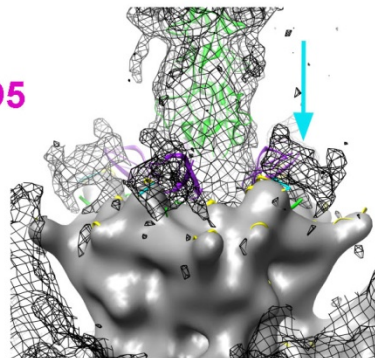
**A**

Ad35f+HD5  
67%



**B**

Ad35f+HD5  
12%



**C**

Ad35f

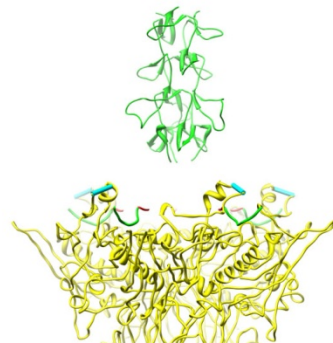
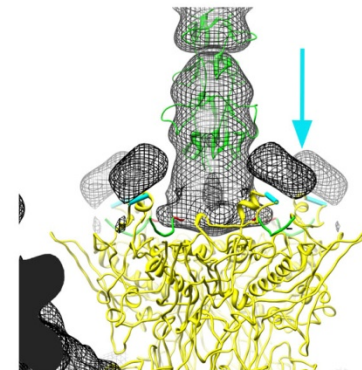




**Figure 4.8.** Side views of the vertex region in the Ad35f+HD5 67% and 12% structures and the Ad35f structure. (A) The difference density (mesh) from the Ad35f+HD5 67% structure is shown with 4 fiber shaft repeats (green) from crystal structure of the Ad2 fiber (PDB ID: 1QIU). In addition, 15 copies of the HD5 crystal structure (purple) were manually docked into the observed difference density. The difference density is removed in the right panel. (B) Same as (A) but for the Ad35f+HD5 12% structure. Five copies of HD5 were docked within the observed difference density. (C) The difference density from the Ad35f structure corresponding to the RGD-loops of the penton base and the fiber shaft. The crystal structure of the Ad2 penton base (yellow) and N-terminal fiber peptide (green) with red at the position of residues E18 and D19 is shown. Cyan bars represent the missing RGD loops of the penton base. The cryoEM density for penton base (gray) is shown in panels A and B. The light blue arrows point to the position of the RGD loop in all 3 cryoEM structures. Scale bar is 100Å.

## Discussion

A possible mechanism of Ad neutralization by HD5 is to stabilize the vertices of the capsid, as suggested by Smith and Nemerow, though the critical binding sites for neutralization remained elusive (10). Given that the Ad5/HD5 complex enters the endosome but then is targeted for degradation, we considered which possible HD5 binding sites identified by cryoEM might stabilize the Ad virion and prevent release of the membrane lytic protein VI.

We examined all of the possible HD5 binding sites on the Ad capsid identified by the cryoEM difference mapping analysis and considered which of these sites may be related to the increased stability of the Ad/HD5 particle. Multiple possible HD5 binding sites are found around the hexon towers and at the central depression of the hexon trimer. There are many negatively charged residues and flexible loops in these locations, making them ideal surfaces for binding of numerous copies of the positively charged HD5 molecule. We observed more HD5 bound to the hexons in position 1 than the other 3 hexon positions of the asymmetric unit. The hexon 1 position is also called the peripentonal hexon position, as it is adjacent to the penton base in the vertex. We also observe significant HD5 binding over the penton base. It is possible that multiple copies of HD5 form a bridge between the peripentonal hexons (those at position 1) and the penton base. The cryoEM structures represent an icosahedral average of the particle images included in the reconstruction. Therefore, the HD5 connection between the peripentonal hexons and the penton base would be difficult to visualize unless it was present in the same manner in the majority of

the asymmetric units and particle images. Since not all of the peripentonal hexons and penton bases are connected by HD5 bridges, it is not obvious how HD5 binding to the tops of the hexons could significantly increase the stability of the Ad virion.

Multiple possible HD5 binding sites are also found above the penton base and around the fiber shaft. There are many negatively charged residues, as well as one flexible surface loop (the RGD loop) at the top of penton base and numerous flexible loops along the fiber shaft, which could be ideal binding sites for the positively charged HD5 molecule. Following the manual docking of HD5 in the vertex region difference density, we carefully examined the sites where HD5 binds. In both the Ad35f+HD5 67% and 12% structures HD5 is docked in the vicinity of the fiber N-terminal peptide at the top of the penton base.

In the crystal structure of the Ad2 penton base and fiber peptide, the N-terminal fiber peptide (aa 10-19) binds to the top of the penton base near the flexible RGD loop. A conserved hydrophobic stretch of fiber residues (FNPVYPY, aa 11-17 in Ad2) forms the interaction region with the top of the penton base (**Figure 4.9**). Following this conserved fiber region is a stretch of four residues that are negatively charged or polar in many Ad types including Ad2, Ad5 and Ad35, but positively charged in other Ad types including Ad17 and Ad37, which are not neutralized by HD5. We considered whether HD5 binding at this site, when it is negatively charged as in the Ad35 fiber, may lead to enhanced Ad stability.

An early step in Ad programmed disassembly is the loss of the fiber concurrent with, or followed shortly by, the loss of the penton base and the peripentonal hexons (37, 118). If the loss of the fiber is a necessary first step (as a primer) for the subsequent loss of other viral components, binding of the HD5 to the N-terminal fiber region may stabilize the Ad virion by stabilizing the fiber/penton base complex. In support of this idea, it has been noted that fiberless Ad5 vectors are less stable than Ads with fiber (57, 109). These Ad5 fiberless vectors tend to release their viral DNA genome prematurely.

Our working hypothesis is that HD5 binding to the negatively charged and polar fiber residues, aa 18-21 in Ad35, stabilizes the fiber/penton base complex and thereby stabilizes the Ad virion and leads to its inability to escape the endosome. These four residues are near the top of the penton base and in the vicinity of the fiber shaft (**Figure 4.9**). When HD5 is bound at this proposed critical site involving the N-terminal region of the fiber, it is also likely to interact with residues in the RGD loop of the penton base, therefore stabilizing the fiber/penton base complex. This hypothesis also explains why some types of Ad are neutralized by HD5 and other types, like those of species D, are not neutralized by HD5. We speculate that there is a correlation between non-neutralization by HD5 and a positively charged sequence after the conserved penton base interaction region of the Ad fiber.

The Nemerow group has tested various types of human Ads to determine whether or not they are neutralized by HD5 (**Figure 4.10**). Ad2 and Ad5, which belong to species C Ads, are strongly neutralized by HD5. Similarly, species A

and B Ads are also neutralized by HD5. The Ad35f vector, which is Ad5 pseudotyped with the Ad35 fiber, is also neutralized by HD5 (J. Smith and G. Nemerow, personal communication). None of the species D Ads that have been tested thus far are neutralized by HD5. The fiber sequence is known for all but two of the Ads types tested (Ad23p and Ad51p). So far there is a perfect correlation between non-neutralization by HD5 and a positively charged fiber sequence after the conserved penton base interaction region (**Figure 4.10**). All of the species D types tested that are not neutralized by HD5 and for which we know the fiber sequence, contain a GYAR fiber sequence after the conserved hydrophobic stretch. This sequence has a positively charged arginine (R) residue, which would likely repel HD5 away from this site.

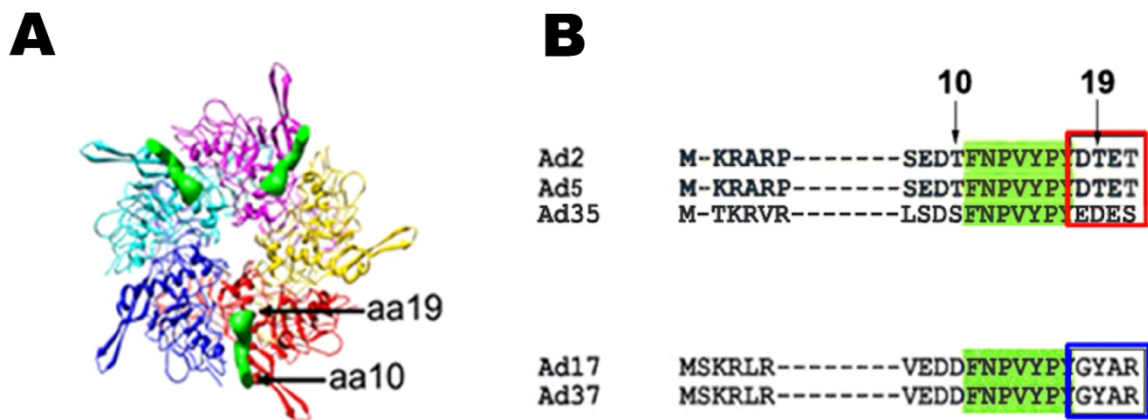


**Figure 4.9.** Postulated critical neutralization site for HD5 based on a combined cryoEM and sequence analysis. (A) Three fiber N-terminal peptides (green) are shown above the penton base (multicolor) (PDB ID: 1X9T). (B) Sequence alignment of the N-terminal regions of the fiber for Ad types 2, 5, 35 which are neutralized by HD5, and types 17, and 37, which are not neutralized by HD5. Ad types 2, 5 and 35 have a negatively charged and polar sequence at positions 18-21 in the N-terminal fiber sequence (outlined with red box). Ad types 17 and 37, both species D viruses, contain a positively charged sequence of residues at this position (outlined with a blue box). Residues highlighted in green are conserved among different Ad species and form the penton base association region shown as a green ribbon in panel A.

A negatively charged and polar sequence after the conserved penton base interaction region, such as DTET in the Ad2 and Ad5 fibers or EDES in the Ad35 fiber, would form a favorable binding pocket for HD5 at the top of the penton base. Difference density is observed in this vicinity in both the Ad35f+HD5 12% and 67% structures (**Figure 4.11**). Without an atomic resolution structure of an Ad/HD5 complex we cannot precisely define the HD5 binding sites on the Ad capsid. The size of HD5 (with molecular dimensions of 17Å x 22Å x 31Å) is similar to the resolutions of the Ad35f+HD5 cryoEM structures (9-12Å). Thus, visualizing the precise orientations of the HD5 molecules relative to the Ad capsid is not feasible in these cryoEM structures. Also, cryoEM structure determination relies on image averaging. If HD5 binds in multiple overlapping sites as we suspect, then we would observe only an average of the bound HD5 rather than discrete binding sites. HD5 binding probably does not follow icosahedral symmetry and, therefore, during the symmetry averaging process some of the HD5 density will be inappropriately averaged. In addition, if HD5 binds to flexible surface loops of Ad as the cryoEM results indicate, this is likely to cause conformational changes further complicating our ability to resolve discrete HD5 binding sites. Despite all of these factors, the intermediate resolution cryoEM structures of Ad35f+HD5, combined with difference mapping using a pseudoatomic facet, have enabled us to visualize the general areas of HD5 binding on the Ad capsid.

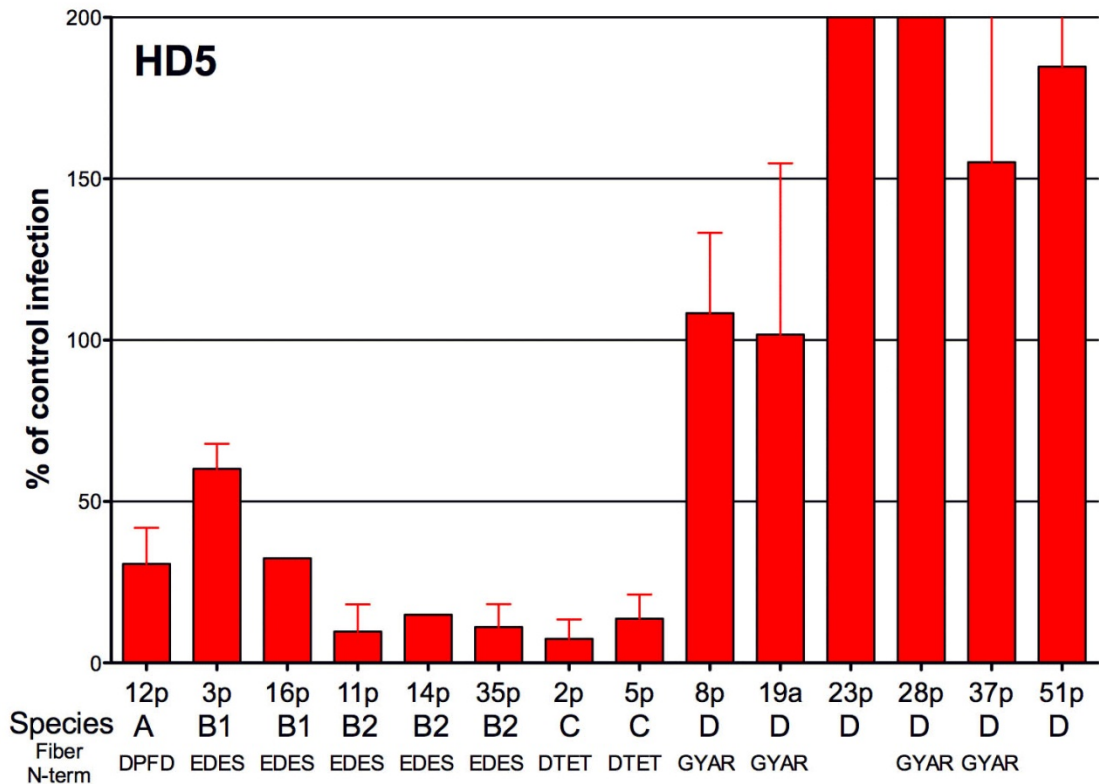


**Figure 4.10.** Infectivity assay for various Ad types in the presence of HD5. The Ad types and their species classifications are indicated at the bottom of the figure. We hypothesize, based on our cryoEM study together with the biochemical and cell entry analyses performed in the Nemerow lab, that the residues 18-EDES-21 for Ad35f, and similar negatively charged sequences in other Ad types, form the critical neutralization binding site for HD5. The sequence of this N-terminal fiber region is shown at the bottom of the figure. The complete fiber sequences for types 23p and 51p have not been determined. The concentration of HD5 was 15 $\mu$ M in the neutralization assay. Note that in some cases HD5 (for example Ad23p and Ad28p) enhances Ad infectivity. Unpublished data from the Nemerow laboratory (J.G. Smith and G.R. Nemerow).



Manual docking with the HD5 crystal structure into the cryoEM difference density suggests that it is plausible for one or more of the arginine residues on the surface of HD5 to interact with the negatively charged region of the fiber and with the flexible RGD loop of penton base. This interaction may “trap” the fiber and anchor it to the penton base. After the Ad/HD5 complex enters the host cell endosome, we speculate that the trapped fiber cannot be released from the virion preventing release of the vertex proteins. Since release of the vertex proteins including protein VI is critical for escape from the endosome, HD5 effectively blocks the Ad capsid from undergoing programmed disassembly and therefore blocks the viral course of infection.

Our cryoEM study of an Ad/HD5 complex has led to the hypothesis that the critical binding site for HD5 neutralization involves the negatively charged and polar fiber residues, aa 18-21 in Ad35, at the top of the penton base. This hypothesis is currently being tested in the Nemerow laboratory with chimeric Ad vectors containing either negatively or positively charged residues at this site in the fiber protein. The combined structural, biochemical, and neutralization studies indicate that HD5 stabilizes the Ad vertex region and prevents viral disassembly in the endosome. This neutralization mechanism may also be relevant for other non-enveloped viruses. Defensins neutralize several non-enveloped viruses in addition to Ad, such as human papillomavirus (HPV) and rotaviruses. If the defensin neutralization mechanism can be determined for Ad, this knowledge may be applicable for other non-enveloped viruses. Understanding the

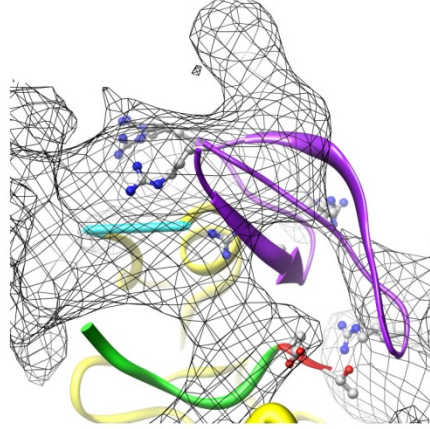
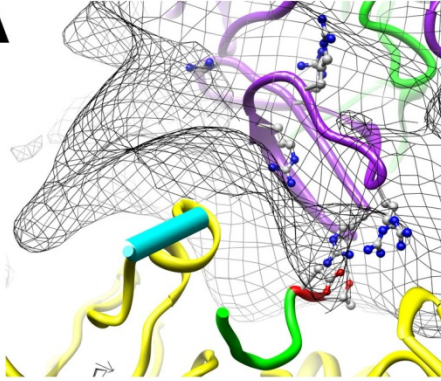
mechanism of action of defensins may also help in the development of new effective treatments against Ad infections.

In the case of Ad, rather than forming membrane pores or interfering with the interaction between the pathogen and host cell receptors, HD5 appears to coat the capsid and interfere with programmed disassembly. This allows the host cell enough time to degrade the virion in the lysosome and thus block the normal course of viral infection.

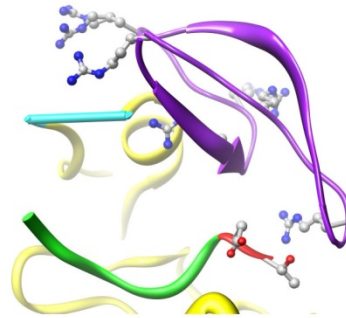
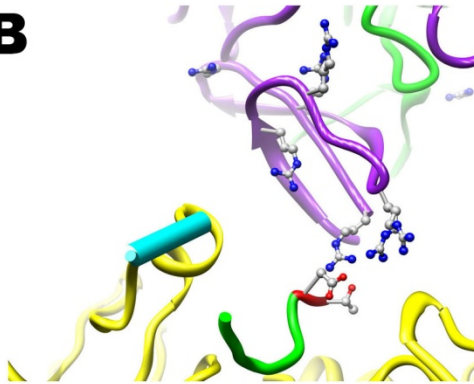
**Ad35f+HD5 67%**

**Ad35f+HD5 12%**

**A**



**B**



**C**

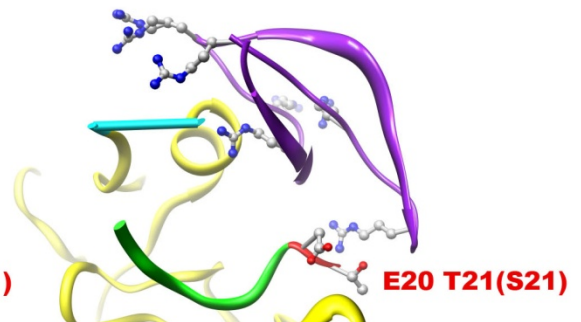
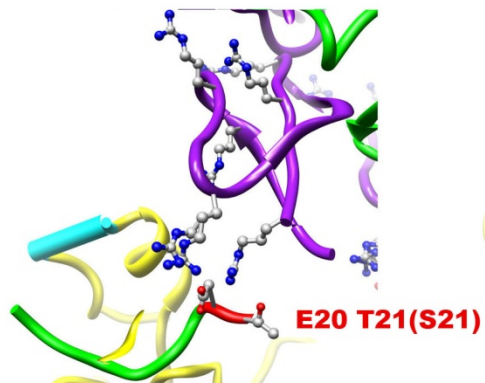


**Figure 4.11.** Close up view the postulated critical binding site of HD5 involving the Ad fiber N-terminal region and the penton base RGD loop. The crystal structure of the Ad2 penton base (yellow) and fiber N-terminal peptide (green and red), is shown together with docked HD5 molecules (purple) and triple  $\beta$ -spiral fiber shaft repeats (green). Fiber residues 18-21 (DTET in Ad2 and Ad5; EDES in Ad35) contribute to the postulated critical binding site. Only residues 10-19 of the Ad2 fiber N-terminal region are observed in the penton base/fiber crystal structure. Ad2 fiber residues D18 and T19 are negatively charged and polar (red ribbon) and their sidechains are shown in a ball and stick representation colored by atom type (O=red, C=white). The corresponding residues in the Ad35 fiber are E18 and D19, both negatively charged residues. A cyan bar denotes the location of the missing RGD loop (residues 297 to 374) of the Ad2 penton base, which may also interact with HD5 at this binding site. The sidechains of the 6 arginine residues of HD5 are shown in a ball and stick representation (N= blue, C= white). (A) The difference density (mesh) from the 67% map (left) or 12% map (right) together with one copy of HD5 in the position near the postulated critical binding site. Note that the HD5 molecule could make favorable electrostatic interactions with the fiber N-terminal residues 18-19 even when docked in a variety of different orientations. (B) Same as in (A), but without the difference density to more clearly show the possible interaction between HD5 and the fiber N-terminal residues. (C) Same as in (B), but rotated 60° around the vertical axis. The approximate positions of fiber residues E20 and T21(S21) of the Ad2(Ad35) fiber are shown schematically with alphanumeric characters since they are missing from the penton base/fiber crystal structure. They are represented by red characters as they are negatively charged and polar residues.

## CHAPTER V

### Summary and Conclusions

#### Implications for Adenovirus cell entry from our cryoEM study of Ad2ts1

The cryoEM studies presented here provide insight into the structural events leading to escape of adenovirus from the endosome, a critical step during its lifecycle. First, we studied Ad2ts1, a mutant generated in the 1970's, which represents a fully assembled but immature Ad. Ad2ts1 contains the immature forms of both capsid-associated proteins (IIIa, VI and VIII) and core-associated proteins (VII, mu and terminal protein) that depend on the Ad protease for maturation (17, 43, 69, 70, 99, 111, 113, 119). When produced at non-permissive temperature (39°C), the Ad2ts1 mutant incorporates a 5-fold reduced copy number of the viral protease due to a proline to leucine substitution at position 137 of its sequence. This defect causes the virus to be targeted for degradation in the lysosome or recycled to the cell membrane (6, 37).

The structure of the Ad2ts1 mutant reveals a connection between the capsid and core formed by the uncleaved precursor proteins. Based on this finding, we propose that Ad2ts1 cannot undergo the necessary conformational changes that result in successful disassembly of the vertex and release of the membrane lytic factor protein VI for endosomal lysis. Failure of the Ad2ts1 mutant to disassemble in the endosome highlights a critical role for the Ad protease in viral maturation (6, 37, 43, 83, 111, 112). The Ad protease primes the virus for disassembly in the host cell by separating the core and inner capsid surface,

allowing the penton bases and peripentonal hexons along with protein VI to dissociate from the virus in the endosome.

*Ad2ts1* contains precursor VI, which is processed by the virally-encoded protease, yet it is fully functional and exhibits similar membrane-lytic activity as mature VI (118). Our structural study shows that the precursor proteins present in *Ad2ts1* lock the capsid from the inside. Locking of the capsid and association of precursor protein VI with the core appear to interfere with the release of the Ad proteins at the appropriate time.

#### Future directions for *Ad2ts1*

CryoEM relies on image averaging, and reaching high-resolution is dependent on the degree of uniformity or homogeneity of the imaged sample. The *Ad2ts1* cryoEM structure contains only ~16% of the collected data, possibly due to heterogeneity in the sample (96). In comparison, the *Ad35f* 6Å structure includes more than one third of the collected particle images. Estimates of the copy number of protease in the mature Ad virion and in *Ad2ts1* differ. It has been estimated that *Ad2ts1* contains fivefold fewer copies of the protease than wild-type mature virions (3). A study of the Ad protease in 1990 by Anderson noted that low levels of protease could be detected. This finding suggests that there is a degree of leakiness, or incomplete penetrance, of the *Ad2ts1* phenotype, which results in an incorporation defect. There could be different populations of the *Ad2ts1* virions with different protease copy numbers, which cannot be distinguished visually. Some virions might have no protease and remain in a

completely immature state, while other virions might contain 1 to 2 copies of the protease and undergo limited proteolytic processing. Such a scenario would give rise to a heterogeneous *Ad2ts1* sample for cryoEM studies. Having different populations of immature Ad means that some virions might undergo programmed disassembly, resembling mature Ad, while others will be arrested at the step of endosomal escape.

To reach subnanometer resolution and facilitate a more in depth interpretation of the *Ad2ts1* structure, it would be ideal to collect *Ad2ts1* data from a more homogeneous sample. Producing a more homogeneous *Ad2ts1* sample could be achieved by deleting the Ad protease gene from the *Ad2ts1* genome or inserting a stop codon in the protease ORF. Uniformity of the immature *Ad2ts1* sample would then allow a higher number of particles to be included in the reconstruction to possibly achieve a high resolution structure, facilitating assignment of the density for the precursor proteins.

Another way to understand Ad maturation and disassembly would be to investigate the interaction between hexon and protein VI, in both its mature and precursor forms by cryoEM. Protein VI is a ~23 kDa protein and would not be feasible for cryoEM analysis as an isolated protein. However, the hexon trimer is over 300 kDa, and a hexon/protein VI complex or hexon/precursor VI should be amenable to single particle cryoEM analysis. A high-resolution structure of the hexon-VI complex could facilitate interpretation of the *Ad2ts1* density and deduce which regions of protein VI might be interacting with the core components. Even if only moderate resolution structures of the hexon-VI and hexon-precursor VI

complexes were obtained, difference mapping analyses could provide information on the position of the cleaved N- and C- termini. Changes in the conformation between mature and immature VI have been postulated as a way of preventing the release of protein VI from the virus while maturation occurs. Concordantly, our studies show that hexon shields the lytic function of protein VI by ~60% (69, 70, 118). Structures of the hexon-VI and hexon-precursor VI complexes would help us understand the viral maturation steps related to the protein VI proteolytic cleavage. These studies might also enable us to determine whether the predicted amphipathic helix of protein VI, which is critical for membrane lytic activity (aa 36-53), is shielded inside the hexon cavity. If so, protein VI must dissociate from hexon to perform its lytic function.

#### Ad-mediated gene delivery

Gene therapy, which is in essence the delivery of a corrective gene to affected tissues, emerged as a discipline in the late 1970's and 80's due to advances in genetic manipulation. The original goal of replacing a defective gene has expanded into the delivery of genetic material for the treatment of various diseases; possible oncolytic therapies include delivery of tumor suppressors and immunomodulating factors (5, 26, 31, 64, 94, 103, 107, 120). Various vectors are being developed to deliver therapeutic genes and they belong to one of two classes: non-viral and viral vectors. Non-viral vectors (such as DNA-containing liposomes and plasmids) have the advantage of by-passing the immune response elicited by viral vectors, but the effectiveness of delivery is low when compared to viral-based therapies.



Viral vectors, including retroviruses, pox viruses, adeno-associated virus, and adenovirus, have evolved efficient ways to deliver genetic material to target cells. Adenovirus has emerged as a powerful vector for gene delivery and currently a third of all ongoing gene therapy clinical trials in the US use Ad as the vector (5, 26, 31).

Among the serious considerations when using Ad vectors is the rapid immune response that the capsid proteins produce in the host. Since no integration of the Ad genome occurs, boosting doses of Ad vectors are required for continued therapeutic treatment. In the late 1990's a costly lesson was learned when a young man, Jesse Gelsinger was provided a high dose of Ad as treatment for an X-linked deficiency, ornithine transcarbamylase. His death halted gene therapy trials temporarily in order to determine the safe-dosage conditions.

To date, Ads are being explored to treat several diseases, including heart failure and cancer. Recombinant human Ads are being used in clinical gene therapy trails aiming to treat heart failure due to damage to cardiomyocytes caused by coronary artery disease, inflammation or hypertension. Treatment of these cells is facilitated by the expression of CAR in the cardiovascular system (64), in particular on cardiomyocytes and vascular endothelial cells. The goals of this approach are to ensure that healthy cardiomyocytes are not adversely affected and to provide a "cure" to those cardiomyocytes that have been affected but not lost by arterial disease or hypertension (40, 64, 103). Ad-mediated gene delivery in the cardiovascular system has been recently studied, for the

prevention of cardiac arrhythmias (by providing Ad carrying the beta-adrenergic receptor kinase inhibitor gene), and for delivery of angiogenic growth factors (like hepatocyte growth factor) (40, 64, 103). These therapies could potentially help in the regeneration of damaged cardiomyocytes and improve recovery of patients suffering from different forms of heart disease.

In cancer, Ad-based vectors can be used to provide a variety of therapies and boost the results of chemotherapy. Several studies have been conducted using Ad as the vector for the treatment of cancer, including the delivery of tumor suppressors (p53, p21, Rb), immunomodulating cytokines (such as IL-2, TNF $\alpha$ , etc), or to stimulate antigen production for tumor vaccines and inhibitors of angiogenesis (4, 5, 94, 120).

Despite the significant progress in this area, much work remains to be done to optimize Ad vectors and create new vectors that can evade the strong immune response which hampers Ad-based therapies. Our cryoEM studies of Ad have suggested several possible approaches for improving Ad vectors. Hexon has been shown to bind to blood coagulation factor X, an important factor in the cascade of clot production, which targets Ads towards the liver (4, 52). If the organ targeted for therapy is not the liver, mutations to the hexon protein could be introduced to avoid delivery to the liver. The Ad-factor X binding sites appears to be at the hexon towers, which are highly variable and could possibly tolerate sequence alterations. A second avenue is to modify the outer-capsid protein IX, which helps to stabilize hexon-hexon interactions. Modifications to this protein (such as labeling with GFP) appear to be well tolerated and could be used to re-

target the virus to the desired organ or tissue. A third important alteration would be to evade the innate immune system by preventing association of Ads with human defensins. Human  $\alpha$ -defensins were recently shown to inhibit Ad infection by binding to the Ad capsid and preventing disassembly (10). We have shown that a possible important site for defensin binding is at the interface of the penton base and fiber proteins and if mutations were to be produced in this region, Ad vectors may be able to evade defensin-mediated neutralization.

#### Antiviral peptides: human Ads and defensins

The cryoEM structural study presented in Chapter 4 enabled us to propose a mechanism for how human  $\alpha$ -defensin HD5 neutralizes Ad infection. Human  $\alpha$ -defensin HD5 exhibits potent anti-adenoviral activity through binding and stabilization of the capsid resulting in failure of the virion to escape the endosome during cell entry (10). Stabilization of the vertex in the capsid appears to block disassembly of the capsid as these components are among the first to be released upon entry of the virus into host cells (10). Human papillomavirus appears to be arrested at a similar stage as adenovirus when exposed to defensins (11). Therefore, understanding how defensins neutralize Ad infection may impact an understanding of defensin-mediated neutralization of other non-enveloped viruses. Also knowledge of the way in which defensins neutralize Ad may pave the way for the next generation of Ad vectors that by-pass detection by the innate immune system.

## Results and implications from the Ad35f+HD5 studies

The cryoEM study on the interaction of a human defensin with adenovirus enabled us to hypothesize possible sites for virus neutralization. A defensin-mediated immune response has been described for both bacteria and enveloped viruses. For human adenovirus, a non-enveloped virus, Smith and Nemerow, have shown that defensins HD5 and HNP-1 inhibit Ad infection causing the neutralized virus to behave in a similar manner as Ad2ts1 produced at 39°C (10). The Ad-defensin interaction was shown (a) to be direct, (b) to target the incoming virus for degradation in the lysosome and (c) to prevent disassembly of the capsid by stabilization at the vertex region. Unpublished studies have found that HD5 is effective at preventing infection of species A, B and C Ads but not of species D (Chapter 4, **Figure 4.9**). HD5 binds to the Ad capsid, but the site(s) important for neutralization remained elusive. This prompted our investigation into the structure of human Ad complexed with HD5 defensin.

The cryoEM structure of the Ad35f vector complexed with HD5 shows that HD5 binds to hexons, penton bases, and fibers of the capsid. The main sites of defensin binding on the Ad capsid are on the towers and central depressions of the hexons (which are negatively charged), along the fiber shaft and the tops of the penton base at the interface where the penton base and fiber interact. A detailed analysis of the Ad35f-HD5 structural results, together with biochemical and sequence analysis of the Ad serotypes that are neutralized by defensin and those that are not neutralized, led us to hypothesize that binding of defensin to the interface formed by the penton base and fiber serves as a key site for

neutralization. Density assigned to HD5 is observed near the N-terminal region of the fiber. Residues 18 to 21 of the Ad35 fiber form a negatively charged pocket. Modeling of the HD5 atomic resolution structure into the difference density indicates that this pocket can fit HD5. As HD5 is predominantly positively charged, it would have charge complementarity with the pocket created by the N-terminal region of the Ad35 fiber. In contrast, the corresponding residues of non-neutralized Ads, such as Ad17 and Ad37 (species D Ads), have positively charged residues in this pocket which would repel HD5. Currently, the Nemerow group is testing this site by creating chimeric Ads, in which the N-terminal portion of the fiber from a defensin-neutralized species is swapped with that of a non-neutralized species. We anticipate that these studies will definitively test the hypothesis of the critical neutralization site. If the hypothesis is refuted, then the Ad-defensin structure will be re-examined for other possible critical sites.

This mechanism of defensin neutralization of Ad differs from that used by defensins to neutralize bacteria, fungi and enveloped viruses. Defensins appear to stabilize the Ad capsid and prevent the release of the membrane-lytic factor in the endosome, thus targeting the virus for lysosomal degradation.

#### Future directions for Ad-defensin

The cryoEM structure of the Ad35f+HD5 complex reveals binding of HD5 to the outer capsid of Ad and no other noticeable changes to the Ad structure. The resolution of 9.6Å facilitates data interpretation, but given the small size of HD5 it is difficult to uniquely position HD5 relative to the Ad capsid in all of its

multiple binding sites. Specifically, we cannot determine which surface of HD5 is interacting with the Ad capsid proteins. The cryoEM structure of Ad35f+HD5 allows for visualization of the general areas of binding for HD5 on the Ad surface, but not their precise positioning. A high-resolution structure of the Ad/defensin complex might allow precise analyses of the interaction between this peptide and Ad. If all of the HD5 binding sites are on flexible loops, then even a high-resolution structure might not reveal the precise interaction between peptide and Ad. Using the moderate resolution cryoEM structure of this complex and our knowledge of the electrostatic surface of HD5, we propose that HD5 binds to a negatively charged pocket of residues located at the interface of the fiber and penton base of Ad. This region of residues on the Ad surface may serve as one important location for neutralization of Ad infection.

To allow a more detailed understanding of the Ad-defensin interaction, a significantly higher number of cryoEM particle images could be collected and averaged. An atomic-resolution structure of adenovirus might be within reach in the near future, as four near-atomic (3.8-4.5Å) resolution cryoEM structures (rotavirus, Epsilon 15 bacteriophage, GroEL and cytoplasmic polyhedrosis virus) were reported last year (123). These near-atomic resolution cryoEM structures involved averaging one million to several million asymmetric units. Higher resolution data would facilitate a more precise modeling of the defensin interaction with the fiber and penton base surfaces. This information might also lead to an understanding of how similar defensins neutralize other non-enveloped viruses. By carefully examining the binding regions of HD5 on the Ad

surface combined with sequence analysis, locations with similar structure/organization in other non-enveloped viruses could be mutated to test for loss of HD5 neutralization. Additionally other defensins (such as HNP-1 and human beta defensins) could be studied in complex with Ad by cryoEM, as well as complexes of HD5 with the isolated penton (the complex formed by the penton base and fiber proteins). This would likely reveal a more detailed view of how HD5 stabilizes the penton base and fiber complex.

CryoEM structures of adenovirus have increased our understanding of the cell entry and programmed disassembly as presented in the two aims of this thesis. The cryoEM structure of the Ad2ts1 mutant highlights the importance of the incorporation of the protease for priming Ad virions for disassembly. Studies of the Ad+HD5 complex enabled us to hypothesize how this innate immune peptide neutralizes infection. These studies provide us with a more detailed understanding on how Ad disassembly is exquisitely controlled, and moreover, how interference with disassembly leads to degradation of the virus in lysosomes. It is of particular interest for the gene delivery field how Ads are neutralized by defensins, which are a first line of defense for the host. These and future studies may pave the way for the next generation of Ad vectors that can avert neutralization by defensins and more successfully deliver the therapeutic gene.

## **Appendix 1**

### Difference Mapping Scripts

Developed by Mariena Silvestry Ramos and Phoebe L. Stewart



## Scripts for Difference Map Analysis

### Notes:

1. The following scripts work with the IMAGIC-5 release from 080206. IMAGIC commands can change depending on the release date, thus the command lines that call for each IMAGIC routine may vary from what is presented here. The order and/or specifications for the answers may vary too depending on the IMAGIC version/release.
2. To use the following difference mapping scripts several components are needed:
  - a. Experimental Map (the best cryoEM structure that has been calculated) in MRC (CCP4) format (possibly in  $750^3$  if the adenovirus sample is of the capsid alone or  $640^3$  or  $960^3$  if it is a complex).
  - b. Control Map in MRC format with dimensions of  $750^3$  (for adenovirus, this varies according to the sample).
  - c. Pixel sizes for both the experimental and control maps at their respective dimensions.
  - d. A “top” directory to which these scripts and the input maps should be copied.
  - e. When using these scripts for adenovirus difference mapping, you will need an initial PDB facet.

## DM-script # 1 – Prepares the maps

```
#!/bin/csh -f
echo " "
echo "DIFFERENCE MAP STEP 1"
echo "Please have full experimental map and control map in starting directory"
echo "Both maps should be in CCP4 format"
echo "Experimental map dimensions should be 6403"
echo "Control map should be 7503 "
echo "If Experimental map is at 9603, then comment out BLOWUP section"
echo " And fix input name to the next subfile section"
echo " "
# EDIT the following lines about the input
set TOP = (for example: /janus1/msilvest/diff_map_test1)
set MAINMAP = experimental_map.mrc
set CTRLMAP = control_map.mrc
set MAINPIX = pixel size for experimental map at 9603
set MAINPIX_640 = pixel size for experimental map at 6403
set CTRLPIX = pixel size for experimental map at 7503
set MAINRESN = final resolution of experimental map
set FRACTION = 2*CTRLPIX/MAINRESN
# Calculate fraction 2*CTRLPIX/MAINRESN
#Generate settings
set MAINMAPIMG = `echo $MAINMAP | awk -F. ' '`
set MAINMAPIMG_960 = $MAINMAPIMG"_960"
set MAINMAPIMG_750 = $MAINMAPIMG"_750"
set MAINMAPIMG_CH = $MAINMAPIMG"_ch"
set MAINMAPMRC_CH = $MAINMAPIMG"_ch.mrc"
```

```

set CTRLMAPIMG = `echo $CTRLMAP | awk -F. '{print $1}`
set CTRLMAPIMG_FILT = $CTRLMAPIMG"_filt"
set CTRLMAPIMG_FILT_ZOOM = $CTRLMAPIMG"_filt_zoom"

# Automatic main map conversion
echo "Performing main map conversion"
cd $TOP
echo "Performing main map conversion"
cd $TOP

/programs/imagi/imagi/stand/em2em.e << END1
CCP4
IMAGIC
3D
$MAINMAP
$MAINMAPIMG
$MAINPIX,$MAINPIX,$MAINPIX
YES
END1

/programs/imagi/imagi/threed/blowup3d.e << END2
BLOWUP
$MAINMAPIMG
$MAINMAPIMG_960
960,960,960
END2

/programs/imagi/imagi/threed/subfile3d.e << END3
$MAINMAPIMG_960
$MAINMAPIMG_750

```

```
CENTER
750,750,750
0,0,0
END3
```

```
rm -f *960*
echo "*****"
echo "Please proceed with dm-step2"
```

**DM-script # 2 – Cuts chunks of the experimental and control maps for display in later steps and filters control map**

```
#Generate settings
set MAINMAPIMG = `echo $MAINMAP | awk -F. '{print $1}`
set MAINMAPIMG_750 = $MAINMAPIMG"_750"
set MAINMAPIMG_CH = $MAINMAPIMG"_ch"
set MAINMAPMRC_CH = $MAINMAPIMG"_ch.mrc"
set CTRLMAPIMG = `echo $CTRLMAP | awk -F. '{print $1}`
set CTRLMAPIMG_FILTER = $CTRLMAPIMG"_filt"
set CTRLMAPIMG_FILTER_ZOOM = $CTRLMAPIMG"_filt_zoom"
/programs/imagc/imagc/threed/subfile3d.e << END1
$MAINMAPIMG_750
$MAINMAPIMG_CH
GENERAL
115,175,190
520,520,520
0,0,0
END1
/programs/imagc/imagc/stand/em2em.e << END2
```

```

IMAGIC
CCP4
3D
$MAINMAPIMG_CH
$MAINMAPMRC_CH
$MAINPIX,$MAINPIX,$MAINPIX
YES
END2
# Automatic control map conversion
echo "Performing control map conversion"
/programs/imagic/imagic/stand/em2em.e << END3
CCP4
IMAGIC
3D
$CTRLMAP
$CTRLMAPIMG
$CTRLPIX,$CTRLPIX,$CTRLPIX
YES
END3
/programs/imagic/imagic/threed/fft3d.e << END4
FILTER
$CTRLMAPIMG
$CTRLMAPIMG_FILT
GAUSS
$FRACTION
END4
echo "*****"

```

```
echo " Please proceed with dm-step3"
```

### **DM-script # 3 - Adjusts control map dimensions to match experimental map dimensions**

```
#!/bin/csh -f
```

```
echo " "
```

```
echo "DF-MAP STEP 3"
```

```
echo " "
```

```
# EDIT the following lines about the input (refer to previous steps to name files accordingly)
```

```
# IMPORTANT!!!! ENTER ZOOMF MANUALLY (CTRLPIX/MAINPIX)
```

```
# MAIN MAP is now the 750 version of the 640 version of your starting map
```

```
set TOP =
```

```
set MAINMAP =
```

```
set CTRLMAP =
```

```
set MAINPIX =
```

```
set CTRLPIX = CTRLPIX/MAINPIX
```

```
set MAINRESN =
```

```
set ZOOMF =
```

```
#Generate settings
```

```
set MAINMAPIMG = `echo $MAINMAP | awk -F. '{print $1}`
```

```
set MAINMAPIMG_CH = $MAINMAPIMG"_ch"
```

```
set MAINMAPMRC_CH = $MAINMAPIMG"_ch.mrc"
```

```
set CTRLMAPIMG = `echo $CTRLMAP | awk -F. '{print $1}`
```

```
set CTRLMAPIMG_FILTER = $CTRLMAPIMG"_filt"
```

```
set CTRLMAPIMG_FILTER_ZOOM = $CTRLMAPIMG"_filt_zoom"
```

```
set CTRLMAPIMG_FILTER_ZOOM_TRANS = $CTRLMAPIMG"_filt_zoom_trans"
```

```

set CTRLMAPIMG_FILT_ZOOM_TRANS_CH =
$CTRLMAPIMG"_filt_zoom_trans_ch"

set CTRLMAPMRC_FILT_ZOOM_TRANS_CH =
$CTRLMAPIMG"_filt_zoom_trans_ch.mrc"

/programs/imagi/imagi/threed/blowup3d.e << END1

ZOOM

$CTRLMAPIMG_FILT

$CTRLMAPIMG_FILT_ZOOM

$ZOOMF

END1

echo "*****"

echo "Please continue to dm-step4"

```

**DM-script # 4 – Cuts chunk of control map for later steps**

```

#!/bin/csh -f

echo " "

echo "DF-MAP STEP 4"

echo " "

# EDIT the following lines about the input (refer to previous steps to name files
accordingly)

set TOP =

set MAINMAP =

set CTRLMAP =

set MAINPIX =

set CTRLPIX =

set MAINRESN =

#Generate settings

```

```
set MAINMAPIMG = `echo $MAINMAP | awk -F. '{print $1}`  
set MAINMAPIMG_CH = $MAINMAPIMG"_ch"  
set MAINMAPMRC_CH = $MAINMAPIMG"_ch.mrc"  
set CTRLMAPIMG = `echo $CTRLMAP | awk -F. '{print $1}`  
set CTRLMAPIMG_FILT = $CTRLMAPIMG"_filt"  
set CTRLMAPIMG_FILT_ZOOM = $CTRLMAPIMG"_filt_zoom"  
set CTRLMAPIMG_FILT_ZOOM_TRANS = $CTRLMAPIMG"_filt_zoom_trans"  
set CTRLMAPIMG_FILT_ZOOM_TRANS_CH =  
$CTRLMAPIMG"_filt_zoom_trans_ch"  
set CTRLMAPMRC_FILT_ZOOM_TRANS_CH  
= $CTRLMAPIMG"_filt_zoom_trans_ch.mrc"  
echo "Aligning zoomed control map to cryo map"
```

```
/programs/imagi/imagi/threed/align3d.e << END1  
$CTRLMAPIMG_FILT_ZOOM  
$MAINMAPIMG  
YES  
$CTRLMAPIMG_FILT_ZOOM_TRANS  
NO  
YES  
0,0,0  
NO  
NO  
10  
scratch3d  
END1  
rm -f scratch3d.*  
/programs/imagi/imagi/threed/subfile3d.e << END2
```



```
$CTRLMAPIMG_FILT_ZOOM_TRANS
$CTRLMAPIMG_FILT_ZOOM_TRANS_CH
GENERAL
115,175,190
520,520,520
0,0,0
END2
/programs/imagi/imagi/stand/em2em.e << END3
IMAGIC
CCP4
3D
$CTRLMAPIMG_FILT_ZOOM_TRANS_CH
$CTRLMAPMRC_FILT_ZOOM_TRANS_CH
$MAINPIX,$MAINPIX,$MAINPIX
YES
END3
echo "The following two files are ready to look at in Chimera"
echo "Remember to set origin to 0,0,0"
echo $MAINMAPMRC_CH
echo $CTRLMAPMRC_FILT_ZOOM_TRANS_CH
echo "Please continue to df-step5"
```

**DM-script # 5 – Uses UCSF Chimera to coarsely position facet in PDB format within experimental map**

```
# INSTRUCTIONS
# Sit at alpha, beta or gamma and login
# cd to dir with threed...ch.mrc and coarserefn_facet_v1.pdb
# NOTE: You will need to cp coarserefn_facet_v1.pdb from another dir
```

```
# Edit the lines below to have the correct map chunk filename
# and correct voxel size
# Start chimera
# Get a command line window with favorites, command line
# In the Chimera command line type the following command:
# source df-step5
# When the Side view window opens, then it is time to do the following
# move x 40 (adjust number until facet is aligned in x
# move y 100 (adjust number until facet is aligned in y
# move z 90 (adjust number until facet is aligned in z
# write relative 0 1 coarserefn_facet_v2.pdb
# then close session and see df-step6
#
open experimental_map_chunk.mrc
volume #0 origin 0,0,0
volume #0 voxelsize ADD the correct voxel size here
volume #0 level 0.03
window
open coarserefn_facet_v1.pdb
~show #1
ribbon #1
window
~select 0
select 1
start Side View
#move x 10
#move y 10
```

```
#move z 10
#write relative 0 1 coarserefn_facet_v2.pdb
```

**DM-script # 6 - Saves individual coordinate files for each capsomer from the coarsely positioned facet from step 5**

```
#!/bin/csh -f
# EDIT SECTION BELOW and RUN THIS IN A TERMINAL WINDOW
echo " "
echo "DF-STEP6 SELECT CAPSID PROTEINS FROM FACET PDB"
echo " "
# EDIT the following lines about the input (refer to previous steps to name files accordingly)
set TOP =
set MAINMAPMRC_CH = experimental_map_chunk.mrc
set FACET_COARSE = coarserefn_facet_v2.pdb
set MAINPIX = experimental map pixel size
set MAINRESN = experimental map resolution
#Generate settings
set MAINMAP_CH = `echo $MAINMAPMRC_CH | awk -F. '{print $1}'`
echo "Selecting out hexon and penton coordinates from facet pdb file"
cat $FACET_COARSE | grep -v '^CONNECT' > temp1.pdb
cat temp1.pdb | grep -v '^HELIX' > temp2.pdb
cat temp2.pdb | grep -v '^SHEET' > temp3.pdb
cat temp3.pdb | grep -v '^TER' > temp4.pdb
head -n 21002 temp4.pdb | tail -n 21002 > hex1a_pre_refn.pdb
head -n 42004 temp4.pdb | tail -n 21002 > hex2a_pre_refn.pdb
head -n 63006 temp4.pdb | tail -n 21002 > hex3a_pre_refn.pdb
head -n 84008 temp4.pdb | tail -n 21002 > hex4a_pre_refn.pdb
```

```
head -n 105010 temp4.pdb | tail -n 21002 > hex1b_pre_refn.pdb
head -n 126012 temp4.pdb | tail -n 21002 > hex2b_pre_refn.pdb
head -n 147014 temp4.pdb | tail -n 21002 > hex3b_pre_refn.pdb
head -n 168016 temp4.pdb | tail -n 21002 > hex4b_pre_refn.pdb
head -n 189018 temp4.pdb | tail -n 21002 > hex1c_pre_refn.pdb
head -n 210020 temp4.pdb | tail -n 21002 > hex2c_pre_refn.pdb
head -n 231022 temp4.pdb | tail -n 21002 > hex3c_pre_refn.pdb
head -n 252024 temp4.pdb | tail -n 21002 > hex4c_pre_refn.pdb
head -n 273026 temp4.pdb | tail -n 21002 > hex1d_pre_refn.pdb
head -n 294028 temp4.pdb | tail -n 21002 > hex2d_pre_refn.pdb
head -n 315030 temp4.pdb | tail -n 21002 > hex1e_pre_refn.pdb
head -n 336032 temp4.pdb | tail -n 21002 > hex2e_pre_refn.pdb
head -n 357034 temp4.pdb | tail -n 21002 > hex1f_pre_refn.pdb
head -n 378036 temp4.pdb | tail -n 21002 > hex2f_pre_refn.pdb
head -n 396063 temp4.pdb | tail -n 18027 > pena_pre_refn.pdb
head -n 414090 temp4.pdb | tail -n 18027 > penb_pre_refn.pdb
head -n 432117 temp4.pdb | tail -n 18027 > penc_pre_refn.pdb

rm temp1.pdb
rm temp2.pdb
rm temp3.pdb
rm temp4.pdb

echo "*****"
echo "Please continue with df-step7"
```

**DM-script # 7 – Uses UCSF Chimera to select and refine the positions of individual hexons and penton bases in the facet**

# INSTRUCTIONS

# Sit at alpha, beta or gamma and login

```

# cd to dir with threed...ch.mrc and hex1a_pre_refn.pdb etc.
# Edit the lines below to have the correct map chunk filename
# and correct voxel size
# Start chimera
# Get a command line window with favorites, command line
# In the Chimera command line type the following command:
# source df-step7
# When the Side view window opens, then it is time to do the following
# Click on Fit button in Fit Model in Map
# Click on Fit button in Fit Model in Map a second time
#
##### REPEAT FOR SECOND PROTEIN #####
# select #2
# Click on Fit button in Fit Model in Map
# Click on Fit button in Fit Model in Map a second time
#
##### REPEAT FOR THIRD PROTEIN #####
# select #3
# Click on Fit button in Fit Model in Map
# Click on Fit button in Fit Model in Map a second time
#
##### REPEAT FOR REST OF THE PROTEINS UNTIL #####
# select #21
# Click on Fit button in Fit Model in Map
# Click on Fit button in Fit Model in Map a second time
#
##### FINAL STEPS #####

```

```
# at command line type
# source df-step8
# In Chimera below the command line you will see a message about
# which file it wrote. When it has finished writing the penc file
# you may close chimera and move on to df-step9.
##### NOTE #####
# NOTE - the Fit Model in Map result is the same
# even when the map is coarsely displayed, at 8 or 4 or 1
#
open experimental_map_chunk.mrc
volume #0 origin 0,0,0
volume #0 voxelsize ADD the correct voxel size here
volume #0 level 0.03
window
open hex1a_pre_refn.pdb
open hex2a_pre_refn.pdb
open hex3a_pre_refn.pdb
open hex4a_pre_refn.pdb
open hex1b_pre_refn.pdb
open hex2b_pre_refn.pdb
open hex3b_pre_refn.pdb
open hex4b_pre_refn.pdb
open hex1c_pre_refn.pdb
open hex2c_pre_refn.pdb
open hex3c_pre_refn.pdb
open hex4c_pre_refn.pdb
open hex1d_pre_refn.pdb
```

```
open hex2d_pre_refn.pdb
open hex1e_pre_refn.pdb
open hex2e_pre_refn.pdb
open hex1f_pre_refn.pdb
open hex2f_pre_refn.pdb
open pena_pre_refn.pdb
open penb_pre_refn.pdb
open penc_pre_refn.pdb
~show #1-21
ribbon #1-21
window
~select 0
select 1
select #1
start Fit Model in Map
start Side View
```

**DM-script # 8 – The docked coordinates for each hexon and penton base in step 7 are saved relative to the experimental map**

**# INSTRUCTIONS**

# When you have completed all of the manual fits in chimera (df-step7)

# then at Chimera command line type the following

# source df-step8

# and the fit coordinates will be saved to 21 files

```
write relative 0 1 hex1a_post_refn.pdb
```

```
write relative 0 2 hex2a_post_refn.pdb
```

```
write relative 0 3 hex3a_post_refn.pdb
```

```
write relative 0 4 hex4a_post_refn.pdb
```

```
write relative 0 5 hex1b_post_refn.pdb
write relative 0 6 hex2b_post_refn.pdb
write relative 0 7 hex3b_post_refn.pdb
write relative 0 8 hex4b_post_refn.pdb
write relative 0 9 hex1c_post_refn.pdb
write relative 0 10 hex2c_post_refn.pdb
write relative 0 11 hex3c_post_refn.pdb
write relative 0 12 hex4c_post_refn.pdb
write relative 0 13 hex1d_post_refn.pdb
write relative 0 14 hex2d_post_refn.pdb
write relative 0 15 hex1e_post_refn.pdb
write relative 0 16 hex2e_post_refn.pdb
write relative 0 17 hex1f_post_refn.pdb
write relative 0 18 hex2f_post_refn.pdb
write relative 0 19 pena_post_refn.pdb
write relative 0 20 penb_post_refn.pdb
write relative 0 21 penc_post_refn.pdb
```

**DM-script # 9 – Converts all the hexon and penton base PDB files to a density map (MRC/CCP4 format), filters the calculated map to the appropriate resolution. Note that the PDB2MRC command with the “center” option in this script applies an unwanted translation to the calculated map. Therefore this script also aligns the calculated map with the experimental map using the IMAGIC threed-align (align3d.e) command.**

```
#!/bin/csh -f
```

```
echo " "
```

```
echo "DF-MAP STEP 9"
```

```
echo "Please have map chunk and 18 hexon and 3 penton pdb files in the
starting directory"
```

```
echo "The hexon pdbs should be named with the following convention"
```



```

echo "hex1a_post_refn.pdb"
echo "The penton pdbs should be named with the following convention"
echo "pena_post_refn.pdb"
echo " "
# EDIT the following lines about the input (refer to previous steps to name files
accordingly)
set TOP =
set SAMP = name of the experimental map
set DIFN = difference map test number (if you have run other diffmap rounds)
set MAP_CHUNK = experimental map chunk
set MAINPIX = experimental map pixel size
set RESN = experimental map resolution
set BOX = 520
cd $TOP
echo "Putting all hexon coords into one file"
set HEXPDB = "facet_18hexon_"$SAMP_"$DIFN".pdb"
set HEXMRC = "facet_18hexon_"$SAMP_"$DIFN".mrc"
set HEXIMG = "facet_18hexon_"$SAMP_"$DIFN
set HEXIMG_TRANS = "facet_18hexon_"$SAMP_"$DIFN"_trans"
set HEXMRC_TRANS = "facet_18hexon_"$SAMP_"$DIFN"_trans.mrc"
cat hex1a_post_refn.pdb | grep '^ATOM' > $HEXPDB
cat hex2a_post_refn.pdb | grep '^ATOM' >> $HEXPDB
cat hex3a_post_refn.pdb | grep '^ATOM' >> $HEXPDB
cat hex4a_post_refn.pdb | grep '^ATOM' >> $HEXPDB
cat hex1b_post_refn.pdb | grep '^ATOM' >> $HEXPDB
cat hex2b_post_refn.pdb | grep '^ATOM' >> $HEXPDB
cat hex3b_post_refn.pdb | grep '^ATOM' >> $HEXPDB
cat hex4b_post_refn.pdb | grep '^ATOM' >> $HEXPDB

```

```

cat hex1c_post_refn.pdb | grep '^ATOM' >> $HEXPDB
cat hex2c_post_refn.pdb | grep '^ATOM' >> $HEXPDB
cat hex3c_post_refn.pdb | grep '^ATOM' >> $HEXPDB
cat hex4c_post_refn.pdb | grep '^ATOM' >> $HEXPDB
cat hex1d_post_refn.pdb | grep '^ATOM' >> $HEXPDB
cat hex2d_post_refn.pdb | grep '^ATOM' >> $HEXPDB
cat hex1e_post_refn.pdb | grep '^ATOM' >> $HEXPDB
cat hex2e_post_refn.pdb | grep '^ATOM' >> $HEXPDB
cat hex1f_post_refn.pdb | grep '^ATOM' >> $HEXPDB
cat hex2f_post_refn.pdb | grep '^ATOM' >> $HEXPDB
echo "Putting all penton coords into one file"
set PENTPDB = "facet_3penton_"$SAMP_"$DIFN".pdb"
set PENTMRC = "facet_3penton_"$SAMP_"$DIFN".mrc"
set PENTIMG = "facet_3penton_"$SAMP_"$DIFN
set PENTIMG_TRANS = "facet_3penton_"$SAMP_"$DIFN"_trans"
set PENTMRC_TRANS = "facet_3penton_"$SAMP_"$DIFN"_trans.mrc"
cat pena_post_refn.pdb | grep '^ATOM' > $PENTPDB
cat penb_post_refn.pdb | grep '^ATOM' >> $PENTPDB
cat penc_post_refn.pdb | grep '^ATOM' >> $PENTPDB
echo "Making complete facet with hexon and penton pdbs"
set FACETPDB = "facet_18hex3pent_"$SAMP_"$DIFN".pdb"
set FACETMRC = "facet_18hex3pent_"$SAMP_"$DIFN".mrc"
set FACETIMG = "facet_18hex3pent_"$SAMP_"$DIFN
set FACETIMG_TRANS = "facet_18hex3pent_"$SAMP_"$DIFN"_trans"
set FACETMRC_TRANS = "facet_18hex3pent_"$SAMP_"$DIFN"_trans.mrc"
cat $HEXPDB > $FACETPDB
cat $PENTPDB >> $FACETPDB

```

```
echo "Converting complete facet with penton and hexon pdb files to mrc"

/programs/EMAN/bin/pdb2mrc $FACETPDB $FACETMRC apix=$MAINPIX
res=$RESN box=$BOX center

/programs/imagick/imagick/stand/em2em.e << END7

CCP4

IMAGIC

3D

$FACETMRC

$FACETIMG

$MAINPIX,$MAINPIX,$MAINPIX

YES

END7

echo "Aligning facet MRC to map chunk"

/programs/imagick/imagick/threed/align3d.e << END10

$FACETIMG

$MAP_CHUNK

YES

$FACETIMG_TRANS

NO

YES

0,0,200

NO

NO

10

scratch3d3

END10

rm -f scratch*

/programs/imagick/imagick/stand/em2em.e << END13
```

```

IMAGIC
CCP4
3D
$FACETIMG_TRANS
$FACETMRC_TRANS
$MAINPIX,$MAINPIX,$MAINPIX
YES
END13
echo " "
echo "*****"
echo "The following files are ready for Chimera"
echo "Remember to set origin to 0 0 0 for all MRC files"
echo $MAP_CHUNK
echo $FACETMRC_TRANS
echo "Select Thresh level for each map in Chimera"
echo "Then continue with df-step10"

```

**DM-script # 10 – Normalizes the cryoEM maps and calculated facet**

```

#!/bin/csh -f
echo " "
echo "DF-MAP STEP 10"
echo " "
echo " Remember to change thresh value to appropriate value"
echo " as obtained from Chimera in step "
# EDIT the following lines about the input (refer to previous steps to name files
accordingly)
set TOP =

```

```

set SAMP =
set DIFN =
set MAP_CHUNK =
set MAP_CTRL =
set MAINPIX =
set RESN =
set BOX = 520
set FACET = facet_18hex3pent_
# Settings from df-step9
set MAP1 = `echo $MAP_CHUNK | awk -F. '{print $1}`
set MAP_IMG = $MAP1
set MAP_CTRLMRC = $MAP_CTRL".mrc"
set FACETPDB = "facet_18hex3pent_"$SAMP_"$DIFN".pdb"
set FACETMRC = "facet_18hex3pent_"$SAMP_"$DIFN".mrc"
set FACETIMG = "facet_18hex3pent_"$SAMP_"$DIFN
set FACETIMG_TRANS = "facet_18hex3pent_"$SAMP_"$DIFN"_trans"
set FACETMRC_TRANS = "facet_18hex3pent_"$SAMP_"$DIFN"_trans.mrc"
set FACETIMG_TRANS_NORM =
"facet_18hex3pent_"$SAMP_"$DIFN"_trans_norm"
set FACETMRC_TRANS_NORM =
"facet_18hex3pent_"$SAMP_"$DIFN"_trans_norm.mrc"
# Settings for df-step10
set MAP_IMG_NORM = $MAP1"_norm"
set MAP_MRC_NORM = $MAP1"_norm.mrc"
set MAP_IMG_NORM_ADD = $MAP1"_norm_add"
set MAP_IMG_NORM_ADD_THR = $MAP1"_norm_add_thr"
set MAP_CTRL_NORM = $MAP_CTRL"_norm"
set MAP_CTRL_NORM_MRC = $MAP_CTRL"_norm.mrc"

```

```

set MAP_CTRL_NORM_ADD = $MAP_CTRL"_norm_add"
set MAP_CTRL_NORM_ADD_THR = $MAP_CTRL"_norm_add_thr"
set FACETIMG_TRANS_THR =
"facet_18hex3pent_"$SAMP_"$DIFN"_trans_thr"
set FACETIMG_TRANS_THR_NORM =
"facet_18hex3pent_"$SAMP_"$DIFN"_trans_thr_norm"
set DIFFIMG_CRYO_MIN_FACET = "diff_cryo_min_facet_"$SAMP_"$DIFN
set DIFFMRC_CRYO_MIN_FACET =
"diff_cryo_min_facet_"$SAMP_"$DIFN".mrc"
set DIFFIMG_CRYO_MIN_MAP_CTRL =
"diff_cryo_min_map_ctrl_"$SAMP_"$DIFN
set DIFFMRC_CRYO_MIN_MAP_CTRL =
"diff_cryo_min_map_ctrl_"$SAMP_"$DIFN".mrc"
set DIFFIMG_MAP_CTRL_MIN_CRYO =
"diff_map_ctrl_min_cryo_"$SAMP_"$DIFN
set DIFFMRC_MAP_CTRL_MIN_CRYO =
"diff_map_ctrl_min_cryo_"$SAMP_"$DIFN".mrc"
cd $TOP

```

```

/programs/imagc/imagc/threed/norm3d.e << END1

```

```

$MAP_IMG

```

```

$MAP_IMG_NORM

```

```

NORM

```

```

10.0

```

```

END1

```

```

/programs/imagc/imagc/threed/norm3d.e << END2

```

```

$MAP_CTRL

```

```

$MAP_CTRL_NORM

```

```

NORM

```

```

10.0

```

```
END2
/programs/imagic/imagic/threed/norm3d.e << END3
$FACETIMG_TRANS
$FACETIMG_TRANS_NORM
NORM
10.0
END3
echo "*****"
echo " Preparing facet for ccp4 conversion and normalization"
echo "*****"
/programs/imagic/imagic/stand/headers.e << END4
$FACETIMG_TRANS
WRITE
INDEX
61
INTERACTIVE
0
END4
/programs/imagic/imagic/stand/em2em.e << END 5
IMAGIC
CCP4
3D
$FACETIMG_TRANS_NORM
$FACETMRC_TRANS_NORM
$MAINPIX,$MAINPIX,$MAINPIX
YES
END5
```

```
echo "*****"
```

```
echo "Please continue with df-step11"
```

**DM-script # 11 – Steps 11 to 13 are necessary to apply the appropriate threshold values to all the maps (experimental, control and facet) to ensure that the subtraction process is performed correctly.**

```
#!/bin/csh -f
```

```
echo " "
```

```
echo "DF-MAP STEP 10"
```

```
echo " "
```

```
echo " Remember to change thresh value to appropriate value"
```

```
echo " as obtained from Chimera in step "
```

```
# EDIT the following lines about the input (refer to previous steps to name files accordingly)
```

```
set TOP =
```

```
set SAMP =
```

```
set DIFN =
```

```
set MAP_CHUNK =
```

```
set MAP_CTRL =
```

```
set MAINPIX =
```

```
set RESN =
```

```
set BOX = 520
```

```
set FACET = facet_18hex3pent_
```

```
# Settings from df-step9
```

```
set MAP1 = `echo $MAP_CHUNK | awk -F. '{print $1}'`
```

```
set MAP_IMG = $MAP1
```

```
set MAP_CTRLMRC = $MAP_CTRL".mrc"
```

```
set FACETPDB = "facet_18hex3pent_"$SAMP_"$DIFN".pdb"
```



```

set FACETMRC = "facet_18hex3pent_"$SAMP_"$DIFN".mrc"
set FACETIMG = "facet_18hex3pent_"$SAMP_"$DIFN
set FACETIMG_TRANS = "facet_18hex3pent_"$SAMP_"$DIFN"_trans"
set FACETMRC_TRANS = "facet_18hex3pent_"$SAMP_"$DIFN"_trans.mrc"

set FACETIMG_TRANS_NORM =
"facet_18hex3pent_"$SAMP_"$DIFN"_trans_norm"

set FACETMRC_TRANS_NORM =
"facet_18hex3pent_"$SAMP_"$DIFN"_trans_norm.mrc"

# Settings for df-step10

set MAP_IMG_NORM = $MAP1"_norm"
set MAP_MRC_NORM = $MAP1"_norm.mrc"
set MAP_IMG_NORM_ADD = $MAP1"_norm_add"
set MAP_IMG_NORM_ADD_THR = $MAP1"_norm_add_thr"
set MAP_CTRL_NORM = $MAP_CTRL"_norm"
set MAP_CTRL_NORM_MRC = $MAP_CTRL"_norm.mrc"
set MAP_CTRL_NORM_ADD = $MAP_CTRL"_norm_add"
set MAP_CTRL_NORM_ADD_THR = $MAP_CTRL"_norm_add_thr"

set FACETIMG_TRANS_THR =
"facet_18hex3pent_"$SAMP_"$DIFN"_trans_thr"

set FACETIMG_TRANS_THR_NORM =
"facet_18hex3pent_"$SAMP_"$DIFN"_trans_thr_norm"

set DIFFIMG_CRYO_MIN_FACET = "diff_cryo_min_facet_"$SAMP_"$DIFN
set DIFFMRC_CRYO_MIN_FACET =
"diff_cryo_min_facet_"$SAMP_"$DIFN".mrc"

set DIFFIMG_CRYO_MIN_MAP_CTRL =
"diff_cryo_min_map_ctrl_"$SAMP_"$DIFN
set DIFFMRC_CRYO_MIN_MAP_CTRL =
"diff_cryo_min_map_ctrl_"$SAMP_"$DIFN".mrc"

set DIFFIMG_MAP_CTRL_MIN_CRYO =
"diff_map_ctrl_min_cryo_"$SAMP_"$DIFN

```

```
set DIFFMRC_MAP_CTRL_MIN_CRYO =
"diff_map_ctrl_min_cryo_"$SAMP_"_$DIFN".mrc"

cd $TOP

/programs/imagic/imagic/stand/em2em.e << END 1

IMAGIC

CCP4

3D

$MAP_IMG_NORM

$MAP_MRC_NORM

$MAINPIX,$MAINPIX,$MAINPIX

YES

END1

/programs/imagic/imagic/stand/em2em.e << END 2

IMAGIC

CCP4

3D

$MAP_CTRL_NORM

$MAP_CTRL_NORM_MRC

$MAINPIX,$MAINPIX,$MAINPIX

YES

END2

echo "*****"

echo "Please continue with df-step12"
```

**DM-script # 12 - Steps 11 to 13 are necessary to apply the appropriate threshold values to all the maps (experimental, control and facet) to ensure that the subtraction process is performed correctly.**

```
#!/bin/csh -f

echo " "

echo "DF-MAP STEP 10"

echo " "

echo " Remember to change thresh value to appropriate value"

echo " as obtained from Chimera in step "

# EDIT the following lines about the input (refer to previous steps to name files
accordingly)

set TOP =

set SAMP =

set DIFN =

set MAP_CHUNK =

set MAP_CTRL =

set MAINPIX =

set RESN =

set BOX = 520

set FACET = facet_18hex3pent_

# Settings from df-step9

set MAP1 = `echo $MAP_CHUNK | awk -F. '{print $1}`

set MAP_IMG = $MAP1

set MAP_CTRLMRC = $MAP_CTRL".mrc"

set FACETPDB = "facet_18hex3pent_"$SAMP_"$DIFN".pdb"

set FACETMRC = "facet_18hex3pent_"$SAMP_"$DIFN".mrc"

set FACETIMG = "facet_18hex3pent_"$SAMP_"$DIFN

set FACETIMG_TRANS = "facet_18hex3pent_"$SAMP_"$DIFN"_trans"
```

```

set FACETMRC_TRANS = "facet_18hex3pent_"$SAMP_"$DIFN"_trans.mrc"

set FACETIMG_TRANS_NORM =
"facet_18hex3pent_"$SAMP_"$DIFN"_trans_norm"

set FACETMRC_TRANS_NORM =
"facet_18hex3pent_"$SAMP_"$DIFN"_trans_norm.mrc"

# Settings for df-step10

set MAP_IMG_NORM = $MAP1"_norm"
set MAP_MRC_NORM = $MAP1"_norm.mrc"
set MAP_IMG_NORM_ADD = $MAP1"_norm_add"
set MAP_IMG_NORM_ADD_THR = $MAP1"_norm_add_thr"
set MAP_CTRL_NORM = $MAP_CTRL"_norm"
set MAP_CTRL_NORM_MRC = $MAP_CTRL"_norm.mrc"
set MAP_CTRL_NORM_ADD = $MAP_CTRL"_norm_add"
set MAP_CTRL_NORM_ADD_THR = $MAP_CTRL"_norm_add_thr"

set FACETIMG_TRANS_THR =
"facet_18hex3pent_"$SAMP_"$DIFN"_trans_thr"

set FACETIMG_TRANS_THR_NORM =
"facet_18hex3pent_"$SAMP_"$DIFN"_trans_thr_norm"

set DIFFIMG_CRYO_MIN_FACET = "diff_cryo_min_facet_"$SAMP_"$DIFN

set DIFFMRC_CRYO_MIN_FACET =
"diff_cryo_min_facet_"$SAMP_"$DIFN".mrc"

set DIFFIMG_CRYO_MIN_MAP_CTRL =
"diff_cryo_min_map_ctrl_"$SAMP_"$DIFN

set DIFFMRC_CRYO_MIN_MAP_CTRL =
"diff_cryo_min_map_ctrl_"$SAMP_"$DIFN".mrc"

set DIFFIMG_MAP_CTRL_MIN_CRYO =
"diff_map_ctrl_min_cryo_"$SAMP_"$DIFN

set DIFFMRC_MAP_CTRL_MIN_CRYO =
"diff_map_ctrl_min_cryo_"$SAMP_"$DIFN".mrc"

cd $TOP

/programs/imagc/imagc/stand/em2em.e << END 4

```

```

IMAGIC
CCP4
3D
$MAP_CTRL_NORM
$MAP_CTRL_NORM_MRC
$MAINPIX,$MAINPIX,$MAINPIX
YES
END4
echo "*****"
echo "Now look at MRC files for cryomap, map ctrl and facet"
echo "Decide on add values for difference map calculation"

```

**DM-script # 13 - Steps 11 to 13 are necessary to apply the appropriate threshold values to all the maps (experimental, control and facet) to ensure that the subtraction process is performed correctly.**

```

#!/bin/csh -f
echo " "
echo "DF-MAP STEP 10"
echo " "
echo " Remember to change thresh value to appropriate value"
echo " as obtained from Chimera in step "
# EDIT the following lines about the input (refer to previous steps to name files
accordingly)
set TOP =
set SAMP =
set DIFN =
set MAP_CHUNK =
set MAP_CTRL =

```

```

set MAINPIX =
set RESN =
set BOX = 520
set FACET = facet_18hex3pent_
# Settings from df-step9
set MAP1 = `echo $MAP_CHUNK | awk -F. '{print $1}`
set MAP_IMG = $MAP1
set MAP_CTRLMRC = $MAP_CTRL".mrc"
set FACETPDB = "facet_18hex3pent_"$SAMP_"$DIFN".pdb"
set FACETMRC = "facet_18hex3pent_"$SAMP_"$DIFN".mrc"
set FACETIMG = "facet_18hex3pent_"$SAMP_"$DIFN
set FACETIMG_TRANS = "facet_18hex3pent_"$SAMP_"$DIFN"_trans"
set FACETMRC_TRANS = "facet_18hex3pent_"$SAMP_"$DIFN"_trans.mrc"
# Settings for df-step10
set MAP_IMG_NORM = $MAP1"_norm"
set MAP_IMG_NORM_ADD = $MAP1"_norm_add"
set MAP_IMG_NORM_ADD_THR = $MAP1"_norm_add_thr"
set MAP_CTRL_NORM = $MAP_CTRL"_norm"
set MAP_CTRL_NORM_ADD = $MAP_CTRL"_norm_add"
set MAP_CTRL_NORM_ADD_THR = $MAP_CTRL"_norm_add_thr"
set FACETIMG_TRANS_THR =
"facet_18hex3pent_"$SAMP_"$DIFN"_trans_thr"
set FACETIMG_TRANS_THR_NORM =
"facet_18hex3pent_"$SAMP_"$DIFN"_trans_thr_norm"
set DIFFIMG_CRYO_MIN_FACET = "diff_cryo_min_facet_"$SAMP_"$DIFN
set DIFFMRC_CRYO_MIN_FACET =
"diff_cryo_min_facet_"$SAMP_"$DIFN".mrc"
set DIFFIMG_CRYO_MIN_MAP_CTRL =
"diff_cryo_min_map_ctrl_"$SAMP_"$DIFN

```

```
set DIFFMRC_CRYO_MIN_MAP_CTRL =  
"diff_cryo_min_map_ctrl_"$SAMP_"$DIFN".mrc"
```

```
set DIFFIMG_MAP_CTRL_MIN_CRYO =  
"diff_map_ctrl_min_cryo_"$SAMP_"$DIFN"
```

```
set DIFFMRC_MAP_CTRL_MIN_CRYO =  
"diff_map_ctrl_min_cryo_"$SAMP_"$DIFN".mrc"
```

```
cd $TOP
```

```
/programs/imagic/imagic/threed/inc3dmenu.e << END2
```

```
ARITHMETIC
```

```
ADD
```

```
$MAP_IMG_NORM
```

```
$MAP_IMG_NORM_ADD
```

```
Write the appropriate value here as determined by using UCSF Chimera
```

```
END2
```

```
/programs/imagic/imagic/threed/inc3dmenu.e << END3
```

```
THRESH
```

```
$MAP_IMG_NORM_ADD
```

```
$MAP_IMG_NORM_ADD_THR
```

```
BELOW
```

```
0
```

```
END3
```

```
/programs/imagic/imagic/threed/inc3dmenu.e << END5
```

```
ARITHMETIC
```

```
ADD
```

```
$MAP_CTRL_NORM
```

```
$MAP_CTRL_NORM_ADD
```

```
Write the appropriate value here as determined by using UCSF Chimera
```

```

END5
/programs/imagick/imagick/threed/inc3dmenu.e << END6
THRESH
$MAP_CTRL_NORM_ADD
$MAP_CTRL_NORM_ADD_THR
BELOW
0
END6
rm -f *750*.img
rm -f *750*.hed
rm -f *pre*.pdb
echo "*****"
echo "Now you are ready to perform the difference maps"

```

### **DM-script # 14 – Calculates difference maps**

```

#!/bin/csh -f
echo " "
echo "DF-MAP STEP 10"
echo " "
echo " Remember to change thresh value to appropriate value"
echo " as obtained from Chimera in step "

# EDIT the following lines about the input
set TOP =
set SAMP =
set DIFN = dm4

```



```

set MAP_CHUNK =
set MAP_CTRL =
set MAINPIX =
set RESN =
set BOX = 520
set FACET = facet_18hex3pent_
# Settings from df-step10
set MAP1 = `echo $MAP_CHUNK | awk -F. '{print $1}`
set MAP_IMG = $MAP1
set MAP_MRC = $MAP1".mrc"
set MAP_CTRLMRC = $MAP_CTRL".mrc"
set FACETPDB = "facet_18hex3pent_"$SAMP"_"$DIFN".pdb"
set FACETMRC = "facet_18hex3pent_"$SAMP"_"$DIFN".mrc"
set FACETIMG = "facet_18hex3pent_"$SAMP"_"$DIFN
set FACETIMG_TRANS = "facet_18hex3pent_"$SAMP"_"$DIFN"_trans"
set FACETMRC_TRANS = "facet_18hex3pent_"$SAMP"_"$DIFN"_trans.mrc"
# Settings for df-step11
set MAP_IMG_NORM = $MAP1"_norm"
set MAP_IMG_NORM_ADD = $MAP1"_norm_add"
set MAP_IMG_NORM_ADD_THR = $MAP1"_norm_add_thr"
set MAP_CTRL_NORM = $MAP_CTRL"_norm"
set MAP_CTRL_NORM_ADD = $MAP_CTRL"_norm_add"
set MAP_CTRL_NORM_ADD_THR = $MAP_CTRL"_norm_add_thr"
set FACETIMG_TRANS = "facet_18hex3pent_"$SAMP"_"$DIFN"_trans"

```

```

set FACETIMG_TRANS_NORM =
"facet_18hex3pent_"$SAMP_"$DIFN"_trans_norm"

set DIFFIMG_CRYO_MIN_FACET = "diff_cryo_min_facet_"$SAMP_"$DIFN

set DIFFMRC_CRYO_MIN_FACET =
"diff_cryo_min_facet_"$SAMP_"$DIFN".mrc"

set DIFFIMG_CRYO_MIN_MAP_CTRL =
"diff_cryo_min_map_ctrl_"$SAMP_"$DIFN

set DIFFMRC_CRYO_MIN_MAP_CTRL =
"diff_cryo_min_map_ctrl_"$SAMP_"$DIFN".mrc"

set DIFFIMG_MAP_CTRL_MIN_CRYO =
"diff_map_ctrl_min_cryo_"$SAMP_"$DIFN

set DIFFMRC_MAP_CTRL_MIN_CRYO =
"diff_map_ctrl_min_cryo_"$SAMP_"$DIFN".mrc"

cd $TOP

echo "*****"

echo "Creating difference maps"

echo "*****"

/programs/imagic/imagic/threed/inc3dmenu.e << END10

TWO3DIM

SUBTRACT

$MAP_IMG

$FACETIMG_TRANS_NORM

$DIFFIMG_CRYO_MIN_FACET

END10

/programs/imagic/imagic/threed/inc3dmenu.e << END12

TWO3DIM

SUBTRACT

```

```
$MAP_IMG
$MAP_CTRL_NORM_ADD_THR
$DIFFIMG_CRYO_MIN_MAP_CTRL
END12
/programs/imagick/imagick/threed/inc3dmenu.e << END14
TWO3DIM
SUBTRACT
$MAP_CTRL_NORM_ADD_THR
$MAP_IMG
$DIFFIMG_MAP_CTRL_MIN_CRYO
END14
/programs/imagick/imagick/stand/em2em.e << END15
IMAGIC
CCP4
3D
$DIFFIMG_MAP_CTRL_MIN_CRYO
$DIFFMRC_MAP_CTRL_MIN_CRYO
$MAINPIX,$MAINPIX,$MAINPIX
YES
END15
/programs/imagick/imagick/stand/em2em.e << END11
IMAGIC
CCP4
3D
$DIFFIMG_CRYO_MIN_FACET
```

```

$DIFFMRC_CRYO_MIN_FACET
$MAINPIX,$MAINPIX,$MAINPIX
YES
END11
/programs/imagc/imagc/stand/em2em.e << END13
IMAGIC
CCP4
3D
$DIFFIMG_CRYO_MIN_FACET
$DIFFMRC_CRYO_MIN_MAP_CTRL
$MAINPIX,$MAINPIX,$MAINPIX
YES
END13

echo " "
echo "*****"
echo "The following file is ready for Chimera"
echo "Remember to set origin to 0 0 0 for all MRC files"
echo $DIFFMRC_CRYO_MIN_FACET
echo $DIFFMRC_CRYO_MIN_MAP_CTRL
echo $DIFFMRC_MAP_CTRL_MIN_CRYO
echo "Cut chunks of the diff-density to easy viewing in Chimera at 1,1,1"

```

## **Appendix 2**

Adenovirus serotype 5 hexon is critical for virus infection of hepatocytes in vivo

O. Kalyuzhniy , N.C. Di Paolo, M. Silvestry, S.E. Hofherr, M.A. Barry,

P.L. Stewart, and D.M. Shayakhmetov

Proceedings of the National Academy of Sciences U S A. Apr 8;105(14):5483-8.

2008

### **Appendix 3**

Visualization of alpha-helices in a 6-angstrom resolution cryoelectron microscopy structure of adenovirus allows refinement of capsid protein assignments

Susan D. Saban, Mariena Silvestry, Glen R. Nemerow, and Phoebe L. Stewart

Journal of Virology Dec;80(24):12049-59. 2006

## **Appendix 4**

Targeting vault nanoparticles to specific cell surface receptors

V.A. Kickhoefer, M. Han, S. Raval-Fernandes, M.J. Poderycki, R.J. Moniz, D.

Vaccari, M. Silvestry, P.L. Stewart, K.A. Kelly, and L.H. Rome

ACS Nano. Jan 27;3(1):27-36. 2009

## REFERENCES

1. **Adiga, U., W. T. Baxter, R. J. Hall, B. Rockel, B. K. Rath, J. Frank, and R. Glaeser.** 2005. Particle picking by segmentation: a comparative study with SPIDER-based manual particle picking. *J Struct Biol* **152**:211-220.
2. **Alba, R., A. C. Bradshaw, A. L. Parker, D. Bhella, S. N. Waddington, S. A. Nicklin, N. van Rooijen, J. Custers, J. Goudsmit, D. H. Barouch, J. H. McVey, and A. H. Baker.** 2009. Identification of coagulation factor (F)X binding sites on the adenovirus serotype 5 hexon: effect of mutagenesis on FX interactions and gene transfer. *Blood*. In Press
3. **Anderson, C. W.** 1990. The proteinase polypeptide of adenovirus serotype 2 virions. *Virology* **177**:259-272.
4. **Baker, A. H., J. H. McVey, S. N. Waddington, N. C. Di Paolo, and D. M. Shayakhmetov.** 2007. The influence of blood on in vivo adenovirus bio-distribution and transduction. *Mol Ther* **15**:1410-1416.
5. **Bangari, D. S., and S. K. Mittal.** 2006. Current strategies and future directions for eluding adenoviral vector immunity. *Curr Gene Ther* **6**:215-226.
6. **Begin, M., and J. Weber.** 1975. Genetic analysis of adenovirus type 2. I. Isolation and genetic characterization of temperature-sensitive mutants. *J Virol* **15**:1-7.
7. **Bergelson, J. M., J. A. Cunningham, G. Droguett, E. A. Kurt-Jones, A. Krithivas, J. S. Hong, M. S. Horwitz, R. L. Crowell, and R. W. Finberg.** 1997. Isolation of a common receptor for Coxsackie B viruses and adenoviruses 2 and 5. *Science* **275**:1320-1323.
8. **Bernard M. Fields, D. M. K., Peter M. Howley, Robert M. Chanock, Joseph L. Melnick, Thomas P. Monath, Bernard Roizman and Stephen E. Straus.** 1996. Fields Virology, p. 2111-2172. *In* B. N. Fields (ed.), *Fields Virology*, 3rd ed, vol. 2. Lippincott-Raven, Philadelphia.
9. **Brown, D. T., M. Westphal, B. T. Burlingham, U. Winterhoff, and W. Doerfler.** 1975. Structure and composition of the adenovirus type 2 core. *J Virol* **16**:366-387.
10. **Buck, C. B.** 2008. Defensins' offensive play: exploiting a viral achilles' heel. *Cell Host Microbe* **3**:3-4.
11. **Buck, C. B., P. M. Day, C. D. Thompson, J. Lubkowski, W. Lu, D. R. Lowy, and J. T. Schiller.** 2006. Human alpha-defensins block



papillomavirus infection. Proc Natl Acad Sci U S A **103**:1516-1521.

12. **Challberg, M. D., S. V. Desiderio, and T. J. Kelly, Jr.** 1980. Adenovirus DNA replication in vitro: characterization of a protein covalently linked to nascent DNA strands. Proc Natl Acad Sci U S A **77**:5105-5109.
13. **Chandonia, J. M., and M. Karplus.** 1999. New methods for accurate prediction of protein secondary structure. Proteins **35**:293-306.
14. **Chang, T. L., J. Vargas, Jr., A. DelPortillo, and M. E. Klotman.** 2005. Dual role of alpha-defensin-1 in anti-HIV-1 innate immunity. J Clin Invest **115**:765-773.
15. **Chatterjee, P. K., M. E. Vayda, and S. J. Flint.** 1986. Identification of proteins and protein domains that contact DNA within adenovirus nucleoprotein cores by ultraviolet light crosslinking of oligonucleotides 32P-labelled in vivo. J Mol Biol **188**:23-37.
16. **Chatterjee, P. K., M. E. Vayda, and S. J. Flint.** 1985. Interactions among the three adenovirus core proteins. J Virol **55**:379-386.
17. **Chatterjee, P. K., U. C. Yang, and S. J. Flint.** 1986. Comparison of the interactions of the adenovirus type 2 major core protein and its precursor with DNA. Nucleic Acids Res **14**:2721-2735.
18. **Chelius, D., A. F. Huhmer, C. H. Shieh, E. Lehmberg, J. A. Traina, T. K. Slattery, and E. Pungor, Jr.** 2002. Analysis of the adenovirus type 5 proteome by liquid chromatography and tandem mass spectrometry methods. J Proteome Res **1**:501-513.
19. **Cole, A. M., and A. L. Cole.** 2008. Antimicrobial polypeptides are key anti-HIV-1 effector molecules of cervicovaginal host defense. Am J Reprod Immunol **59**:27-34.
20. **Coombs, D. H., A. J. Robinson, J. W. Bodnar, C. J. Jones, and G. D. Pearson.** 1979. Detection of covalent DNA-protein complexes: the adenovirus DNA-terminal protein complex and HeLa DNA-protein complexes. Cold Spring Harb Symp Quant Biol **43 Pt 2**:741-753.
21. **Corden, J., H. M. Engelking, and G. D. Pearson.** 1976. Chromatin-like organization of the adenovirus chromosome. Proc Natl Acad Sci U S A **73**:401-404.
22. **Cotten, M., and J. M. Weber.** 1995. The adenovirus protease is required for virus entry into host cells. Virology **213**:494-502.

23. **Cuzange, A., J. Chroboczek, and B. Jacrot.** 1994. The penton base of human adenovirus type 3 has the RGD motif. *Gene* **146**:257-259.
24. **Daher, K. A., M. E. Selsted, and R. I. Lehrer.** 1986. Direct inactivation of viruses by human granulocyte defensins. *J Virol* **60**:1068-1074.
25. **Dietrich, D. E., X. Xiao, D. V. Dawson, M. Belanger, H. Xie, A. Progulske-Fox, and K. A. Brogden.** 2008. Human alpha- and beta-defensins bind to immobilized adhesins from *Porphyromonas gingivalis*. *Infect Immun* **76**:5714-5720.
26. **Dmitriev, I. P., E. A. Kashentseva, and D. T. Curiel.** 2002. Engineering of adenovirus vectors containing heterologous peptide sequences in the C terminus of capsid protein IX. *J Virol* **76**:6893-6899.
27. **Durmort, C., C. Stehlin, G. Schoehn, A. Mitraki, E. Drouet, S. Cusack, and W. P. Burmeister.** 2001. Structure of the fiber head of Ad3, a non-CAR-binding serotype of adenovirus. *Virology* **285**:302-312.
28. **Everitt, E., L. Lutter, and L. Philipson.** 1975. Structural proteins of adenoviruses. XII. Location and neighbor relationship among proteins of adenovirion type 2 as revealed by enzymatic iodination, immunoprecipitation and chemical cross-linking. *Virology* **67**:197-208.
29. **Fabry, C. M., M. Rosa-Calatrava, J. F. Conway, C. Zubieta, S. Cusack, R. W. Ruigrok, and G. Schoehn.** 2005. A quasi-atomic model of human adenovirus type 5 capsid. *EMBO J* **24**:1645-1654.
30. **Fabry, C. M., M. Rosa-Calatrava, C. Moriscot, R. W. Ruigrok, P. Boulanger, and G. Schoehn.** 2009. The C-terminal domains of adenovirus serotype 5 protein IX assemble into an antiparallel structure on the facets of the capsid. *J Virol* **83**:1135-1139.
31. **Flotte, T. R.** 2007. Gene therapy: the first two decades and the current state-of-the-art. *J Cell Physiol* **213**:301-305.
32. **Furci, L., F. Sironi, M. Tolazzi, L. Vassena, and P. Lusso.** 2007. Alpha-defensins block the early steps of HIV-1 infection: interference with the binding of gp120 to CD4. *Blood* **109**:2928-2935.
33. **Furcinitti, P. S., J. van Oostrum, and R. M. Burnett.** 1989. Adenovirus polypeptide IX revealed as capsid cement by difference images from electron microscopy and crystallography. *EMBO J* **8**:3563-3570.
34. **Gaggar, A., D. M. Shayakhmetov, and A. Lieber.** 2003. CD46 is a cellular receptor for group B adenoviruses. *Nat Med* **9**:1408-1412.

35. **Gastaldelli, M., N. Imelli, K. Boucke, B. Amstutz, O. Meier, and U. F. Greber.** 2008. Infectious adenovirus type 2 transport through early but not late endosomes. *Traffic* **9**:2265-2278.
36. **Greber, U. F., P. Webster, J. Weber, and A. Helenius.** 1996. The role of the adenovirus protease on virus entry into cells. *EMBO J* **15**:1766-1777.
37. **Greber, U. F., M. Willetts, P. Webster, and A. Helenius.** 1993. Stepwise dismantling of adenovirus 2 during entry into cells. *Cell* **75**:477-486.
38. **Grigorieff, N.,** Bfactor:  
[http://emlab.rose2.brandeis.edu/grigorieff/download\\_b.html](http://emlab.rose2.brandeis.edu/grigorieff/download_b.html).
39. **Grigorieff, N.** 2007. FREALIGN: high-resolution refinement of single particle structures. *J Struct Biol* **157**:117-125.
40. **Gupta, D., E. J. Molina, J. Palma, J. P. Gaughan, W. Long, and M. Macha.** 2008. Adenoviral beta-adrenergic receptor kinase inhibitor gene transfer improves exercise capacity, cardiac contractility, and systemic inflammation in a model of pressure overload hypertrophy. *Cardiovasc Drugs Ther* **22**:373-381.
41. **Gura, T.** 2001. Innate immunity. Ancient system gets new respect. *Science* **291**:2068-2071.
42. **Hancock RE, S. H.** 2006. Antimicrobial and host-defense peptides as new anti-infective therapeutic strategies. *Nat Biotechnol* **24**:1551-1557.
43. **Hannan, C., L. H. Raptis, C. V. Dery, and J. Weber.** 1983. Biological and structural studies with an adenovirus type 2 temperature-sensitive mutant defective for uncoating. *Intervirology* **19**:213-223.
44. **Harpst, J. A., J. F. Ennever, and W. C. Russell.** 1977. Physical properties of nucleoprotein cores from adenovirus type 5. *Nucleic Acids Res* **4**:477-490.
45. **Harter, M. L., J. B. Lewis, and C. W. Anderson.** 1979. Adenovirus type 2 terminal protein: purification and comparison of tryptic peptides with known adenovirus-coded proteins. *J Virol* **31**:823-835.
46. **Harvey, S. A., E. G. Romanowski, K. A. Yates, and Y. J. Gordon.** 2005. Adenovirus-directed ocular innate immunity: the role of conjunctival defensin-like chemokines (IP-10, I-TAC) and phagocytic human defensin-alpha. *Invest Ophthalmol Vis Sci* **46**:3657-3665.
47. **Hassell, J. A., and J. Weber.** 1978. Genetic analysis of adenovirus type 2. VIII. Physical locations of temperature-sensitive mutations. *J Virol*

28:671-678.

48. **Hasson, T. B., D. A. Ornelles, and T. Shenk.** 1992. Adenovirus L1 52- and 55-kilodalton proteins are present within assembling virions and colocalize with nuclear structures distinct from replication centers. *J Virol* **66**:6133-6142.
49. **Honkavuori, K. S., B. D. Pollard, M. S. Rodriguez, R. T. Hay, and G. D. Kemp.** 2004. Dual role of the adenovirus pVI C terminus as a nuclear localization signal and activator of the viral protease. *J Gen Virol* **85**:3367-3376.
50. **Hosokawa, K., and M. T. Sung.** 1976. Isolation and characterization of an extremely basic protein from adenovirus type 5. *J Virol* **17**:924-934.
51. **Jones, D. T.** 1999. Protein secondary structure prediction based on position-specific scoring matrices. *J Mol Biol* **292**:195-202.
52. **Kalyuzhniy, O., N. C. Di Paolo, M. Silvestry, S. E. Hofherr, M. A. Barry, P. L. Stewart, and D. M. Shayakhmetov.** 2008. Adenovirus serotype 5 hexon is critical for virus infection of hepatocytes in vivo. *Proc Natl Acad Sci U S A* **105**:5483-5488.
53. **Karplus, K., K. Sjolander, C. Barrett, M. Cline, D. Haussler, R. Hughey, L. Holm, and C. Sander.** 1997. Predicting protein structure using hidden Markov models. *Proteins Suppl* **1**:134-139.
54. **Kickhoefer, V. A., M. Han, S. Raval-Fernandes, M. J. Poderycki, R. J. Moniz, D. Vaccari, M. Silvestry, P. L. Stewart, K. A. Kelly, and L. H. Rome.** 2009. Targeting vault nanoparticles to specific cell surface receptors. *ACS Nano* **3**:27-36.
55. **Kirby, I., E. Davison, A. J. Beavil, C. P. Soh, T. J. Wickham, P. W. Roelvink, I. Kovesdi, B. J. Sutton, and G. Santis.** 2000. Identification of contact residues and definition of the CAR-binding site of adenovirus type 5 fiber protein. *J Virol* **74**:2804-2813.
56. **Kuhn, L., D. Trabattoni, C. Kankasa, K. Semrau, P. Kasonde, F. Lissoni, M. Sinkala, M. Ghosh, C. Vwalika, G. M. Aldrovandi, D. M. Thea, and M. Clerici.** 2005. Alpha-defensins in the prevention of HIV transmission among breastfed infants. *J Acquir Immune Defic Syndr* **39**:138-142.
57. **Legrand, V., D. Spehner, Y. Schlesinger, N. Settelen, A. Pavirani, and M. Mehtali.** 1999. Fiberless recombinant adenoviruses: virus maturation and infectivity in the absence of fiber. *J Virol* **73**:907-919.

58. **Lehmborg, E., J. A. Traina, J. A. Chakel, R. J. Chang, M. Parkman, M. T. McCaman, P. K. Murakami, V. Lahidji, J. W. Nelson, W. S. Hancock, E. Nestaas, and E. Pungor, Jr.** 1999. Reversed-phase high-performance liquid chromatographic assay for the adenovirus type 5 proteome. *J Chromatogr B Biomed Sci Appl* **732**:411-423.
59. **Lehrer RI, L. A., Ganz T.** 1993. Defensins: antimicrobial and cytotoxic peptides of mammalian cells. *Annu Rev Immunol* **11**:105-128.
60. **Leopold, P. L., and R. G. Crystal.** 2007. Intracellular trafficking of adenovirus: many means to many ends. *Adv Drug Deliv Rev* **59**:810-821.
61. **Liu, G. Q., L. E. Babiss, F. C. Volkert, C. S. Young, and H. S. Ginsberg.** 1985. A thermolabile mutant of adenovirus 5 resulting from a substitution mutation in the protein VIII gene. *J Virol* **53**:920-925.
62. **Liu, Y.-H., G. Vellekamp, G. Chen, U. A. Mirza, D. Wylie, B. Twarowska, J. T. Tang, F. W. Porter, S. Wang, T. L. Nagabhushan, and B. N. Pramanik.** 2003. Proteomic study of recombinant adenovirus 5 encoding human p53 by matrix-assisted laser desorption/ionization mass spectrometry in combination with database search. *International Journal of Mass Spectrometry* **226**:55-69.
63. **Lortat-Jacob, H., E. Chouin, S. Cusack, and M. J. van Raaij.** 2001. Kinetic analysis of adenovirus fiber binding to its receptor reveals an avidity mechanism for trimeric receptor-ligand interactions. *J Biol Chem* **276**:9009-9015.
64. **Ly, H., Y. Kawase, R. Yoneyama, and R. J. Hajjar.** 2007. Gene therapy in the treatment of heart failure. *Physiology (Bethesda)* **22**:81-96.
65. **Mangel, W. F., M. L. Baniecki, and W. J. McGrath.** 2003. Specific interactions of the adenovirus proteinase with the viral DNA, an 11-amino-acid viral peptide, and the cellular protein actin. *Cell Mol Life Sci* **60**:2347-2355.
66. **Mangel, W. F., D. L. Toledo, M. T. Brown, J. H. Martin, and W. J. McGrath.** 1996. Characterization of three components of human adenovirus proteinase activity in vitro. *J Biol Chem* **271**:536-543.
67. **Marsh, M. P., S. K. Campos, M. L. Baker, C. Y. Chen, W. Chiu, and M. A. Barry.** 2006. Cryoelectron microscopy of protein IX-modified adenoviruses suggests a new position for the C terminus of protein IX. *J Virol* **80**:11881-11886.
68. **Matthews, D. A., and W. C. Russell.** 1998. Adenovirus core protein V is

delivered by the invading virus to the nucleus of the infected cell and later in infection is associated with nucleoli. *J Gen Virol* **79 ( Pt 7)**:1671-1675.

69. **Matthews, D. A., and W. C. Russell.** 1994. Adenovirus protein-protein interactions: hexon and protein VI. *J Gen Virol* **75 ( Pt 12)**:3365-3374.
70. **Matthews, D. A., and W. C. Russell.** 1995. Adenovirus protein-protein interactions: molecular parameters governing the binding of protein VI to hexon and the activation of the adenovirus 23K protease. *J Gen Virol* **76 ( Pt 8)**:1959-1969.
71. **McPhee JB, H. R.** 2005. Function and therapeutic potential of host defence peptides. *J Pept Sci* **11**:677-687.
72. **Meiler, J., and D. Baker.** 2003. Coupled prediction of protein secondary and tertiary structure. *Proc Natl Acad Sci U S A* **100**:12105-12110.
73. **Meiler, J., J. J. Prompers, W. Peti, C. Griesinger, and R. Bruschweiler.** 2001. Model-free approach to the dynamic interpretation of residual dipolar couplings in globular proteins. *J Am Chem Soc* **123**:6098-6107.
74. **Mindell, J. A., and N. Grigorieff.** 2003. Accurate determination of local defocus and specimen tilt in electron microscopy. *J Struct Biol* **142**:334-347.
75. **Mirza, A., and J. Weber.** 1980. Infectivity and uncoating of adenovirus cores. *Intervirology* **13**:307-311.
76. **Mirza, M. A., and J. Weber.** 1982. Structure of adenovirus chromatin. *Biochim Biophys Acta* **696**:76-86.
77. **Mirza, M. A., and J. Weber.** 1979. Uncoating of adenovirus type 2. *J Virol* **30**:462-471.
78. **Mondel, M., B. O. Schroeder, K. Zimmermann, H. Huber, S. Nuding, J. Beisner, K. Fellermann, E. F. Stange, and J. Wehkamp.** 2009. Probiotic *E. coli* treatment mediates antimicrobial human beta-defensin synthesis and fecal excretion in humans. *Mucosal Immunol* **2**:166-172.
79. **Mookherjee N, H. R.** 2007. Cationic host defence peptides: innate immune regulatory peptides as a novel approach for treating infections. *Cell Mol Life Sci* **64**:922-933.
80. **Nemerow, G. R., L. Pache, V. Reddy, and P. L. Stewart.** 2009. Insights into adenovirus host cell interactions from structural studies. *Virology* **384**:380-388.

81. **Nermut, M. V., J. A. Harpst, and W. C. Russell.** 1975. Electron microscopy of adenovirus cores. *J Gen Virol* **28**:49-58.
82. **Pettersen, E. F., T. D. Goddard, C. C. Huang, G. S. Couch, D. M. Greenblatt, E. C. Meng, and T. E. Ferrin.** 2004. UCSF Chimera--a visualization system for exploratory research and analysis. *J Comput Chem* **25**:1605-1612.
83. **Rancourt, C., H. Keyvani-Amineh, S. Sircar, P. Labrecque, and J. M. Weber.** 1995. Proline 137 is critical for adenovirus protease encapsidation and activation but not enzyme activity. *Virology* **209**:167-173.
84. **Rekosh, D. M., W. C. Russell, A. J. Bellet, and A. J. Robinson.** 1977. Identification of a protein linked to the ends of adenovirus DNA. *Cell* **11**:283-295.
85. **Rosenthal, P. B., and R. Henderson.** 2003. Optimal determination of particle orientation, absolute hand, and contrast loss in single-particle electron cryomicroscopy. *J Mol Biol* **333**:721-745.
86. **Russell, W. C., and B. Precious.** 1982. Nucleic acid-binding properties of adenovirus structural polypeptides. *J Gen Virol* **63 (Pt 1)**:69-79.
87. **Rux, J. J., P. R. Kuser, and R. M. Burnett.** 2003. Structural and phylogenetic analysis of adenovirus hexons by use of high-resolution x-ray crystallographic, molecular modeling, and sequence-based methods. *J Virol* **77**:9553-9566.
88. **Saban, S. D., R. R. Nepomuceno, L. D. Gritton, G. R. Nemerow, and P. L. Stewart.** 2005. CryoEM structure at 9A resolution of an adenovirus vector targeted to hematopoietic cells. *J Mol Biol* **349**:526-537.
89. **Saban, S. D., M. Silvestry, G. R. Nemerow, and P. L. Stewart.** 2006. Visualization of alpha-helices in a 6-angstrom resolution cryoelectron microscopy structure of adenovirus allows refinement of capsid protein assignments. *J Virol* **80**:12049-12059.
90. **Salvatore M, G.-S. A., Ruchala P, Lehrer RI, Chang T, Klotman ME.** 2007. alpha-Defensin inhibits influenza virus replication by cell-mediated mechanism(s). *J Infect Dis* **196**:835-843.
91. **San Martin, C., J. N. Glasgow, A. Borovjagin, M. S. Beatty, E. A. Kashentseva, D. T. Curiel, R. Marabini, and I. P. Dmitriev.** 2008. Localization of the N-terminus of minor coat protein IIIa in the adenovirus capsid. *J Mol Biol* **383**:923-934.

92. **Schlee, M., J. Wehkamp, A. Altenhoefer, T. A. Oelschlaeger, E. F. Stange, and K. Fellermann.** 2007. Induction of human beta-defensin 2 by the probiotic *Escherichia coli* Nissle 1917 is mediated through flagellin. *Infect Immun* **75**:2399-2407.
93. **Schneider, J. J., A. Unholzer, M. Schaller, M. Schafer-Korting, and H. C. Korting.** 2005. Human defensins. *J Mol Med* **83**:587-595.
94. **Seth, P.** 2005. Vector-mediated cancer gene therapy: an overview. *Cancer Biol Ther* **4**:512-517.
95. **Shi, J., D. R. Williams, and P. L. Stewart.** 2008. A Script-Assisted Microscopy (SAM) package to improve data acquisition rates on FEI Tecnai electron microscopes equipped with Gatan CCD cameras. *J Struct Biol* **164**:166-169.
96. **Silvestry, M., S. Lindert, J. G. Smith, O. Maier, C. M. Wiethoff, G. R. Nemerow, and P. L. Stewart.** 2009. Cryo-electron microscopy structure of adenovirus type 2 temperature-sensitive mutant 1 reveals insight into the cell entry defect. *J Virol* **83**:7375-7383.
97. **Smith, J. G., and G. R. Nemerow.** 2008. Mechanism of adenovirus neutralization by Human alpha-defensins. *Cell Host Microbe* **3**:11-19.
98. **Stewart, P. L., R. M. Burnett, M. Cyrklaff, and S. D. Fuller.** 1991. Image reconstruction reveals the complex molecular organization of adenovirus. *Cell* **67**:145-154.
99. **Sung, M. T., T. M. Cao, M. A. Lischwe, and R. T. Coleman.** 1983. Molecular processing of adenovirus proteins. *J Biol Chem* **258**:8266-8272.
100. **Suomalainen, M., M. Y. Nakano, S. Keller, K. Boucke, R. P. Stidwill, and U. F. Greber.** 1999. Microtubule-dependent plus- and minus end-directed motilities are competing processes for nuclear targeting of adenovirus. *J Cell Biol* **144**:657-672.
101. **Szyk, A., Z. Wu, K. Tucker, D. Yang, W. Lu, and J. Lubkowski.** 2006. Crystal structures of human alpha-defensins HNP4, HD5, and HD6. *Protein Sci* **15**:2749-2760.
102. **Takahashi, A., A. Wada, K. Ogushi, K. Maeda, T. Kawahara, K. Mawatari, H. Kurazono, J. Moss, T. Hirayama, and Y. Nakaya.** 2001. Production of beta-defensin-2 by human colonic epithelial cells induced by *Salmonella enteritidis* flagella filament structural protein. *FEBS Lett* **508**:484-488.



103. **Tamamori-Adachi, M., H. Takagi, K. Hashimoto, K. Goto, T. Hidaka, U. Koshimizu, K. Yamada, I. Goto, Y. Maejima, M. Isobe, K. I. Nakayama, N. Inomata, and S. Kitajima.** 2008. Cardiomyocyte proliferation and protection against post-myocardial infarction heart failure by cyclin D1 and Skp2 ubiquitin ligase. *Cardiovasc Res* **80**:181-190.
104. **van Heel, M., G. Harauz, E. V. Orlova, R. Schmidt, and M. Schatz.** 1996. A new generation of the IMAGIC image processing system. *J Struct Biol* **116**:17-24.
105. **van Raaij, M. J., E. Chouin, H. van der Zandt, J. M. Bergelson, and S. Cusack.** 2000. Dimeric structure of the coxsackievirus and adenovirus receptor D1 domain at 1.7 Å resolution. *Structure* **8**:1147-1155.
106. **van Raaij, M. J., A. Mitraki, G. Lavigne, and S. Cusack.** 1999. A triple beta-spiral in the adenovirus fibre shaft reveals a new structural motif for a fibrous protein. *Nature* **401**:935-938.
107. **Vasudevan S, Y. J., Osapay G, Tran P, Tai K, Liang W, Kumar V, Selsted ME, Cocco MJ.** 2008. Synthesis, structure, and activities of an oral mucosal alpha-defensin from rhesus macaque. *J Biol Chem* **283**:35869-35877.
108. **Vigant, F., D. Descamps, B. Jullienne, S. Esselin, E. Connault, P. Opolon, T. Tordjmann, E. Vigne, M. Perricaudet, and K. Benihoud.** 2008. Substitution of hexon hypervariable region 5 of adenovirus serotype 5 abrogates blood factor binding and limits gene transfer to liver. *Mol Ther* **16**:1474-1480.
109. **Von Seggern DJ, C. C., Fleck SK, Stewart PL, Nemerow GR.** 1999. A helper-independent adenovirus vector with E1, E3, and fiber deleted: structure and infectivity of fiberless particles. *J Virol*. **73**:1601-1608.
110. **Waddington, S. N., J. H. McVey, D. Bhella, A. L. Parker, K. Barker, H. Atoda, R. Pink, S. M. Buckley, J. A. Greig, L. Denby, J. Custers, T. Morita, I. M. Francischetti, R. Q. Monteiro, D. H. Barouch, N. van Rooijen, C. Napoli, M. J. Havenga, S. A. Nicklin, and A. H. Baker.** 2008. Adenovirus serotype 5 hexon mediates liver gene transfer. *Cell* **132**:397-409.
111. **Weber, J.** 1976. Genetic analysis of adenovirus type 2 III. Temperature sensitivity of processing viral proteins. *J Virol* **17**:462-471.
112. **Weber, J., M. Begin, and G. Khittoo.** 1975. Genetic Analysis of Adenovirus Type 2 II. Preliminary Phenotypic Characterization of Temperature-Sensitive Mutants. *J Virol* **15**:1049-1056.

113. **Webster, A., R. T. Hay, and G. Kemp.** 1993. The adenovirus protease is activated by a virus-coded disulphide-linked peptide. *Cell* **72**:97-104.
114. **Webster, A., S. Russell, P. Talbot, W. C. Russell, and G. D. Kemp.** 1989. Characterization of the adenovirus proteinase: substrate specificity. *J Gen Virol* **70 ( Pt 12)**:3225-3234.
115. **Weinberg, A., M. E. Quinones-Mateu, and M. M. Lederman.** 2006. Role of human beta-defensins in HIV infection. *Adv Dent Res* **19**:42-48.
116. **Wickham, T. J., E. J. Filardo, D. A. Cheresh, and G. R. Nemerow.** 1994. Integrin alpha v beta 5 selectively promotes adenovirus mediated cell membrane permeabilization. *J Cell Biol* **127**:257-264.
117. **Wickham, T. J., P. Mathias, D. A. Cheresh, and G. R. Nemerow.** 1993. Integrins alpha v beta 3 and alpha v beta 5 promote adenovirus internalization but not virus attachment. *Cell* **73**:309-319.
118. **Wiethoff, C. M., H. Wodrich, L. Gerace, and G. R. Nemerow.** 2005. Adenovirus protein VI mediates membrane disruption following capsid disassembly. *J Virol* **79**:1992-2000.
119. **Wodrich, H., T. Guan, G. Cingolani, D. Von Seggern, G. Nemerow, and L. Gerace.** 2003. Switch from capsid protein import to adenovirus assembly by cleavage of nuclear transport signals. *EMBO J* **22**:6245-6255.
120. **Yang D, L. Z., Tewary P, Chen Q, de la Rosa G, Oppenheim JJ.** 2007. Defensin participation in innate and adaptive immunity. *Curr Pharm Des* **13**:3131-3139.
121. **Yedery, R. D., and K. V. Reddy.** 2005. Antimicrobial peptides as microbicidal contraceptives: prophecies for prophylactics--a mini review. *Eur J Contracept Reprod Health Care* **10**:32-42.
122. **Zhang, W., and R. Arcos.** 2005. Interaction of the adenovirus major core protein precursor, pVII, with the viral DNA packaging machinery. *Virology* **334**:194-202.
123. **Zhou, Z. H.** 2008. Towards atomic resolution structural determination by single-particle cryo-electron microscopy. *Curr Opin Struct Biol* **18**:218-228.
124. **Zubieta, C., G. Schoehn, J. Chroboczek, and S. Cusack.** 2005. The structure of the human adenovirus 2 penton. *Mol Cell* **17**:121-135.